2014

Analysis of the Role of Astrocyte Elevated Gene-1 in Normal Liver Physiology and in the Onset and Progression of Hepatocellular Carcinoma

Chadia L. Robertson
Virginia Commonwealth University, robertsoncl@vcu.edu

Follow this and additional works at: http://scholarscompass.vcu.edu/etd

Part of the Biochemical Phenomena, Metabolism, and Nutrition Commons, Disease Modeling Commons, Gastroenterology Commons, Genetic Phenomena Commons, Genetic Processes Commons, Hepatology Commons, Immune System Diseases Commons, Medical Immunology Commons, Medical Molecular Biology Commons, and the Oncology Commons

Downloaded from
http://scholarscompass.vcu.edu/etd/3573

Analysis of the Role of Astrocyte Elevated Gene-1 in Normal Liver

Physiology and in the Onset and Progression of Hepatocellular Carcinoma

A dissertation submitted in partial fulfillment of the requirements for the degree of
Doctor of Philosophy at Virginia Commonwealth University

by

Chadia L. Robertson
Bachelor of Science, University of Florida, Gainesville, FL
Master of Science, Barry University, Miami, FL

Advisor: Devanand Sarkar MBBS, PhD
Associate Professor, Department of Human and Molecular Genetics
Blick Scholar
Associate Scientific Director, Cancer Therapeutics
VCU Institute of Molecular Medicine
Massey Cancer Center

Virginia Commonwealth University
Richmond, Virginia
September 2014

Acknowledgements

I would like to take this opportunity to thank the people who have helped and supported me throughout my PhD training. I would first like to thank my mentor Dr. Devanand Sarkar for all of the support and opportunities he has given me. For being there when I really needed guidance and for letting go and allowing me the independence I needed to grow as a scientist I thank you Dr Sarkar- you have lead by example your career your dedication and your accomplishments have truly been a source of inspiration for me. I would also like to thank the members of the Sarkar lab including Rachel Gredler who has helped me with many projects throughout my time in the lab and has always fostered a functional and collaborative lab environment. I also would like to thank Dr. Ayesha Siddiq who taught me many of the techniques I needed to start my project. Thank you to the current members of the Sarkar lab Dr. Jyoti Srivastava and Dr. Devaraja Rajasekaran who have provided great intellectual conversations, collaborations and support. A big thank you to each of my thesis committee members. Dr Phillip Hylemon thank you for so readily sharing ideas and resources, the help that I received from your lab particularly with the primary hepatocyte isolations and bile acid analysis certainly helped move my project forward. Dr. Jolene Windle, thank you for always making time to talk through the animal projects and for offering truly thoughtful suggestions on how to tackle issues large and small. Dr. Suzanne Barbour thank you for all of your guidance, support and words of encouragement, your support has meant more than you know. Dr. Paul Fisher thank you for always offering guidance and support and for making time to pay attention to the projects always finding ways to make them better-I have truly benefited from your experience. To my friends, siblings, aunts, uncles and cousins who have always been there for me and knowing how much this endeavor has meant to me showered me with constant love and support I thank each of you. To Mba Uzoma Mba you are been my best friend and my rock, I thank you for grounding me and believing in me through it all.

Dedication

I dedicate this thesis to my parents Winsome and Neville Robertson. You have inspired me to dream and believe that I can achieve those dreams. You taught me that all should be done with integrity and distinction. You believed in me and in my abilities. You have loved me beyond words. I am all that I am because of you.

Table of Contents

List of Tables

List of Figures

CHAPTER THREE

List of abbreviations and symbols

α……………………………………..…………………………………….Alpha

a.a…………………………….…..…………………….…..………………Amino acid

AEG-1……………………………………………………Astrocyte Elevated Gene-1

ACHH3……………………………………………….…….Acetyl Histone H3

β…………………………………………………………………….……..Beta

C………………………………………………………..….……………Celsius

CBC……………………………………………………….Complete Blood Count

δ…………………………………………………..….……………….Delta

γ…………………………………………………………..….…………Gamma

H3…………………………………………………………….………Histone H3

HDAC………………………………………………….…….Histone Deacetylase

HPLC………………………………………...……High Performance Liquid Chromatography

IgG………………………………………………………..……...Immunoglobulin G

IP……………………………………………………….…………….Immunoprecipitation

KD………………………………………………………………….…..Knockdown

KO……………………………………………………………………..Knockout

H&E………………………………………………..……Hematoxylin and Eosin

MEK…………………………………….............… Mitogen-activated protein extracellular kinase

Erk…….….………………………………….……… Extracellular signal-regulated kinase

PI3K……………………………………………………. Phosphotidyl-inositol-3-kinase

QPCR…………………………………..…..Quantitative real time polymerase chain reaction

RNA……………………………………………….…..…………Ribonucleic acid

μ…..……………………………………..….……………………………Micro

bp……………………………………………………………………Base pair

PBS………………………………………………………..Phosphate buffered saline

PCR………………………………………………….………Polymerase chain reaction

shRNA……………………………………………………….…..Short hairpin rna

siRNA…………………………………………………..…………Small interfering rna

WT……………………………………………………………….…..Wild type

Abstract

ANALYSIS OF THE ROLE OF ASTROCYTE ELEVATED GENE-1 IN NORMAL

LIVER PHYSIOLOGY AND IN THE ONSET AND PROGRESSION OF

HEPATOCELLULAR CARCINOMA

By Chadia L. Robertson, PhD

A dissertation submitted in partial fulfillment of the requirements for the degree of Doctor of Philosophy at Virginia Commonwealth University

Virginia Commonwealth University, 2014

Advisor: Devanand Sarkar MBBS, PhD
Associate Professor, Department of Human and Molecular Genetics
Blick Scholar
Associate Scientific Director, Cancer Therapeutics
VCU Institute of Molecular Medicine
Massey Cancer Center

First identified over a decade ago, Astrocyte Elevated Gene-1 (AEG-1) has been studied extensively due to early reports of its overexpression in various cancer cell lines. Research groups all over the globe including our own have since identified AEG-1 overexpression in cancers of diverse lineages including cancers of the liver, colon, skin, prostate, breast, lung, esophagus, neurons and neuronal glia as compared to matched normal tissue. A comprehensive and convincing body of data currently points to AEG-1 as an essential component, critical to the progression and perhaps onset of cancer. AEG-1 is a potent activator of multiple pro-tumorigenic signal transduction pathways such as mitogen-activated protein extracellular kinase (MEK)/ extracellular signal-regulated kinase (ERK), phosphotidyl-inositol-3-kinase (PI3K)/Akt/mTOR, NF-κB and Wnt/β-catenin pathway. In addition, studies show that AEG-1 not only alters

global gene and protein expression profiles, it also modulates fundamental intracellular processes, such as transcription, translation and RNA interference in cancer cells most likely by functioning as a scaffold protein.

The mechanisms by which AEG-1 is overexpressed in cancer have been studied extensively and it is clear that multiple layers of regulation including genomic amplification, transcriptional, posttranscriptional, and posttranslational controls are involved however; the mechanism by which AEG 1 itself induces its oncogenic effects is still poorly understood. Just as questions remain about the exact role of AEG-1 in carcinogenesis, very little is known about the role of AEG-1 in regulating normal physiological functions in the liver. With the help of the Massey Cancer Center Transgenic/Knockout Mouse Core, our lab has successfully created a germline-AEG-1 knockout mouse (AEG-1-/-) as a model to interrogate AEG-1 function in vivo. Here I present the insights gained from efforts to analyze this novel AEG-1-/- mouse model. Aspects of the physiological functions of AEG-1 will be covered in chapter two wherein details of the characterization of the AEG-1-/- mouse are described including the role of AEG-1 in lipid metabolism. Chapter three discusses novel discoveries about the specific role of AEG-1 in mediating hepatocarcinogenesis by modulating NF-κB, a critical inflammatory pathway.

Chapter One-Introduction

I. Initial Identification and Cloning of Astrocyte Elevated Gene -1

In 2002, Su and colleagues set out to elucidate potential gene expression changes in HIV-1-infected astrocytes. Rapid subtraction hybridization (RaSH) was used as a method to identify differential expression between infected and non-infected primary human fetal astrocytes (PHFAs). Temporal cDNA libraries were prepared from double-stranded cDNAs, which were PCR amplified and then hybridized. Subtracting temporal cDNAs derived from uninfected astrocytes from temporal cDNAs made from HIV-1 infected astrocytes allowed for the identification of several human immunodeficiency virus (HIV)-1 and tumor necrosis factor (TNF)-α-inducible induced genes. These genes termed astrocyte elevated (AEGs) included both novel and previously characterized targets [1]. AEG-1 (also referred to as Metadherin, LYRIC, or 3D3/LYRIC in the literature) was among 15 of the novel genes identified. AEG-1 was shown to be induced following exposure to HIV-1, its cell surface protein gp120, or upon exposure to the HIV-1-induced cytokine tumor necrosis factor-α (TNF-α).

The role of AEG-1 in HIV-1 was not pursued further however soon after the initial identification of AEG-1, another group cloned the murine ortholog of AEG-1 in a study aimed at identifying tumor cell surface molecules mediating metastasis of breast cancer cells using in vivo phage screening methods. In this

study a phage display library of breast carcinoma cDNAs enriched for secreted and transmembrane proteins from mouse 4T1 breast cancer cells was injected into mice intravenously. Phages that localized to the lungs were isolated and sequenced. One of the clones identified in this study encoded amino acids 378-440 of mouse AEG-1, and this particular extracellular protein domain was shown to specifically induce phage homing to the microvasculature of the lung. This was the first identification of the lung homing domain (LHD) in the protein they named metastasis adhesion protein-or metadherin [2]. Immunostaining revealed metadherin overexpression in breast cancer tissue and breast tumor xenografts as compared to normal breast tissue sections [2]. This study also showed that overexpressing metadherin in HEK293T cells enhanced lung localization of the cells while siRNA-mediated knockdown of metadherin inhibited the lung metastasis commonly seen in mouse 4T1 breast cancer cells. Additionally, the use of anti- metadherin antibodies reactive to the lung-homing domain of metadherin inhibited experimental breast cancer lung metastasis providing the first experimental evidence that this murine AEG-1 ortholog played an important role in cancer metastasis [2].

Also in 2004, gene-trapping techniques screening for proteins located at distinct sub-compartments of the nucleus led to the isolation of the mouse/rat AEG-1 by a separate group who assigned the name 3D3/lyric [3]. In this study F9 embryonic carcinoma cells were transfected with a reporter gene possessing an upstream splice acceptor then allowed to fuse with trapped genes through splicing. Localization of the trapped genes was then determined by

immnostaining for the reporter gene. The N-terminal of 3D3/lyric was trapped using this method and found to localize at the nuclear membrane showing a unique, patchy distribution at the nuclear periphery [3]. Sub cellular fractionation and immunostaining showed that the 3D3/lyric protein was located primarily in the endoplasmic reticulum (ER), but staining was also observed in the nuclear envelope and the nucleolus making it a rare example of a protein that travels freely between the nuclear compartment and the ER. Concurrently another group reported cloning the rat AEG-1 homolog as a tight junction protein. This protein was found to have a strong interaction with carcinoembryonic antigen-related cell adhesion molecule 1 protein (CEACAM1), and was thus deemed LYsine-RIch CEACAM1 co-isolated (LYRIC) and the cDNA was cloned by expression library screening [4].

II. Characterization of Astrocyte Elevated Gene-1

BLAST comparison indicates that the AEG-1 gene is unique in that it has no structural similarity to any currently known genes [4]. AEG-1 homologues have been identified in a number of mammals with over 90% rate of identity however AEG-1 homologues have not been detected in invertebrates. Recently, Lee and Kang conducted a phylogenetic analysis probing DNA sequences for the AEG-1 gene in a wide range of vertebrates using computational phylogenetics methods. Bayesian inference using a GTR-Invariants-Gamma model with 1 million generations was used to generate a phylogenetic tree (Fig 1.1). The data

that resulted illustrated the lines of evolutionary descent of the AEG-1 gene from a common ancestor and provided some new and interesting insights regarding the phylogenetic evolution of AEG-1. Extremely long branches or clades were observed in all mammalian species with the exception of primates and carnivores. The clade pattern with respect to the length is suggestive of a strong degree of purifying natural selection within the short-branched clades in the tree. Quantification of the lengths of the clades revealed a fourfold slower rate of change in the AEG-1 gene in primates and carnivores as compared to other mammals. This data indicates that AEG-1 arose in the common ancestor of all jawed vertebrates over 500 million years ago [5]. Taken together it may be presumed that not only is AEG-1 distinct to vertebrates, it may have been a part of the evolutionary process some 500 million years ago incorporated to perform specialized functions in higher vertebrates.
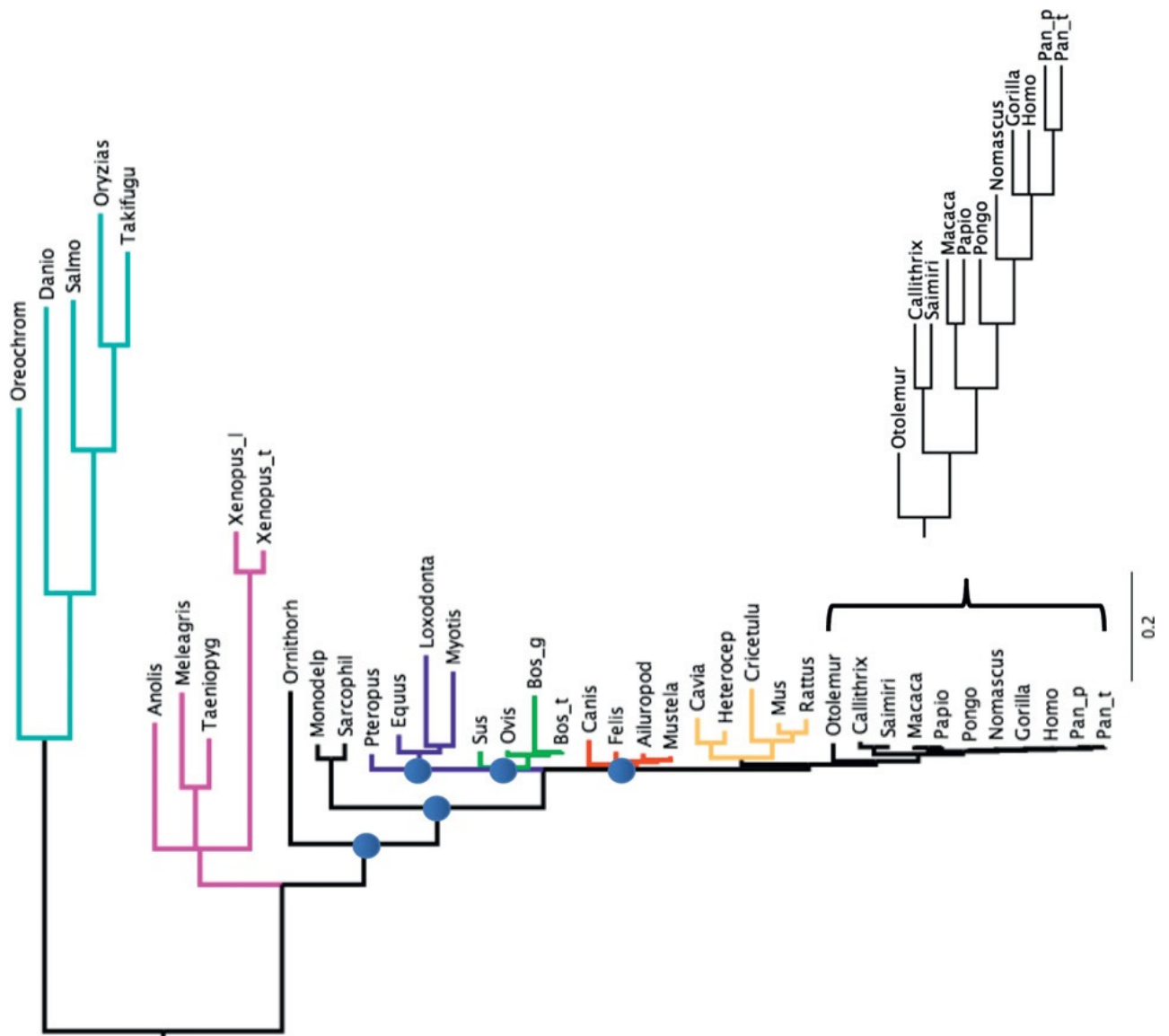
Figure 1.1 Bayesian phylogenetic tree. This tree depicts the relationship between vertebrate AEG-1/MTDH/LYRIC genes.

The human AEG-1 gene has 12 exons and 11 introns and is located at chromosome 8q22-a region identified as a hotspot for recurrent amplification of several human cancer cells by cytogenetic analysis [6] [7] [8]. AEG-1 mRNA consists of 3611 nucleotides excluding the poly-A tail. The open reading frame (from nucleotide 220 to 1,968) of AEG-1 encodes a lysine-rich 64 kDa protein with an isoelectric point of 9.33 as determined by conceptual translational analysis using SMART and von Heijne's technique 9.33 [6].

AEG-1 is recognized as a single-pass transmembrane protein with putative transmembrane domain (TMD) spanning amino acid residues 51 to 72 (Fig 1.2) as determined by analysis of its hydrophobic regions using PSORTII, InterProScan and Simple Modular Architecture Research Tool (SMART) [3]. A hidden Markov model used to predict protein membrane helices and protein topology predicted AEG-1 to be a protein with type II transmembrane topology with an extracellular lung homing domain. This prediction was supported by FACS analysis of AEG-1 tagged with the Myc epitope at the LHD, which indicated extracellular distribution of the C-terminal [2]. The membrane topology of the AG-1 protein is controversial however, due to the fact that type Ib topology of AEG-1 was also predicted in other studies in which intracellular localization of AEG-1 orthologs was confirmed in a number of studies by immunofluorescent microscopy [4] [6] [3].

The localization of AEG-1 and its function is also an area of much dispute. Britt et al. described AEG-1 as a protein localized to tight junctions in polarized rat and human prostate epithelial cells and by immunofluorescence LYRIC

showed co-localization with the tight junction protein ZO-1 [4]. In the same study it was shown that while LYRIC was localized in the tight junctions of normal rat hepatocytes, AS30D-rat hepatoma cells as well as human 293T cells overexpressing LYRIC showed perinuclear localized of the LYRIC protein. Peri-nulcear localization of the protein cloned as 3d3/lyric was also reported by Sutherland and colleagues who also reported detection in the endoplasmic reticulum (ER), nucleus and nucleolus of HeLa and human fibrosarcoma cells [3]. On the other hand, Brown and Ruoslahti, from the Burnham Institute, identified Metadherin as a cell surface protein in mouse breast cancer cells and HEK293T cells overexpressing Metadherin [2]. It has been hypothesized that the large C-terminal domain of the protein is displayed outside of the cell thus facilitating homing of breast cancer cells to the lung and promotes metastasis. In tissue sections of human breast cancer, the protein was localized predominantly in the cytoplasm [9]. However, a recent study from China analyzing 225 breast cancer patients showed increased expression of the protein with the progression of the disease and AEG-1 expression inversely correlated with patient survival [10]. Interestingly, in this study, the metastatic tumors showed more nuclear staining [10]. Our group has also also observed a similar phenomenon in melanoma patient samples showing higher nuclear staining in metastatic disease. In human HCC cells, unpermeabilized cellular conditions result in detection of the AEG-1 protein exclusively on the cell surface however upon permeabilization of cells, AEG-1 can be detected both in the cytoplasm as well as in the nucleus. In malignant glioma cells, strong nuclear staining of AEG-1 is observed and in both

HeLa cells and malignant glioma cells TNF-α treatment results in nuclear translocation of the AEG-1 protein where it interacts with the p65 subunit of NF-κB and the transcription co-activator CBP [11] [12]. Nuclear access is attributed to the three putative nuclear localization signals (NLS) (Fig. 1.2) identified between amino acids 79 to 91 (NLS-1), 432 to 451 (NLS-2), and 561 to 580 (NLS-3) [3]. Each of the three putative NLSs appears to function differently in the nuclear localization of AEG-1. NLS-3 is thought to be the primary determinant of AEG-1 nuclear localization, while NLS-1 is said to regulate nucleolar localization. AEG-1 is monoubiquitinated at NLS 2 and it is believed that this ubiquitination is responsible for trapping AEG-1 in the cytoplasmic compartment a process thought to be responsible for the cytoplasmic distribution of AEG-1 occurring in cancer cells [13]. Based on the available data, it is apparent that AEG-1 might be localized in membrane tight junctions, the cytoplasm, endoplasmic reticulum or the nucleus in a cell type and cell status dependent manner. The role of AEG-1 in each sub cellular compartment and the specific mechanisms facilitating the translocation of AEG-1 requires further investigation.

In an attempt to gain insights into the potential physiological role of AEG-1 in normal development, Jeon and colleagues examined the expression pattern of AEG-1 in mouse embryonic tissues which are similar to humans in that progenitor cells exist for differentiation and cell proliferation for tissue and organ formation [14]. In this study the expression pattern of AEG-1 during mouse embryo development from stage E8.5 through E18.5 was analyzed. Quantitative real-time PCR was used to analyze mRNAs extracted from whole wild-type

mouse embryos at E8.5, E9.5 and E10.5 in varying degrees at each of the three stages. Peak expression of AEG-1 was identified at E10.5. Whole mount immunohistochemistry was also performed to assess the spatial and temporal expression pattern of AEG-1 in E9.5 and E10.5 embryos. AEG-1 expression was detected in mid-to-hindbrain, fronto-nasal processes, limbs, and pharyngeal arches in the early developmental period E9.5–10.5 suggesting that AEG-1 expression plays a pertinent role in progenitor cell differentiation and/or proliferation of early embryos. Expression was increased in the brain, olfactory and skeletal systems, skin, hair follicles, and the liver at specific stages during E12.5–18.5 indicate a potential involvement of AEG-1 in normal cell proliferation during mouse embryonic development. The consistent AEG-1 expression observed through all developmental stages of actively proliferating cells and tissue like liver, skin and hair follicles combined with co-localization of AEG-1 and Ki-67 at the single cell level suggested that AEG-1 expression may be essential to actively proliferating cells and tissues that have a strong regenerative ability.

Analysis of adult human multiple tissue Northern blots (ClonTech) demonstrated that AEG-1 mRNA is ubiquitously expressed at varying levels in all organs [6]. Kang and colleagues did however report higher *AEG*-1 expression in two categories of organs, muscle-dominating organs such as skeletal muscle, heart, tongue and small intestine, and endocrine glands including thyroid and adrenal gland suggesting a possible role of AEG-1 in calcium-associated processes in adult tissue however this potential role has not been studied further.

9

Figure 1.2 Motifs present in AEG-1 protein. The numbers represent amino acid positions. TMD: transmembrane domain. NLS: putative nuclear localization signal.

III. Factors Affecting Astrocyte Elevated Gene-1 Expression

A. Ha-Ras Regulates Expression of Astrocyte Elevated Gene-1

AEG-1 is a downstream target of Ha-ras an oncogenic protein crucial in cellular transformation, tumor progression, and metastasis. The effect of oncogenic Ha-ras on AEG-1 expression was examined in a 2006 study [15]. Specifically examined was the effect of Ha-ras overexpression on the transcription and translation of AEG-1. Transient transfection of a Ha-ras expression plasmid into immortalized adult human astrocytes (THV cells) resulted in significant induction of AEG-1 protein. It was also shown that this AEG-1 protein accumulation was associated with an increase in AEG-1 specific mRNA expression, which was caused by enhanced transcription. Collectively this data suggests that Ha-ras-mediated AEG-1 induction is regulated at the transcriptional level rather than by protein stabilization. Furthermore, promoter analysis of AEG-1 showed that c-Myc binding at two specific E-box elements was critical for Ha-ras-mediated AEG-1 promoter activation as well as for basal promoter activity. Treatment of cells with the PI3K inhibitor, LY294002 significantly attenuated Ha-ras-mediated AEG-1 promoter activation further suggesting that this effect was mediated through the PI3K signaling pathway [15]. This study also identified positive and negative regulatory regions within the AEG-1 promoter. Two E-box elements found within the positive regulatory region were found to be essential for both basal and Ras-induced promoter activity. Additional putative transcription factor binding sites for Sp1, E-box element,

CREB, and Ets-2 were found within the positive regulatory region, and the negative regulatory region held potential RAR-α and YY1 binding sites whose functional relevance require further investigation.

B. Astrocyte Elevated Gene-1 Induction by Pro-inflammatory Factors

AEG-1 was initially identified as neuropathology-associated gene in primary human fetal astrocytes (PHFA) inducible by both HIV-1 and TNF-α [1]. Subsequent studies have proven that TNF-α not only induces AEG-1 expression but also stimulates nuclear translocation of AEG-1 where its interaction with p65 results in activation [12]. Similarly Khuda et al has shown that the Gram-negative bacterial component lipopolysaccharide (LPS) is also a potent activator of AEG-1 in human promonocytic cells [16]. In that study LPS treatment of U937- human promonocytic cells induced AEG-1 by activation of the NF-κB pathway and conversely, AEG-1 activation was shown to be required for LPS-induced NF-κB activation. Furthermore, LPS treatment also induced TNF-α and prostaglandin E2 (PGE2) production in these cells via NF-κB activation [16]. This data confounds previous reports that a relationship exists between AEG-1 and NF-κB primarily in response to inflammatory cues further suggesting that AEG-1 may play a role in the inflammatory response as a regulatory molecule for the control of TLR4 (LPS)-mediated gene expression. Taken together, these studies suggest a possible positive feedback loop between AEG-1 and NF-κB.

C. Micro RNA Regulation of Astrocyte Elevated Gene-1 Expression

Micro RNAs (MiRNAs) are a class of endogenous small noncoding RNAs derived from distinctive hairpin precursors in plants and animals [17]. These endogenous RNAs pair to sites in mRNAs, typically in their 3' untranslated region (3'UTR) to direct post-transcriptional repression. A single miRNA may target multiple genes, and a single gene may be regulated by multiple miRNAs [18]. At least one-third of all human genes are predicted to be miRNA targets and indeed several miRNAs have been identified which target and modulate AEG-1 expression. MiR-375 is perhaps the most well documented example of this. Initially MiR-375 was identified as a specific regulator of pancreatic islet cell function and was found to regulate insulin secretion [19]. Further studies revealed miR-375 to be a multifunctional miRNA participating in multiple aspects of islet cell development as well as glucose homeostasis. Most recently studies have shown that miR-375 is significantly downregulated in multiple types of cancer [20] . TargetScan-the online software provided by MIT for prediction of miRNA targets has identified AEG-1 as a putative target of miR-375 and indeed studies done to examine the functional relevance of these in silico predictions have corroborated this prediction. In one study, miR-375 was shown to directly aim at its predicted binding site in AEG-1s 3' untranslated region (3'UTR) leading to the suppression of luciferase expression of a pLUC-AEG-1 construct, however no such effect was seen with use of a control construct. Furthermore overexpression of miR-375 in HCC-positive HepG2 cells was shown to greatly reduce AEG-1 mRNA and protein levels while inhibition of miR-375 led to

enhanced AEG-1 mRNA and protein expression in normal primary human hepatocytes further corroborating the luciferace data [21]. In separate study focused on the functional significance of miR-375 in cancer cells and identification of miR-375-regulated novel cancer networks in head and neck squamous cell carcinoma (HNSCC) a genome-wide gene expression analysis miR-375 was performed to search for miR-375-regulated molecular targets. This screen identified AEG-1 as a target of miR-375 in SAS and FaDu-head and neck squamous cell carcinoma HNSCC cell lines. It was shown that the aberrant downregulation of miR-375 in these cancer cells was correlated to the AEG-1 overexpression seen in HNSCC patients [22]. Restoration of miR-375 resulted in a decrease in AEG-1 protein levels as well as significant inhibition of cell proliferation and induction of cell apoptosis in the cell lines used.

In addition to miR-375 other micro RNAs have been shown to directly target AEG-1 expression. Under normal conditions miR-26a protects normal liver tissue from inflammation [23]. Aberrant downregulation of miR-26a has however been linked to increased metastasis in breast cancer patients and decreased survival rates in HCC patients [24] [23]. In a recent study, overexpression of miR-26a was shown to initiate breast tumor cell apoptosis by targeting MTDH [24].

MiR-137 expression has also been inversely correlated with AEG-1 levels. In ovarian cancer patient specimens miR-137 was shown to downregulate AEG-1 expression through interaction at AEG-1s 3'UTR [25]. In this study overexpression of miR-137 was shown to repress AEG-1 expression in ovarian cancer cells lines and also significantly inhibit cell growth and colony formation

activity. Restoring an AEG-1 transcript without the 3'UTR rescued miR-137-induced cell growth and colony formation inhibition suggesting that that AEG-1 may in fact be a functional target of miR-137 [25].

AEG-1 was also identified as a target of miR-136 in glioma cells. In this study miR-136 overexpression in glioma cells was shown to decrease AEG-1 expression, increase the apoptotic rate of glioma cells and sensitized cells to Cisplatin induced death [26].

IV. Relevant Astrocyte Elevated Gene-1 Protein Interactions

A. Nuclear Factor Kappa-Light-Chain-Enhancer of Activated B Cells

Although AEG-1 has no DNA binding domains and has not been shown to directly bind to DNA, it does play a role in modulation of transcription and translation via numerous protein interactions such as with Nuclear Factor Kappa-Light-Chain-Enhancer of Activated B Cells (NF-κB). NF-κB is transcription factor regulating the expression of genes involved in a wide variety of physiological processes ranging from regulation of cell growth and cell survival to cell adhesion, inflammation and differentiation. This very critical factor facilitates cell responsiveness to a large number of extracellular stimuli. NF-κB has also been identified as a critical component of numerous essential systemic functions including inflammatory cascades, innate immune responses, adaptive immune responses, secondary lymphoid organ development and osteoclastogenesis.

In a 2006 study Emdad et al described the nuclear translocation of both AEG-1 and the p65 subunit of the NF-κB protein complex following TNF-α treatment in HeLa cells [12]. This was one of the first studies to show that these two proteins physically interacted, suggesting a potential mechanism by which AEG-1 could activate NF-κB. AEG-1 was shown to translocate to the nucleus of TNF-α treated cells where it activated NF-κB by specific interaction at the region - a.a. 101–205. Furthermore AEG-1s N-terminal (specifically a.a. 1–71) was identified as the site of interaction with NF-κB, which was also shown to be critical for NF-κB activation [11]. It is important to note that the interaction between AEG-1 and NF-κB is not seen under basal cellular conditions in which AEG-1 localized both in the cytoplasm and in the perinuclear region. However, upon upregulation of AEG-1 following TNF-α treatment, AEG-1 was shown to facilitate IκBα degradation resulting in an increase in NF-κB DNA binding activity and NF-κB promoter activity [11]. In addition to this, gene array analysis showed that ectopic expression of AEG-1 by adenovirus (Ad.AEG-1) infection in HeLa cells resulted in marked upregulation of numerous NF-κB-responsive cell adhesion molecules. Induced molecules included CAM-2 and ICAM-3, factors frequently overexpressed in B-cell chronic lymphocytic leukemia [27], selectin E, and selectin P ligand, known to regulate the adherence and metastasis of a cancer cells to endothelium [28] [29] and TLR4 which has been implicated in tumor cell immune evasion [30]. Ad.AEG-1 infection of HeLa cells also resulted in marked upregulation of a number of cytokines including IL-8 [12]. This was later corroborated with evidence showing that AEG-1 is able to facilitate the binding of

NF-κB to the cyclic AMP-response element binding protein (CREB)-binding protein (CBP) complex on the IL-8 promoter in inflammatory responses by interacting with CBP [11]. Recently Khuda and colleagues showed that AEG-1 was induced via the NF-κB pathway in U937 human promonocytic cells following lipopolysaccharide (LPS) stimulation. Conversely, shRNA mediated knockdown of AEG-1 in the human breast cancer cells (MDA-MB-231) was shown to abolish NF-κB activation by LPS and effectively blocked LPS-induced IL-8 and MMP9 production [16, 31]. It is clear that the interaction between AEG-1 and NF-κB is an important component of inflammatory cascades however it may also be surmised that innate immune responses, adaptive immune responses, secondary lymphoid organ development and osteoclastogenesis, other processes regulated by NF-κB may also be impacted by AEG-1 expression and activity.

B. Sumoylated Promyelocytic Leukemia Zinc Finger Protein and C-Myc

The interaction between AEG-1 and the sumoylated promyelocytic leukemia zinc finger protein (PLZF) was initially identified by yeast two-hybridization (Y2H) screening methods. PLZF was shown to interact with the AEG-1 protein at two regions (a.a. 1–285 and 487–582) and a.a. 322–404 was shown to be the site important site for this interaction on the PLZF protein [31]. The PLZF protein is a transcriptional repressor that binds to the promoter of various genes including cyclin A2, interleukin-3 receptor (IL-3Rα) and the proto-oncogene c-myc. PLZF also contributes to the regulation of cell growth, death,

and differentiation by functioning as both a proapoptotic and an antiapoptotic factor [32] [33]. Co-expression of AEG-1 with PLZF results in a substantial increase in c-Myc transcript level. Chromatin immunoprecipitation (ChIP) techniques revealed that AEG-1 suppresses the binding of the PLZF to the c-Myc promoter, thus causing increased transcription of c-Myc. MYC expression is frequently deregulated in tumor cells by chromosomal translocation or gene amplification. This deregulation of c-myc is thought to induce a metabolic adaptation wherein tumor cells alter their metabolism in order to support accelerated growth and survival. As an oncoprotein MYC promotes tumorigenesis by inappropriate regulation of transcriptional programs resulting in uncontrolled cell proliferation, independence of growth factors and genomic instability [34]. The interaction of AEG-1 with PLZF prevents the recruitment of PLZF to the c-Myc promoter, ultimately leading to upregulation of c-Myc transcription. This represents another way in which AEG-1 functions as a regulator of transcription through protein-protein interaction and also takes part in the promotion of tumorigenesis.

C. Staphylococcal Nuclease Tudor Domain Containing 1 and the RNA-Induced Silencing Complex

Staphylococcal nuclease tudor domain containing 1 (SND1) was first identified as a transcriptional co-activator for Epstein–Barr virus nuclear antigen 2 and has since been found to be a multifunctional protein with reported roles in transcriptional activation, RNA editing, the apoptotic cascade, regulation of spliceosome activity and formation of the RNA-induced silencing complex [35] [36] [37] [38] [39] [40]. The interaction between AEG-1 and SND1 was first identified by means of an unbiased, mass spectrometry based screen for MTDH-interacting partners [41]. In a recent study AEG-1 was identified as a component of the RNA-induced silencing complex (RISC) [40]. This interaction was determined based on AEG-1s interaction with both Argonaute 2 (Ago2), the major nuclease of the RISC and SND1 also known to function as a nuclease in the RISC [39]. Coimmunoprecipitation analysis using lysates from HCC cell lines demonstrated an interaction between AEG-1 and both SND1 and Ago2. This data was supported by double immunofluorescence studies demonstrating the ability of AEG-1 to co localize with both Ago2 and SND1. In this study AEG-1was shown to interact with SND1 in the cytoplasm to facilitate RISC activity. Furthermore it was demonstrated that both AEG-1 and SND1 are required for optimum RISC activity facilitating small interfering RNA (siRNA) and micro RNA (miRNA)-mediated silencing of luciferase reporter genes. AEG-1 overexpression and binding to SND1 was also shown to aid oncomiR-mediated degradation of tumor-suppressor messenger RNAs. Potential targets of this increased RISC

degradation included tumor suppressor mRNAs such as PTEN, CDKN1C, CDKN1A, p21 and TGFBR2. Indeed expression of all of these targets was shown to be downregulated in response to overexpression of AEG-1 or SND1 and upregulated, upon knockdown of AEG-1 or SND1 [39]. The described study spoke specifically to the impact of the of AEG-1-SND1 interaction on the expression tumor suppressor genes however, SND1 has been identified as an essential component of many aspects of gene expression. For example SND1 has also been shown to associate with the U5 small nuclear ribonucleoprotein component of the spliceosome and enhance spliceosome assembly and activity [42] [43]. In contrast, the role of SND1 as a coactivator and transcriptional activator have also been well studied. Numerous studies also show that AEG-1 expression correlated directly to SND1 expression [39] [41] [44]. This suggests that the two may in fact interact to modulate the expression of a wide range of genes ultimately molding genetic diversity in eukaryotes not only through modulation of RISC activity but perhaps also by manipulation of transcription and/or spliceosome machinery assembly.

D. Retinoid X Receptor

One of the more intriguing structural features of the AEG-1 protein is the "LXXLL" (L, leucine; X, any amino acid) motif located at a.a. 21-25 of its NH2-terminal region (Fig 1.2). The LXXLL sequence was originally identified in proteins that bind the activation function-2 (AF-2) region of nuclear receptor

ligand-binding domains (LBDs) [45]. These conserved motifs were shown to have a key role in nuclear-receptor regulation with many nuclear-receptor-binding proteins and co-repressors capable of interacting with and modulating the activity of liganded nuclear receptors (NR) [46]. While the presence of the LXXLL sequence is not exclusive to molecules involved in regulation of NR activity it is a protein-recognition motif widely used in transcriptional regulation. No previous reports have defined the functional relevance this very important regulatory sequence in AEG-1. Our group has recently put forth efforts to investigate the biological relevance of this motif to AEG-1 function. To this end yeast 2 hybridization (Y2H) screening of a human liver cDNA library was performed using the NH2-terminal (a.a.1-57) of AEG-1 as bait. Interestingly this screen provided evidence of an interaction of between AEG-1 and the Retinoid X Receptor β (RXRβ). RXR is an essential member of the steroid/thyroid hormone super family of nuclear receptors and is a master regulator of a plethora of physiological processes functioning as a transcription factor with roles in development, cell differentiation, metabolism, and cell death. The association between RXRβ/RXRα and AEG-1 was confirmed by co-immunoprecipitation (Co-IP) assays performed using human HCC cell lines. Mutation of AEG-1s LXXLL motif nullified this RXR-AEG-1 association solidifying the importance of the LXXL motif to this interaction. Conversely, deletion of the C-terminal ligand-binding/AF-2 domain (LBD) of RXRα, but not the N-terminal AF-1/DNA binding domain (DBD) also abolished the RXR-AEG-1 interaction suggesting that the LBD is the site of AEG-1 interaction. This data provided evidence in support of the hypothesis that

AEG-1s LXXLL motif is a functional domain and a site of interaction with RXR. RXR plays a major role in regulating genes controlling cell proliferation and differentiation in the context of its heterodimeric binding with the RAR. Interestingly inhibition of basal and ligand-dependent RARE activity was also observed in both AEG-1 overexpressing cancer cells and primary AEG-1 transgenic (Alb/AEG-1) hepatocytes while RARE activity was amplified in AEG-1KO mouse hepatocytes and in cancer cells following siRNA directed AEG-1 knockdown suggesting that AEG-1 expression impacts RXR-binding partner activity. Even more compellingly that study showed that AEG-1 activation of ERK induced RXR phosphorylation leading to its functional inactivation and attenuation of ligand-dependent transactivation [47]. Taken together, these findings show for the first time that that AEG-1 interacts with RXRs AF-2 ligand-binding domain via its own LXXLL motif. This interaction modulates nuclear receptor/co-activator binding activity and subsequently impacts RXR activation. In the absence of ligand, RXR is bound to hormone response elements complexes with corepressor proteins. The binding of agonistic ligands to RXR results in dissociation of corepressors and recruitment of coactivator proteins possessing distinct LXXLL motifs. The negative regulation of RXR by AEG-1 suggests a potential mechanism by which AEG-1 may impact the maintenance of RXR homeostasis. By competing for coactivator binding, AEG-1 may impact RXR activation and the transcription of RXR target genes. The existence of putative transcription factor binding sites for RAR-α within AEG-1s negative regulatory region has previously documented, [15] combined with the data from

this most recent study there is reason to suspect that AEG-1 may be part of a feedback mechanism regulating RXR and RAR binding. This being said, it may be of interest to further explore the role of AEG-1 in the maintenance of RXR homeostasis.

E. Additional Interactions and Regulatory Mechanisms

The AEG-1 molecule possesses a number of interesting domains that may explain some of its proposed functions. Evidence that AEG-1 aids in the homing of metastatic breast cancer cells to the lung vasculature is supported by the presence of a putative lung-homing domain (LHD) (amino acid region 378–440) [2, 48]. The molecule also contains a C-terminal '435-GALPTGKS-442' sequence predicted to as a potential ATP/GTP binding (Sutherland et al., 2004). There are also a number of interesting putative post-translational modification residues and regulatory residues within the AEG-1 protein including potential sites of phosphorylation, ubiquitination and acetylation [49]. The relevance of most of these sites have yet to be explored but evidence exists that suggests that at least some of these modifications impact protein function and localization. AEG-1 protein is detected as a 75-kDa band by Western blot analysis although its predicted molecular weight is 64 kDa. This gap has been attributed to monoubiquitination of lysines within AEG-1s NLS-2 region. Additionally, cell fractionation showed that ubiquitinylated LYRIC/AEG-1 is almost exclusively cytoplasmic indicating that this type of modification is also responsible for cellular

localization of the protein [31]. Furthermore, reduction of AEG-1 ubiquitination has recently been shown to both alter its sub-cellular distribution and impair the interaction between AEG-1and p65/NFκB [50]. The biological significance of these modifications have not yet been determined but certainly warrants additional research efforts.

Chapter Two-Astrocyte Elevated Gene-1 Regulates Lipid Metabolism

I. Introduction

The role of Astrocyte Elevated Gene-1 as an oncogene is well-established [9, 51-53]. AEG-1 plays a crucial role in regulating tumor cell proliferation, invasion and metastasis [2, 9, 51, 54], and positively contributes to tumor-associated angiogenesis, chemoresistance and protection from apoptosis [52, 55-57]. However, the physiological function of AEG-1 is still not known. The AEG-1 gene is present only in vertebrates, in which the protein is highly conserved, suggesting that AEG-1 evolved to perform specific functions in higher organisms [5]. Analysis of AEG-1 expression during mouse development demonstrated AEG-1 expression in mid-to-hindbrain, fronto-nasal processes, limbs and pharyngeal arches in the early development period from E8.5 to E9.5 [14]. At stages of E12.5 to E18.5 AEG-1 expression was detected in the brain, the olfactory and skeletal systems, skin and liver. Co-localization of AEG-1 expression was observed with the proliferation marker Ki-67 and it was hypothesized that AEG-1 might play a role in normal mouse development in the context of cell proliferation and differentiation [14].

We recently identified a novel interaction between AEG-1 and Retinoid X Receptor (RXR), a transcription factor functioning as an obligate heterodimer partner of diverse nuclear receptors mediating the action of hormones, vitamins and lipids [54, 58, 59]. AEG-1 interacts with RXR via a 'LXXLL' motif [45] and this interaction was found to interfere with co-activator recruitment and inhibit RXR-

mediated transcriptional regulation by its heterodimer partners. The current study

unravels a novel physiological function of AEG-1 in lipid homeostasis by

analyzing an AEG-1 knockout (AEG-1KO) mouse. Although AEG-1KO mice

were viable and fertile, they were significantly leaner, had prominently less body

fat and lived significantly longer when compared to wild type (WT) mice. When

maintained on a high fat and cholesterol diet (HFD), WT mice rapidly gained

weight while AEG-1KO mice did not gain weight at all. This phenotype of AEG-

1KO mice was due to decreased fat absorption from the intestines because of

increased activity of Liver X Receptor (LXR) and Peroxisome Proliferator

Activated Receptor (PPAR)-α in enterocytes. LXR and PPARα are both

heterodimer binding partners of RXR, in the intestines. LXR is a nuclear receptor

which functions as a cholesterol sensor and regulator of transcription of a set of

genes associated with cholesterol absorption, transport, efflux and excretion.

Thus LXR is critical for the control of lipid homeostasis and response to

physiological concentrations of sterols [60] [61]. There are two LXR isoforms,

LXRα and LXRβ, both of which form obligate heterodimers with RXR. In

enterocytes, activation of LXR inhibits cholesterol absorption by downregulating

cholesterol transporter Npc1l1 and upregulating cholesterol efflux proteins,

Abca1, Abcg5 and Abcg8 [62]. PPARα, a subtype of the PPAR superfamily, also

interacts with the retinoid X receptor to function as a transcription factor to induce

the expression of a series of genes involved in fatty acid transport and

mitochondrial fatty acid oxidation [63]. Activation of PPARα in the enterocytes

promotes β-oxidation of absorbed fatty acids thereby downregulating fatty acid

absorption into the circulation [64]. Products of cholesterol metabolism, such as the oxysterols 24(S)-hydroxycholesterol, 22(R)-hydroxycholesterol, 24(S), 25-epoxycholesterol and 27-hydroxycholesterol, function as ligands for LXR while fatty acids and fatty acid derivatives are endogenous ligands for PPARα [60, 65]. A high fat diet provides ligands to both LXR and PPARα thereby accentuating this effect and providing a potential mechanism to explain the almost complete inhibition of fat absorption by AEG-1KO mice placed on a HFD. The studies described in this chapter reveal a novel role of AEG-1 in regulating nuclear receptors regulating lipid metabolism. By regulating LXR and PPAR-α function AEG-1 might be a key component of lipid homeostasis. The observed resistance of AEG-1KO mice to HFD suggests that AEG-1 may also significantly modulate the effects of high fat diet, and thereby function as a unique determinant of obesity perhaps also playing a role in obesity-associated diseases.

II. Materials and Methods
Generation of AEG-1 Knockout (AEG-1KO) mice:

To generate AEG-1KO mice, an AEG-1KO targeting vector was constructed. Contiguous AEG-1 genomic regions were generated by high-fidelity PCR from 129/SvEv embryonic stem (ES) cell DNA and sequentially cloned into the NDTV targeting vector, which contains both a floxed neomycin phosphotransferase (*neo*) cassette for positive selection of homologous recombinants with the neomycin analog G418, and a diphtheria toxin A (DT-A) cassette for negative selection of non-homologous recombinants. The final AEG-1KO targeting vector possesses a 5' homology arm containing both the AEG-1promoter and exon 1, and a 3' homology arm containing part of intron 1. The 5' arm also has a *loxP* site inserted just 5' of a 257-bp region of homology (71%) between the human and mouse promoters.

The AEG-1KO targeting vector was linearized with *Nhe* I and electroporated into 129/SvEv ES cells. ES cell clones resistant to G418 were screened for homologous recombination by Southern blot analysis using both 3'-flanking genomic and *neo* cassette probes. Retention of the introduced *loxP* site in homologous recombinants was verified by PCR using a 5'-flanking primer in combination with a unique *loxP* primer. Two ES cell clones possessing the targeted AEG-1KO allele were injected into C57BL/6 blastocysts, which were then implanted into pseudopregnant CD-1 recipients. To generate the final conventional AEG-1KO alleles, chimeric males were bred to homozygous EIIa-*cre* females (Jackson Laboratory, stock number 003724). Agouti offspring were

screened for the conventional KO allele with a 3-primer PCR protocol using a common anti-sense primer (5'-CTTGAGATAGACATCTCTCTCTAC-3') in combination with two sense primers: (5'-GAAGAATCTCAGAAGCGAGGAGC-3') and (5'-GCTTAGCAAGAGTAGCTTATTACG-3'), specific for the wild-type and conventional KO alleles and generating PCR products of 397 bp and 577 bp, respectively.

All animal studies were approved by the Institutional Animal Care and Use Committee at Virginia Commonwealth University, and were conducted in accordance with the Animal Welfare Act, the PHS Policy on Humane Care and Use of Laboratory Animals, and the U.S. Government Principles for the Utilization and Care of Vertebrate Animals Used in Testing, Research, and Training.

AEG-1KO mice were viable and fertile, although litter sizes were very small (1-2 pups per litter). Further, even litters generated by crossing AEG-1+/- breeding pairs were very small (2-3 pups per litter), which precluded generating large numbers of WT and AEG-1KO mice as littermates. Therefore, the majority of the experiments were carried out with age-matched mice generated by breeding WT and AEG-1KO mice separately. However, it should be noted that the same phenotypes (as described in the next sections) were observed in AEG-1KO mice generated from AEG-1+/- X AEG-1+/- matings as from AEG-1KO X AEG-1KO matings. Additionally, the experiments described here were performed with mice on a C57BL/6:129/Sv background. However, we have backcrossed the line to C57BL/6 for 10 generations and obtained similar results for both the WT

and AEG-1KO mice on the C57BL/6 background as on the C57BL/6:129/Sv background. Thus our findings are not restricted to strains or littermates status.

Measurement of food consumption and body weight:

Measured amount of food was given to 4-weeks old age-matched WT and AEG-1KO mice (n=8/group) housed in individual cages. Amount of food consumed per week was determined by measuring the leftover food. Body weight was also measured weekly. The experiment was performed for 12 weeks. Food consumption was calculated by the amount of food (in gm) consumed per gm of body weight.

Mice were fed a regular chow diet. For high fat diet (HFD) experiments, 8 weeks old mice were fed high fat and cholesterol containing diet (Harlan; TD. 88137) for 5 weeks.

MRI of total body fat mapping:

Male WT and AEG-1KO mice at 12 weeks of age were used (n=6/group). Using a Bruker-Biospin Biospec console and a 7 Tesla, 30 cm free bore magnet (Bruker Biospin, USA), T2 weighted multi-slice spin echo images with and without fat suppression were acquired, covering the entire body from the base of skull to the tail, with a field of view of 4 x 4 cm and 256 x 256 matrix size. Animals were anesthetized with isoflurane during preparation (4%) and imaging (1%). The imaging parameters used were: repetition time (TR) of 6.5 s, time of echo (TE) of 56 ms. The resultant 2D images were exported and analyzed using ImageJ software (NIH, Maryland, USA). By subtracting the fat-suppressed images from

the non-fat suppressed images fat-only images were produced, which were then used for ROI analysis of the fat depots. Multiplying the area of the ROI by slice thickness gave the volume.

Indirect Calorimetry:

Male WT and AEG-1KO mice at 12 weeks of age were used (n=6/group). VCO_2, VO_2, and respiratory quotient (RQ) were measured using a four chamber Columbus Instruments Comprehensive Lab Animal Monitoring System CLAMS/Oxymax (Columbus, OH) indirect calorimetry (IDC) machine, which was calibrated based on the O_2 and CO_2 levels of the room dedicated for indirect calorimetry only. The mice were acclimated to the IDC room for 1 week prior to the experiment. The oxygen consumption is calculated by taking the difference between the input oxygen flow and the output oxygen flow. Similarly, the carbon dioxide production is calculated by taking the difference between the output and input carbon dioxide flows. The calculations are described below:

VO2 = Vi O2i -Vo O2o

Vi and Vo are the input and output ventilation rates (LPM)

O2i and O2o are oxygen fractions at the input and output

VCO2 = VoCO2o -ViCO2i

Vi and Vo are the input and output ventilation rates (LPM)

CO2i and CO2o are carbon dioxide fractions at the input and output

The respiratory exchange ratio (RER) is simply the ratio between the carbon dioxide production and the oxygen consumption thus the equation is: RER = $VCO_2/VO2$. Energy expenditure or Heat is calculated before the application of any normalization or correction and, thus, reflect the exact heat of the subject. The calorific value (CV) is based on the observed respiratory exchange ratio. CV is then used with the observed oxygen consumption (VO_2) to calculate heat, the equations are:

Heat = CV × VO2

CV = 3.815 +1.232 × RER

Measurement of triglyceride concentrations and synthesis by stable isotopes

The Case Mouse Phenotyping Center (MMPC) measured the triglyceride content and newly synthesized triglyceride levels. In order to enrich the body water with ~2% ^2H, IP injection of labeled water (20 µL • g-1 of body weight of 9 g/L NaCl in 99% atomic percentage excess $2H_2O$) was administered to adult male mice, and they were returned to their cages and maintained on 5% ^2H-labeled drinking water for 5 d. The mice were sacrificed, and blood and tissue samples were collected and flash-frozen in liquid nitrogen. The samples were stored at -80°C until analysis. Triglyceride concentrations and de novo lipogenesis was determined as previously described [66]. Briefly, triglyceride from tissues was isolated, and labeled glycerol and palmitate were analyzed after derivatization by mass spectrometry. The ^2H-labeled triglyceride covalently linked

to glycerol measures the amount of newly synthesized triglyceride, while the ^{2}H-labeled triglyceride covalently attached to palmitate indicates the amount of new palmitate. In mice given 2H$_2$O for 5 d, the contribution of de novo lipogenesis to the pool of triglyceride and palmitate was calculated using the following equation:

% newly made palmitate = [total ^{2}H-labeled palmitate • (^{2}H-labeled body water × n)]-1 × 100, where n is the number of exchangeable hydrogens, which is assumed to be 22 [67, 68].

The percentage of total newly made triglyceride glycerol is calculated using the following equation:

% total newly made triglyceride-glycerol = [^{2}H-labeled triglyceride-glycerol • (^{2}H-labeled water × n)]-1 × 100, where ^{2}H-labeled triglyceride-glycerol is the M1 isotopomer, ^{2}H-labeled water is the average amount labeled in a given mouse, and n is the exchange factor (experimentally determined from the M2/M1 ratio of triglyceride glycerol). We calculated the total triglyceride pool size (µmol/g tissue) in the tissues using the following equation: total pool size of triglyceride = [^{2}H-labeled triglyceride-glycerol • (^{2}H-labeled water × n)]-1 × 100.

In vivo cholesterol absorption:

Fecal dual isotope ratio method [69] was used in which WT and AEG-1KO mice were gavaged with 0.5 µCi of [^{14}C]-cholesterol and 1 µCi of [^{3}H]-sitostanol in 100 µl of soy bean oil. Mice were fed standard chow diet for three days and the feces were collected daily. The radioactivity of the pooled fecal samples was

determined by a scintillation counter. The percentage of cholesterol absorption was calculated as:

$(([^{14}C]/[^{3}H])$ dosing mixture - $([^{14}C]/[^{3}H])$ feces) / $([^{14}C]/[^{3}H])$ dosing mixture X 100.

In vivo fatty acid absorption:

WT and AEG-1KO mice were fasted overnight and i.v. injected with 500 mg/kg Tyloxapol to block serum lipase activity. After 30 min, mice were gavaged with fat emulsion containing 10 µCi $[^{3}H]$triolein. Blood samples were collected from tail vein at time 0 and hourly for 4 h. Serum radioactivity was determined by a scintillation counter [70].

Metabolomic profiling of plasma samples:

Plasma samples were extracted using ice cold chloroform/methanol (2:1) as described [71]. LC-MS analyses were conducted on a Thermo Fisher Q Exactive mass spectrometer with on-line separation using a Thermo Fisher/Dionex RSLC nano HPLC. HPLC column is Waters Atlantis dC18 (3 µm, 300 µm x 150 mm) with mobile phase A, acetonitrile/water (40:60) containing 10 mM ammonium acetate and mobile phase B, acetonitrile/isopropanol (10:90) containing 10 mM ammonium acetate. Data-dependent MS/MS scans were performed using one full MS scan (m/z 200 – 2000) followed by 6 MS/MS scans in the HCD collision cell with a normalized collision energy (NCE) of 35 arbitrary units. Both positive and negative ion detection were performed through Q Exactive MS at 70,000 resolution (m/z 300). Raw data were acquired under the control of Thermo Xcalibur software (Thermo Fisher). Progenesis CoMet

34

(Nonlinear Dynamics) was used to process the raw data files acquired from the Q Exactive MS analyses to detect the metabolites that exhibit significant differences ($p<0.05$ in ANOVA analysis) in the intensity among the different groups of plasma samples. Peak alignment and integration was performed and the relative abundance was generated for each metabolite among different sample types. The metabolites were identified with accurate mass through METLIN and Lipid Maps databases searching using a 5-ppm mass tolerance and manual interpretation of the MS/MS fragment patterns. The comparison with the retention times with commercially available standards was also performed for further confirmation. The heat map was drawn for significantly different lipids ($p<0.05$ and fold change>2) between WT and KO samples. To assist in visualization and interpretation of the data, we performed a z-score transformation of the abundances for each lipid.

Immunohistochemistry

Immunohistochemistry was performed using formalin-flixed paraffin embedded (FFPE) sections as described previously [51]. The sections were blocked in PBST using 10% normal goat serum. Primary anti-AEG-1 antibody (rabbit polyclonal; 1:800; generated in-house) was diluted in PBST containing 5% normal goat serum. Secondary antibody was diluted in PBST containing 2.5% normal goat serum. The signals were developed by avidin-biotin-peroxidase complexes with a DAB substrate solution (Vector laboratories).

[¹⁸F]-FDG uptake assay

Animals were fasted overnight and anesthetized (2% isoflurane in Oxygen) under warm conditions for about 10 minutes before the intravenous injection of 2-deoxy-2-[^{18}F]Fluoro-D-Glucose (FDG), which was obtained from IBA Molecular Inc., (Sterling, VA). Approximately 300 µCi of FDG (11.5±0.6 MBq) was injected via tail vein and animals were maintained under anesthesia in a warm chamber to maintain normal body temperature. After 60 minutes of FDG uptake animals were positioned in the Inveon Preclinical System (Siemens Healthcare, PA) and PET data was acquired for 20 minutes with no attenuation correction. A CT scan was also acquired for anatomical reference. The PET images were processed using manufacturer recommended calibration procedures using a phantom of known volume and activity acquired prior to the study. OSEM3D-MAP reconstructions were done using Inveon Acquisition Workplace 1.5 (Siemens Healthcare, PA) and were used for region-of-interest (ROI) analysis in the Inveon Research Workplace 4.1 (Siemens Healthcare, PA). The percent injected dose/gram of tissue (%ID/g) values were calculated after appropriate decay corrections using the formula $\%ID/g = C_t/ID \times 100$, where C_t was the concentration of radiotracer in the tissue (MBq/cc), which was obtained from the PET images after ROI analysis. Statistical comparisons were made using Student's *t*-test; $p < 0.05$ was considered significant.

Primary hepatocyte culture and transfection assays:

Primary mouse hepatocytes were isolated as described [54] and were plated on collagen-coated dishes (BD BioCoat collagen type I, BD Biosciences) and cultured in Williams E medium (SIGMA) containing $NaHCO_3$, L-glutamine, insulin (1.5 µM) and dexamethasone (0.1 µM). For transfections, $1X10^5$ hepatocytes were plated in 24-well collagen coated plates and the next day transfected using Promofectin-Hepatocyte transfection reagent in 9:1 ratio of firefly luciferase reporter plasmid containing responsive elements (pGL3.luc, pGL3.*LXRE*.luc, pGL3.*PPRE*.luc) and renilla luciferase reporter plasmid (pGL3.renilla.luc) [54]. After 48 hours, cells were incubated in presence or absence of respective ligands (T0901317; 5 µM and CP775146; 2.5 µM) for another 24 hours. Luciferase assays were measured using Dual Luciferase Reporter Assay kit (Promega) following manufacturer's protocol and firefly luciferase activity was normalized by renilla luciferase activity. Each experiment was performed in triplicates and three times to calculate means and standard deviations.

Total RNA extraction, cDNA preparation and Real time PCR:

Total RNA was extracted from hepatocytes or mouse tissues using the QIAGEN miRNAeasy Mini Kit (QIAGEN, Hilden, Germany). cDNA preparation was done using ABI cDNA synthesis kit (Applied Biosystems, Foster City, CA). Real-time polymerase chain reaction (RT-PCR) was performed using an ABI ViiA7 fast real-time PCR system and Taqman gene expression assays according to the manufacturer's protocol (Applied Biosystems, Foster City, CA).

Glucose tolerance test (GTT):

Mice were fasted overnight (16 h) and glucose was injected intraperitoneally (1.5 g/kg). Blood samples were collected from tail-tip before and at 10, 30, 60, 90 and 120 min after the injection for the measurement of glucose with a glucometer.

Chromatin Immunoprecipitation:

12 week old wild-type and AEG-1KO littermates (n=3) were treated with the LXR agonist T0901317 (30 μg/gm) by a single oral gavage. 24 hours following treatment, the animals were euthanized and livers were immediately removed. The Chromatin immunoprecipitation (ChIP) assay was performed using a SimpleChIP Plus kit (Cell Signaling Technology, Danvers, MA) according to the manufacturer's instruction. Briefly, livers were minced on ice and cross-linking was performed by treatment with a 1.5% formaldehyde solution for 20 min at room temperature. A solution of 0.125M glycine was added at the end of the reaction followed by one wash with cold PBS. Tissue disaggregation was

performed using a dounce homogenizer to obtain cells in single cell suspension and nuclei were digested with Micrococcal Nuclease. 10 μg of cross-linked chromatins were incubated with antibody and allowed to complex overnight at 4 °C, followed by 2 hour incubation with protein G magnetic beads. The protein G magnetic beads immuno-complex was washed four times. DNA/protein complexes were eluted from beads and reverse cross-linked at 65 °C. DNA was purified and quantitative PCR was performed using Power SYBR Green PCR Mastermix (Applied Biosystems Foster City, CA) on the ABI ViiA7 fast real-time PCR system according to the manufacturer's protocol (Applied Biosystems, Foster City, CA). PCR efficiencies of primers were examined by standard curve of serial-diluted liver extracts input and melting curve functionality. The results were analyzed using the software provided with the ABI ViiA7 fast real-time PCR system. PCR efficiencies of primers were examined by standard curve of serial-diluted liver extracts input and melting curve functionality. The primers used were Abca1 forward: 5'-GAACGAGCTTTTCCCCTTTC-3' and Abca1 reverse: 5'-CCCGGCCTCTGTTTATGTAG-3'.

Measurement of fatty acid β-oxidation

Products of fatty acid β-oxidation were measured in fresh liver and small intestine homogenates using ^{14}C-palmitate as previously described [72].

III. Results

A. AEG-1KO Mice are Lean and Have a Longer Life Span

We generated an AEG-1KO mouse in which the promoter region, exon 1 and part of intron 1 of the AEG-1 gene was deleted using a Cre-loxP system (Fig. 2.1). The authenticity of AEG-1 knockout was confirmed by Southern blotting, genomic PCR, Taqman Q-RT-PCR, Western blot analyses and immunohistochemistry (Fig. 2.2 A-D).
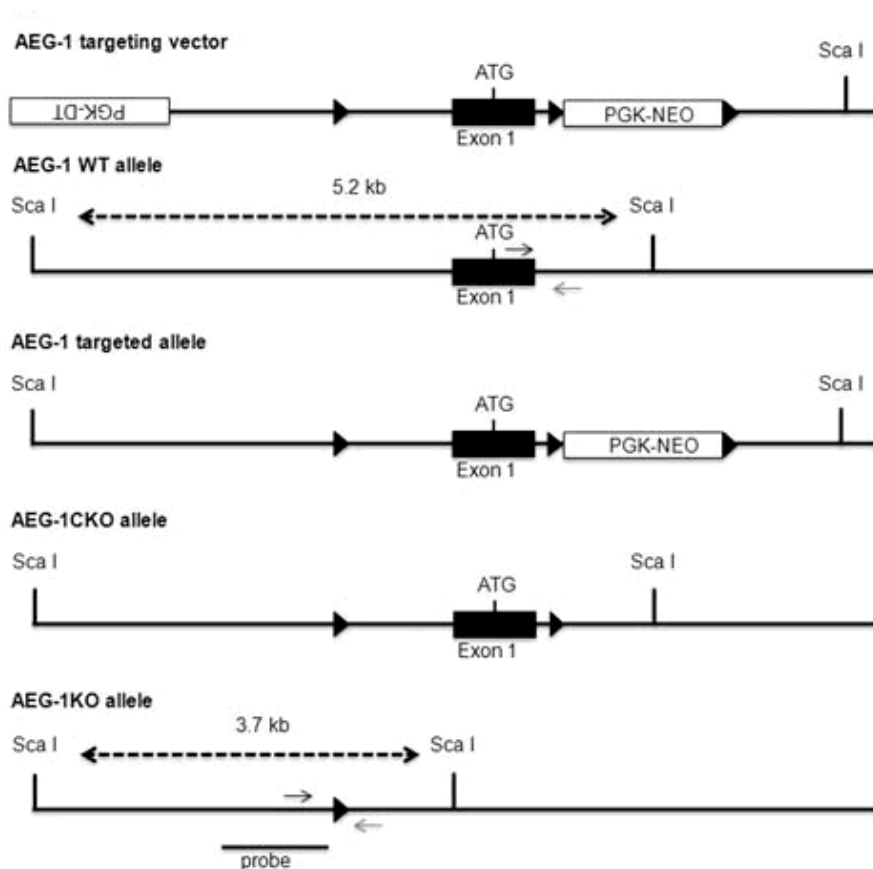

Figure 2. 1 Generation of the AEG-1 Knockout Mouse. A. Targeting strategy. Arrowheads indicate loxP sites.
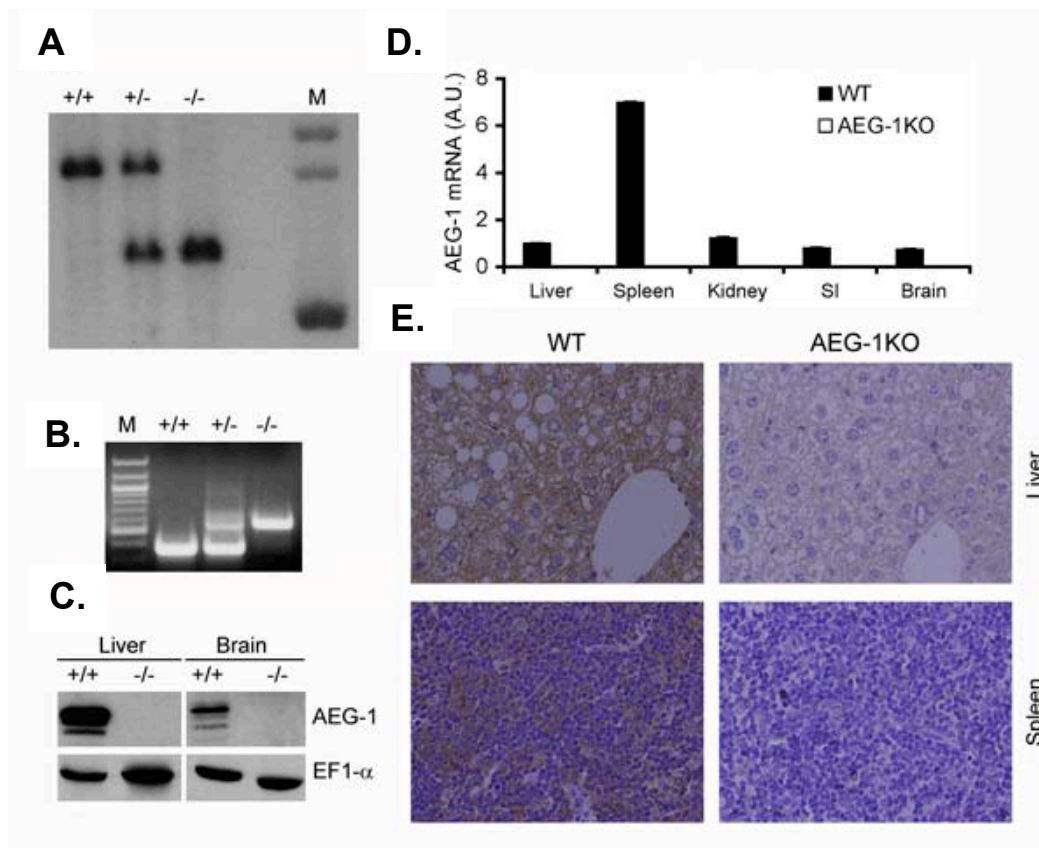
Figure 2.2 Confirmation of knockout of AEG-1 in organs. A. Southern blotting analysis to confirm genotype using the probe shown in Fig2.1. B. PCR using genomic DNA. For A-B, M represents molecular weight marker. C. Western blot analysis for AEG-1 in the indicated organs. D. AEG-1 mRNA expression in different organs by Taqman Q-RT-PCR. A.U.: arbitrary unit. F. Immunohistochemistry for AEG-1 in the indicated organs.

AEG-1KO mice were viable and fertile. At birth no significant difference in appearance and body weight were observed between AEG-1KO and WT mice. Both WT and KO mice developed normally to full adulthood, indicating that AEG-1 is likely not involved in developmental regulation. Histological analysis of the internal organs of the adult mice also did not reveal any significant and noticeable difference between WT and AEG-1KO mice (Fig. 2.3).
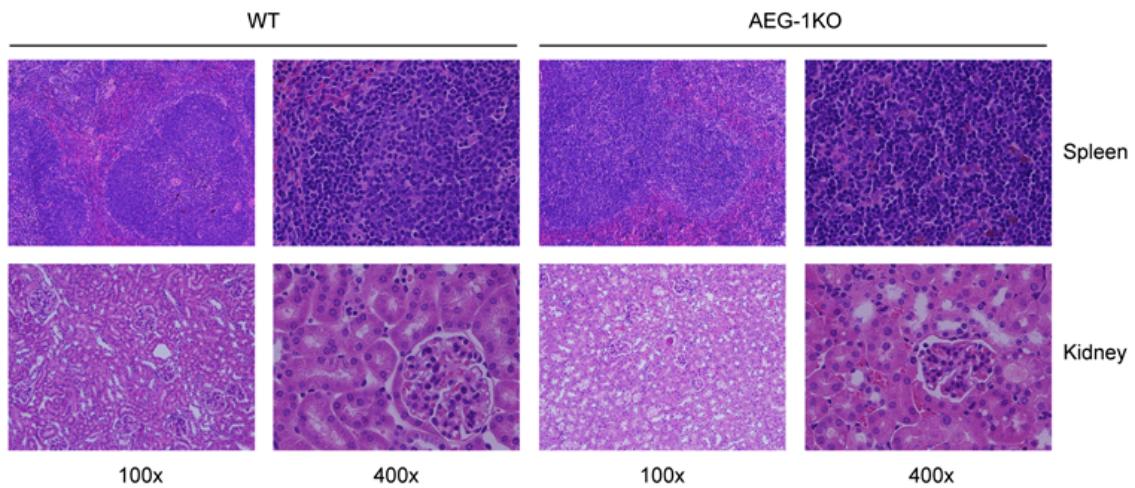

Figure 2.3. AEG-1KO mice do not show histological abnormalities. H&E staining of spleen and kidney of adult WT and AEG-1KO mice.

A marked difference in body weight gain was however observed between age-matched WT and AEG-1KO mice. At 4 weeks of age, male AEG-1KO mice were slightly smaller than their age-matched WT counterparts. However this difference was not statistically significant. Weekly monitoring over the next 12 weeks revealed that the average body weight gain by each WT mouse over that period was ~14 gm, wherein the weight gain of AEG-1KO mice was only ~4 gm (Fig. 2.4A). During this period, food consumption (gm of food/gm of body weight) was similar in both groups (Fig. 2.4B). The substantial difference in body weight gain continued with age (Fig. 2.5 A-B) and was more pronounced in male mice than in female mice (Fig. 2.5 A-B).
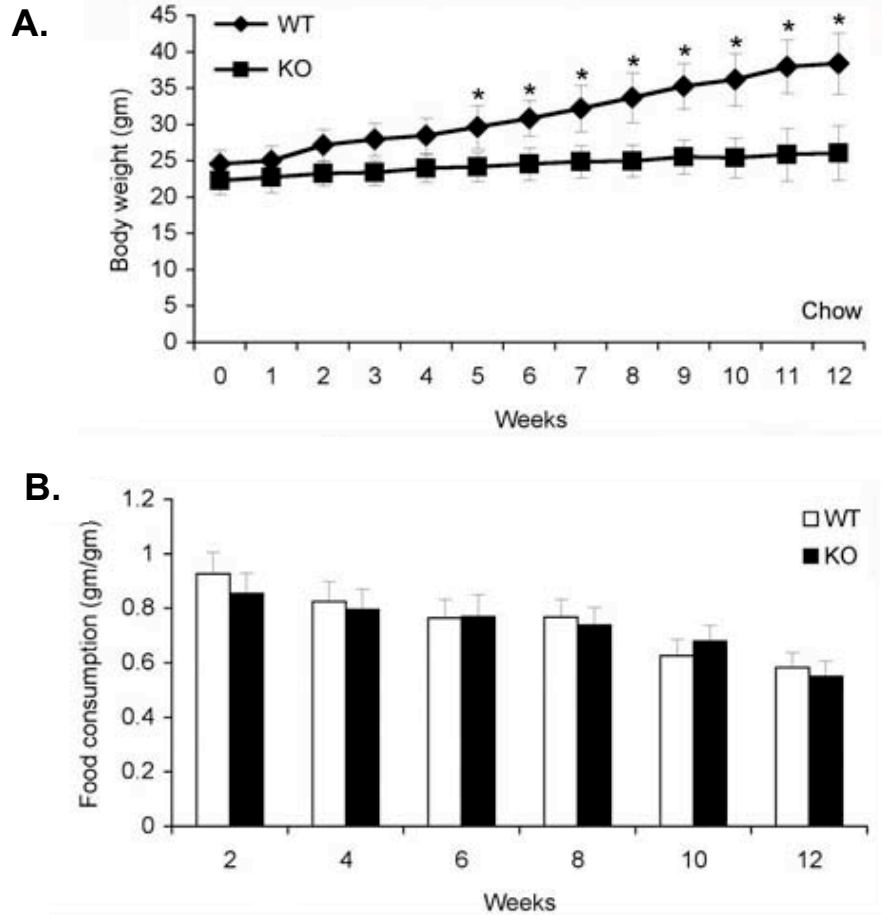
Figure 2.4 Characterization of AEG-1KO mouse. A. Weekly body weight gain. (n = 8/group). B. Bi-weekly food consumption. (n = 8/group). Data represents mean ± SEM. *: p<0.05.
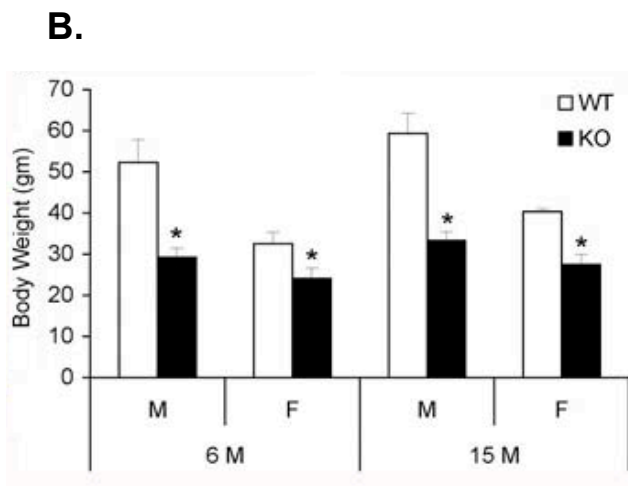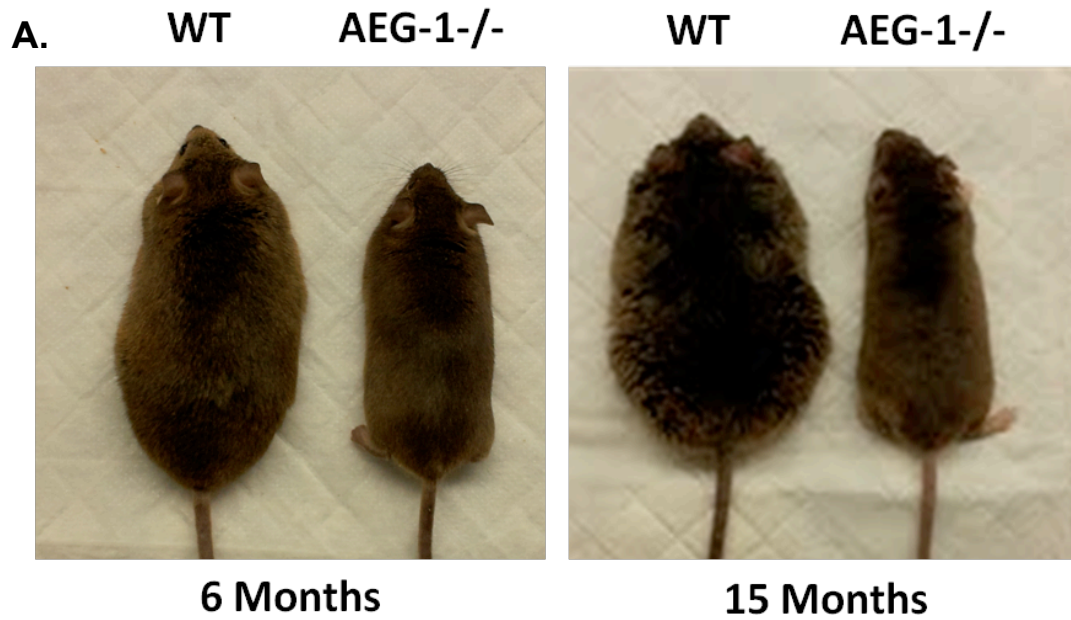
Figure 2.5 Characterization of AEG-1KO mouse. A. Representative photographs of male WT and AEG-1-/- mice at 6 and 15 months of age. B. Average body weight of male (M) and female (F) mice at 6 and 15 months of age. (N = 12/group). For graphs, data represents mean ± SEM. *: p<0.05.

MRI analysis demonstrated a significant decrease in subcutaneous, intramuscular and visceral fat deposits in 6-month-old AEG-1KO mice as compared to WT mice (Fig. 2.6A-B). Both subcutaneous and visceral adipose tissue have potential protective and pathogenic effects however excess accumulation of either may share similar adipose tissue pathologic processes leading to pericardiac and perivascular fat accumulation, as well as fatty infiltration of the liver, muscle, pancreas and heart. Indeed our studies show that aged (15 months old) WT mice demonstrated steatotic changes in the liver, while no such change was observed in AEG-1KO mice (Fig. 2.8B.). Furthermore histological evaluation showed that adipocytes in white and brown adipose tissues were larger and more abundant in WT mice versus AEG-1KO mice (Fig. 2.8A). Glucose tolerance was first evaluated to determine if the observed phenotype was a result of altered glucose management. No significant difference was observed in glucose tolerance, suggesting that insulin signaling is functional in AEG-1KO mice (Fig. 2.7). PET-imaging and [^{18}F]-FDG uptake analysis methods were also used for the assessment of glucose metabolism but did not show any difference between WT and AEG-1KO mice (Table 3.1) suggesting that these differences in fat accumulation were not a result of disparities in glucose tolerance or peripheral glucose metabolism. A cohort of WT and AEG-1KO mice were monitored up until 24 months of age. Over this time period, 19 out of 21 WT mice died, however a significant survival benefit was observed in the leaner AEG-1KO mice, of which only 3 of 20 mice expired (Fig. 2.9).

A.
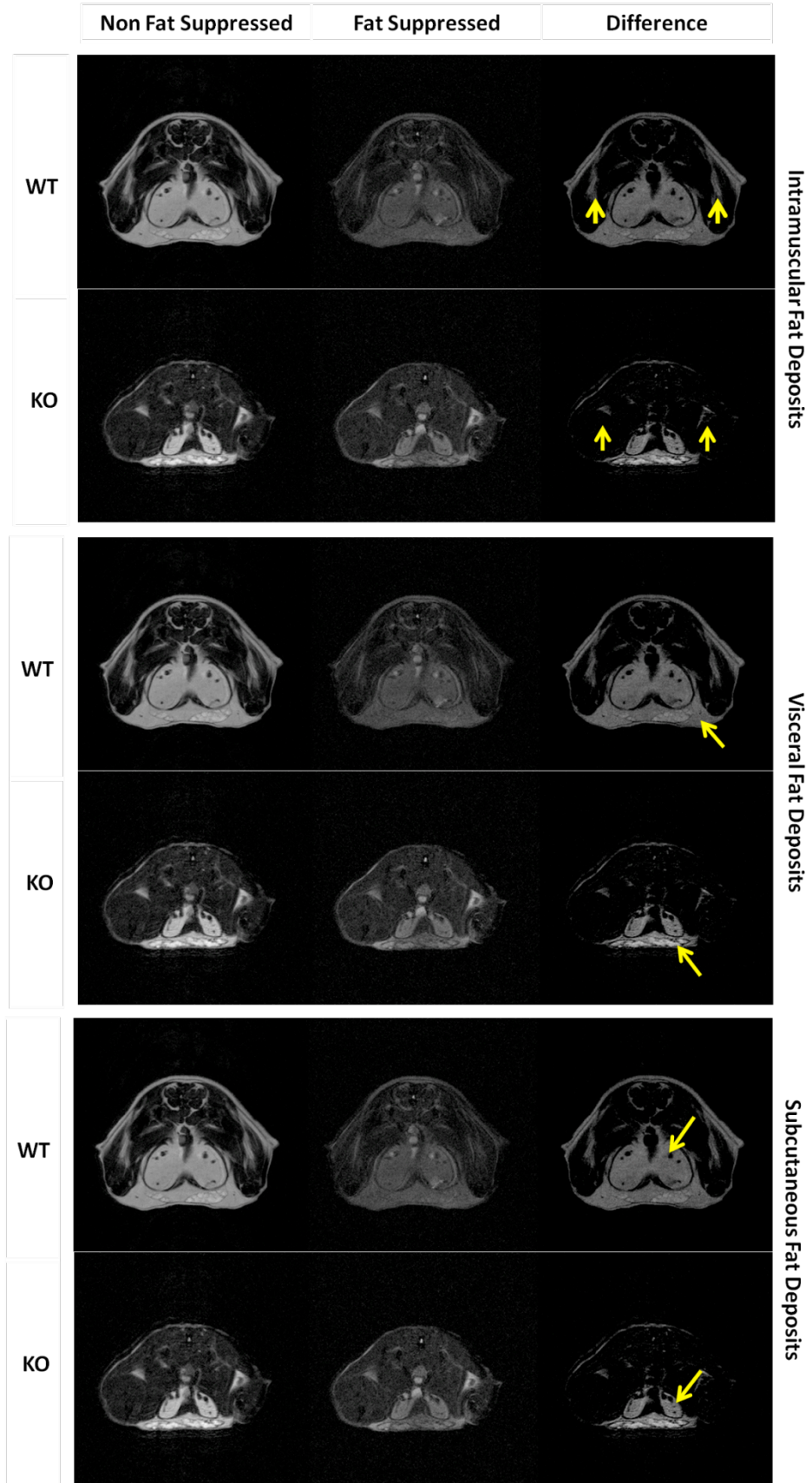
B.
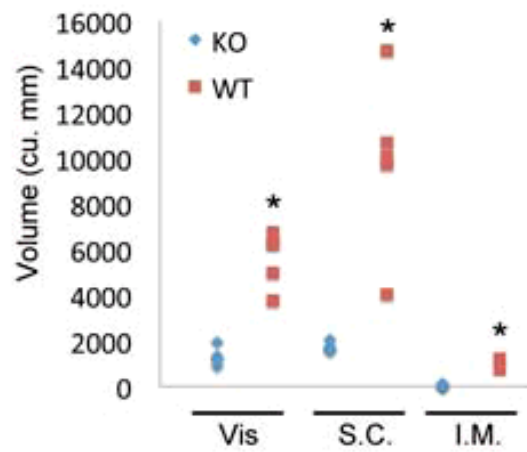
Figure 2.6 MRI Analysis of mice. A. Representative MRI depicting areas of intramuscular (I.M) visceral (Vis) and subcutaneous (S.C.) fat deposits. B. Quantification of body fat distribution determined by MRI. (N = 5/group). Data points represent individual animals; *: $p<0.05$.

Figure 2.7 Glucose tolerance of WT and AEG-1KO mice. Blood glucose was measured at the indicated time points after i.p. injection of a bolus of glucose in fasted mice.

Table 1 Glucose uptake in peripheral tissues. Results of [18F]-FDG uptake assay: The percent injected dose/gram of tissue (%ID/g) values were calculated after appropriate decay corrections.

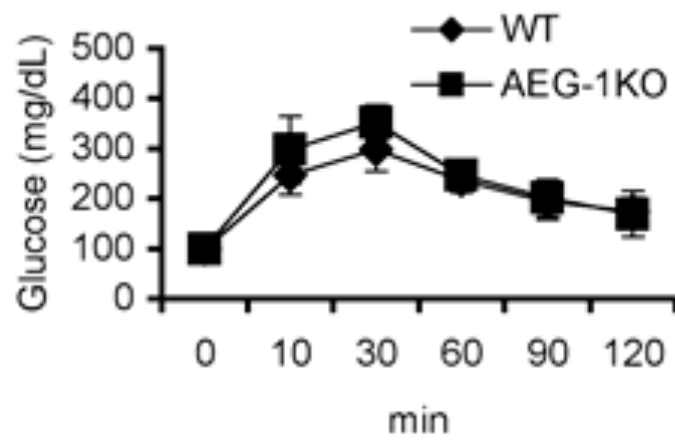|		[18F]-FDG Percent Injected Dose/gram of tissue				Body Weight (grams)	FDG Injected Dose (micro Ci)	Uptake Time (minutes)
Mouse ID	Type	HEART	BRAIN	LIVER	KIDNEY			
CgB-m01	WT	41.09	10.42	6.772	18.820	37.9	320.0	70.00
CgB-m02	WT	18.51	8.76	3.686	8.627	47.1	319.0	69.00
CgB-m03	WT	30.39	9.13	2.311	9.433	50.7	303.0	64.00
CgC-m01	WT	21.92	12.05	3.284	12.344	40.3	283.0	71.00
CgC-m02	WT	53.86	15.18	4.052	13.785	33.1	317.0	77.00
CgC-m03	WT	14.47	16.81	3.955	13.036	39.3	339.8	66.00
AVERAGE		30.04	12.06	4.01	12.67	41.40	313.63	69.50
STD		15.04	3.30	1.49	3.64	6.41	19.06	4.51
CgA-m02	KO	11.26	11.92	1.969	10.317	25.9	310.0	74.00
CgD-m01	KO	26.31	10.58	3.018	7.835	25.2	301.2	77.00
CgE-m01	KO	17.20	4.86	1.775	6.581	31.1	294.3	71.00
CgE-m02	KO	22.88	6.88	2.490	9.517	27.3	309.0	63.00
CgE-m03	KO	21.20	6.84	3.137	8.452	24.1	307.0	55.00
AVERAGE		19.77	8.21	2.48	8.54	26.72	304.30	68.00
STD		5.78	2.92	0.61	1.45	2.71	6.55	8.94
T-test (2 tail, 2 sample)		0.169	0.071	0.056	0.039	0.001	0.302	0.746

The only significant difference in FDG uptake was observed in the kidneys, which could be due to clearance and may not be due to variability in glucose uptake.
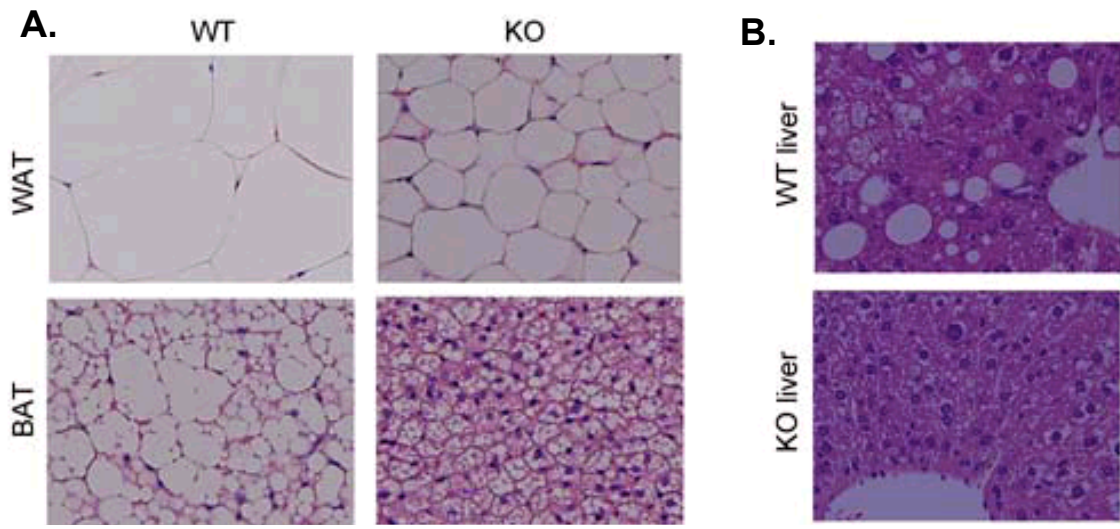
Figure 2.8 Histological Evaluation of Adipose and Liver Tissue. A. H&E staining of white adipose tissue (WAT) and brown adipose tissue (BAT) at 15 months. B. H& E staining of WT and KO liver sections at 15 months.
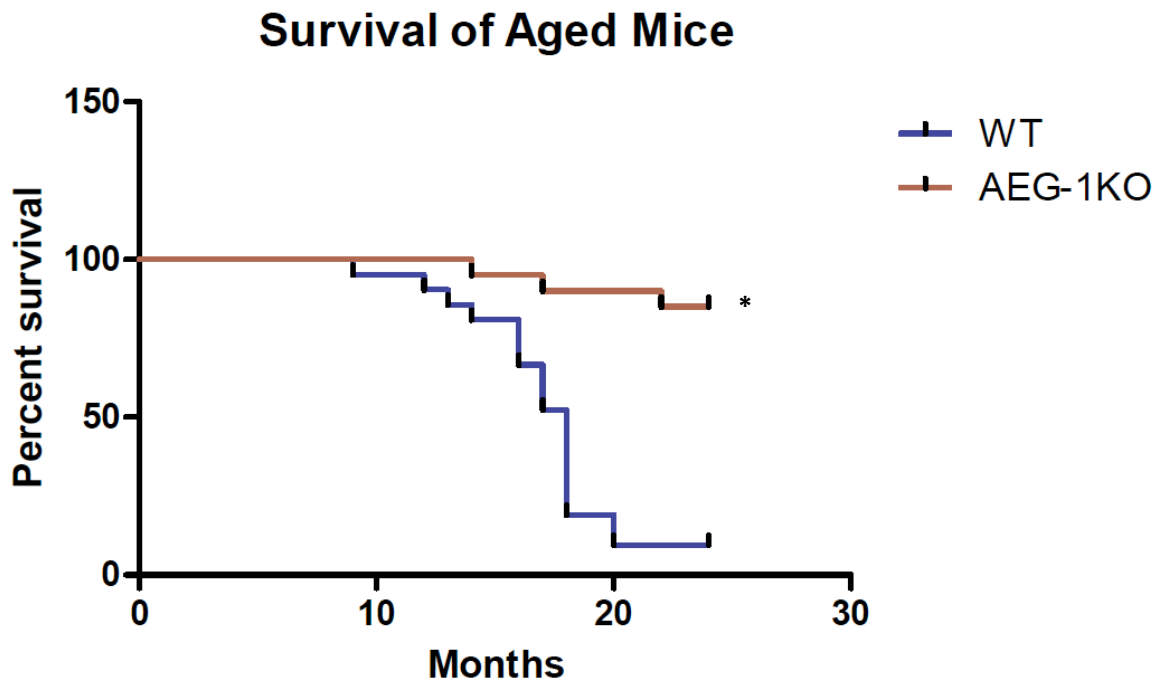
Figure 2.9 Aging Study. Kaplan-Meier survival curve; representing WT and AEG-1KO mouse viability over 24 months. (n = 21 for WT and n =20 for AEG-1KO) *: p<0.05.
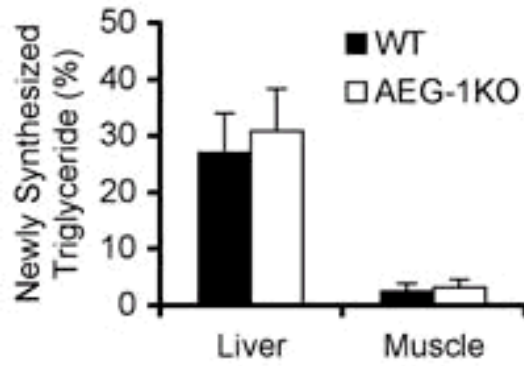
B. Intestinal fat absorption is inhibited in AEG-1KO mice

In the absence of differential glucose tolerance, three potential causative factors remained that could result in the profound lack of fat in AEG-1KO mice. These factors included: (1) defects in fat synthesis, (2) increased energy expenditure (fat burning), and/or (3) decreased fat absorption from the intestine. Each of these factors was interrogated individually as part of the characterization of the AEG-1KO mice. First to be evaluated was serum total triglyceride (TG) and cholesterol levels. Both of which were significantly lower in AEG-1KO compared to WT mice (Fig. 2.10A). Interestingly, although the total TG level was low in AEG-1KO mice, a comprehensive serum lipidomic analysis revealed significantly higher levels of triglycerides (TG) containing long-chain fatty acids in AEG-1KO mice as compared to age-matched WT mice (Fig. 2.11). Levels of newly synthesized TG and palmitate in liver and muscle of WT and AEG-1KO mice were also found to be similar in between WT and AEG-1KO mice (Fig. 2.10B-C).
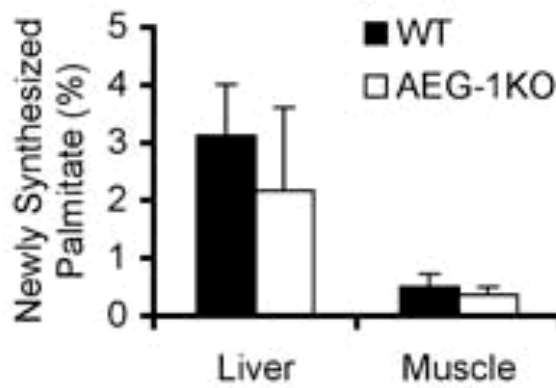
A.
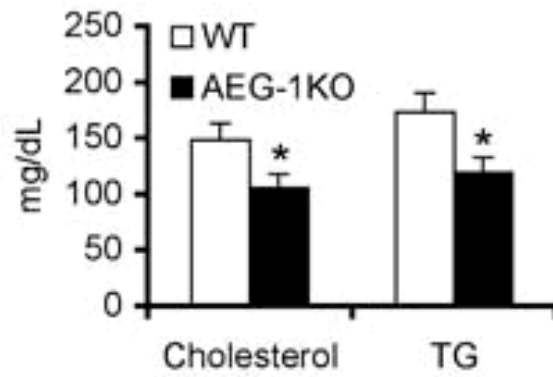
B.

C.

Figure 2.10 Intestinal fat absorption is inhibited in AEG-1KO mouse. A. Serum total cholesterol and triglyceride (TG) levels. (n=5/group). Measurement of newly synthesized triglycerides (B) and palmitate (C).
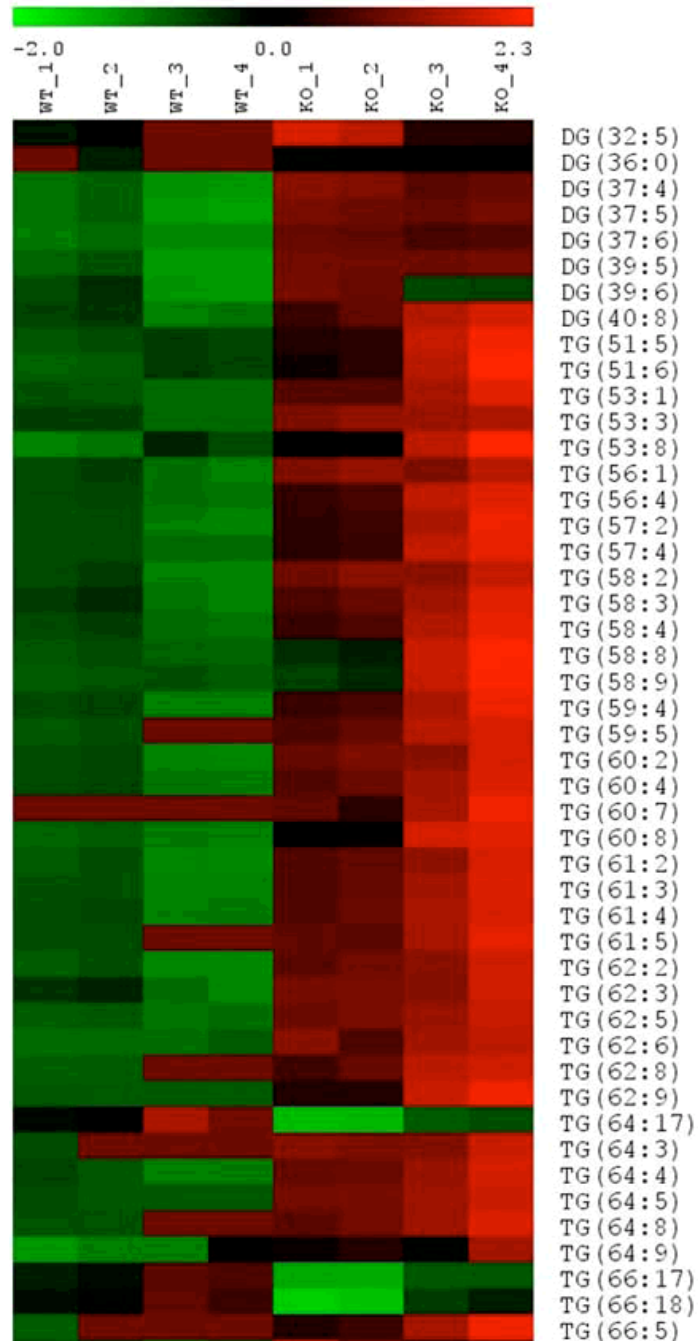
Figure 2.11 Triglycerides containing long-chain fatty acids are increased in AEG-1KO mice Heat map of plasma lipid profile (n=4/group).

To assess rates of energy expenditure, an indirect calorimetry analysis was conducted measuring O_2 consumption and CO_2 production in WT and AEG1-KO mice, however these methods did not reveal any increased fat burning in AEG-1KO mice (Fig. 3.12A-B). In fact, AEG-1KO mice demonstrated a small but statistically significant decrease in energy expenditure compared to WT mice (Fig. 3.12B). No difference was observed in Uncoupling Protein 1 (UCP1) levels in white and brown adipose tissue of WT and AEG-1KO mice (data not shown).

Next to be evaluated was intestinal lipid absorption. Cholesterol absorption was measured by oral gavage delivery of [^{14}C]-cholesterol followed by measurement of radioactive fecal output. Fatty acid absorption was assessed by oral gavage delivery of [^{3}H]-triolein followed by temporal measurement of plasma radioactivity. Both cholesterol and fatty acid absorption by the intestine were markedly inhibited in AEG-1KO as compared to WT mice (Fig. 2.13A-B). Taken together, this data suggested that the lean phenotype observed in AEG-1KO mice might be explained by reduced cholesterol and TG absorption from the intestine.

A.
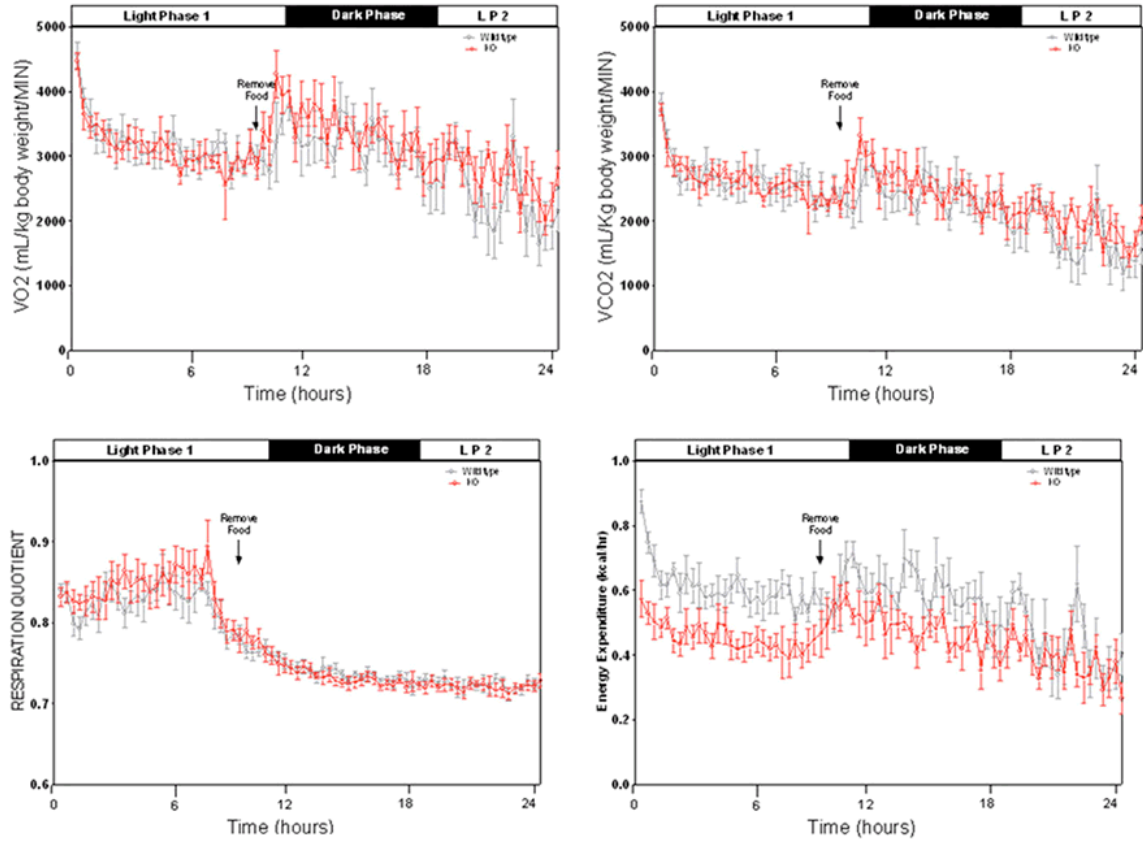
B.
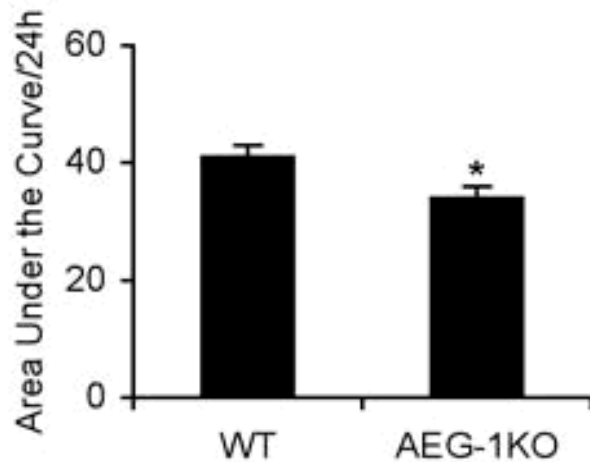
Figure 2.12 AEG-1KO mice do not show increased fat burning. A. Indirect calorimetry analysis measuring O2 consumption and CO2 production. B. Quantification as calculated by quantifying the area under the curve. (n=6/group).

A.
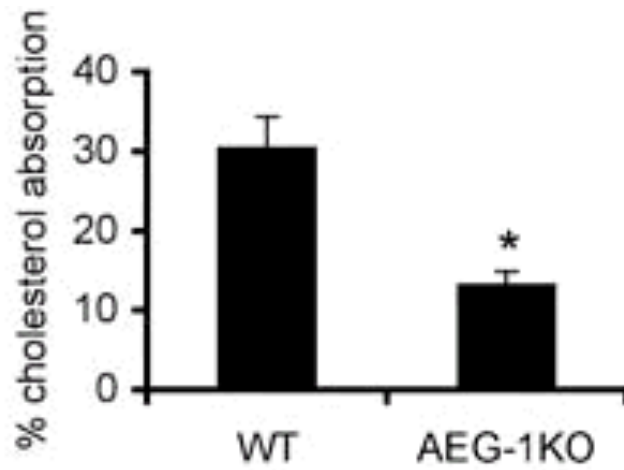
B.
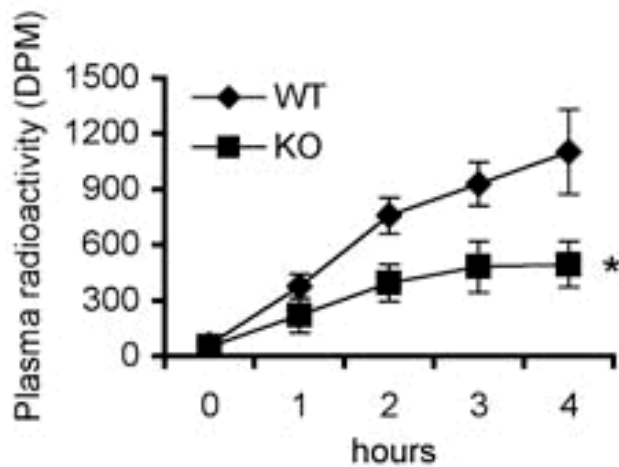
Figure 2.13 Intestinal fat absorption is inhibited in AEG-1KO mouse. A. Measurement of cholesterol absorption from the intestine after oral gavage of [14C]-cholesterol and then measuring fecal radioactivity. B. Measurement of fatty acid absorption by oral gavage of [3H]triolein and then temporally measuring plasma radioactivity.

To determine if intestinal cholesterol and TG absorption was indeed subjugated in AEG-1KO mice, the animals were maintained on a high fat and cholesterol containing diet (HFD). A cohort of WT and AEG-1KO mice were fed a HFD starting at 8 weeks of age. Over a period of 5 weeks, each WT mouse gained ~11 gm of body weight on average, while no weight gain was observed in AEG-1KO mice (Fig. 2.14B). The experiment was terminated early, since the AEG-1KO mice started developing steatorrhea with a tendency to actually lose body weight. Post mortem evaluation revealed evidence of steatosis in the liver of WT mice as a result of the HFD but this phenomenon was absent in AEG-1KO mice (Fig. 2.14A). The resistance of AEG-1KO mice to HFD induced weight gain indicated that intestinal fat and cholesterol absorption was indeed impaired. Moreover, the fact that mice actually lost weight suggests that high levels of fat and cholesterol were not only poorly tolerated but also inaccessible as an energy source in the AEG-1 KO mice. These findings indicate that feeding a HFD further aggravated the reduced cholesterol and TG absorption in AEG-1KO mice.

A.
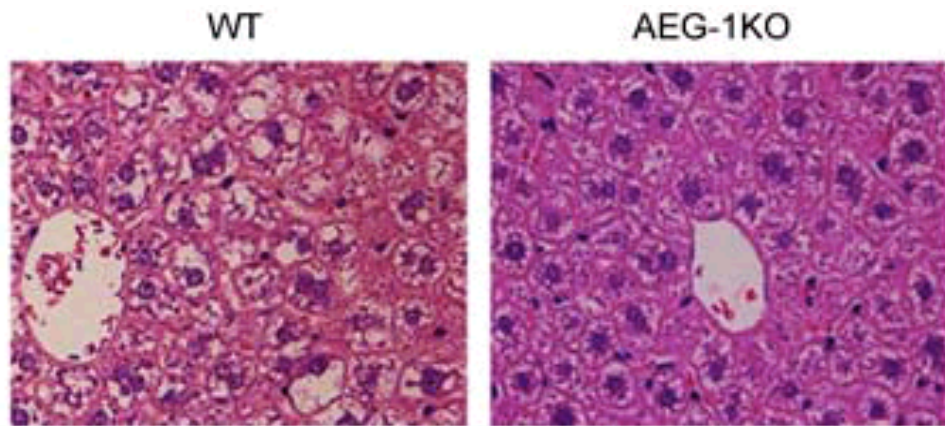
B.
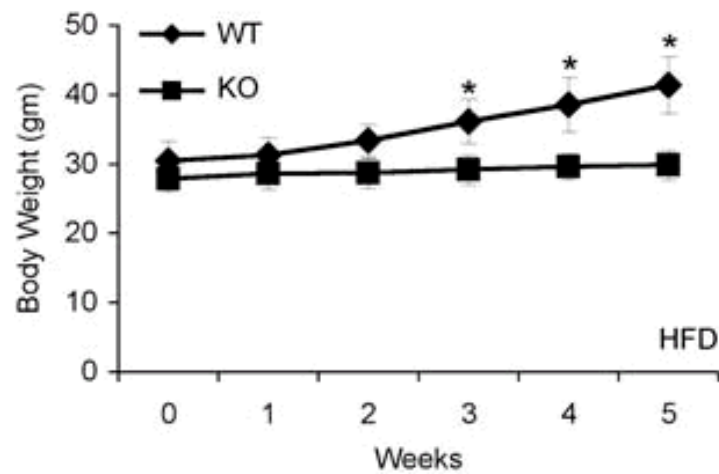
2.14 AEG-1KO Mice are resistant to high fat diet induced weight gain. A. H&E staining of liver sections of mice fed HFD. B. Weekly body weight gain upon feeding high fat and cholesterol diet (HFD). (n=8). For graphs, the data represent mean ± SEM. *: p<0.05.

C. LXR and PPARα Activities are Augmented in the Intestine of AEG-1KO Mice

We next searched for the molecular mechanism conferring the phenotype observed in the AEG-1KO mice. As mentioned previously, our group has recently described a novel interaction between AEG-1 and Retinoid X Receptor (RXR), a transcription factor functioning as an obligate heterodimer partner of diverse nuclear receptors mediating the action of hormones, vitamins and lipids. LXR and PPARα are two heterodimeric binding partners of RXR that are essential to the absorption, transport, efflux and excretion of cholesterol and fatty acids (Fig. 2.15, 2.16, 2.17). Based on the observed phenotype, we speculated that LXR and PPARα activity might be altered in AEG-1KO mice. To test this hypothesis, we first analyzed LXR and PPARα activity by means of luciferase reporter assays wherein primary WT and AEG-1KO hepatocytes were transfected with either LXRE or PPARE then treated with either T0901317 (5 uM) or CP775146 (2.5 uM), synthetic ligands of LXR and PPARα respectively. Both basal and ligand-dependent LXR and PPARα activities were significantly higher in AEG-1KO hepatocytes as compared to WT hepatocytes (Fig. 2.18A-B).
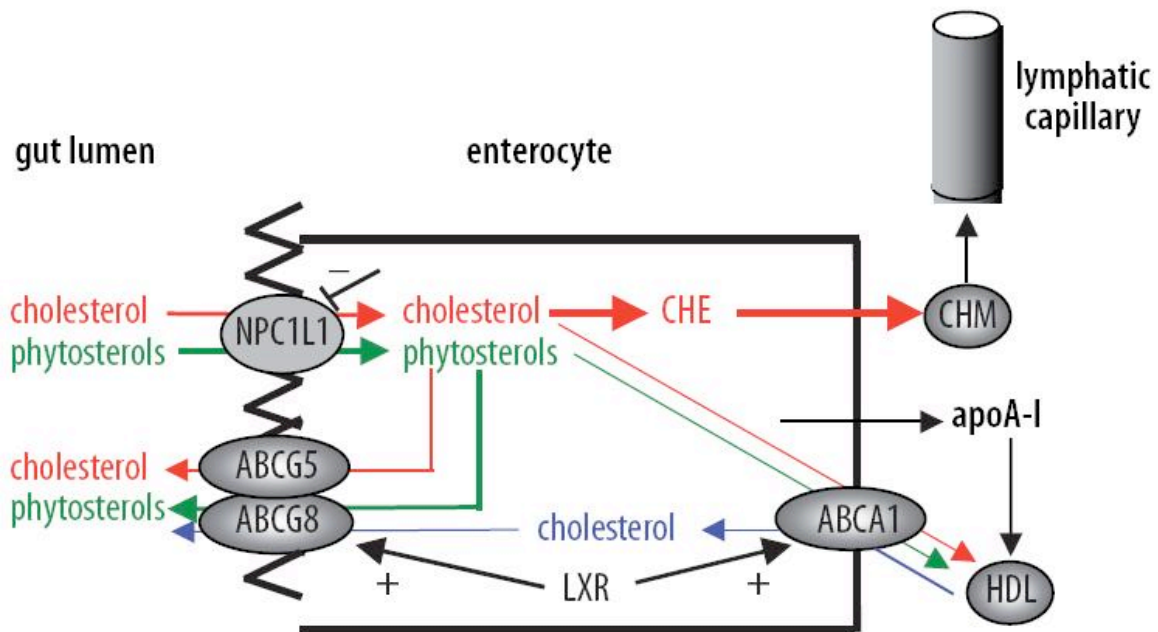
Figure 2.15 Intestinal cholesterol efflux. Intestinal cholesterol absorption (red arrows), intestinal phytosterol handling (green arrows), and the role of enterocytes in fecal excretion of cholesterol delivered from peripheral tissues by HDLs (i.e. alternative reverse cholesterol transport, blue blue arrows). Cholesterol is absorbed from bile micelles through the apical membrane NPC1L1 protein. Most of it is subsequently esterified by ACAT-2, and cholesteryl esters are incorporated into chylomicrons (CHM), which are exocytozed and enter the lymphatic capillaries. Some cholesterol is extruded to the intestinal lumen through the apical ABCG5/ABCG8 heterodimer and the minority of cholesterol is extruded through the basolateral ABCA1 to enter the HDL fraction, in part formed locally in the intestine from locally generated apoAI. Alimentary phytosterols are absorbed by NPC1L1, but are not esterified; most of them are rapidly extruded to the gut lumen through the ABCG5/ABCG8 complex and some phytosterols are transferred to HDLs by basolateral ABCA1. In addition, the intestine may drive the removal of peripheral tissue-derived cholesterol from HDLs to the feces through the concerted action of basolateral ABCA1 and apical ABCG5/ABCG8. LXR agonists inhibit NPC1L1 and increase ABCA1, ABCG5, and ABCG8.

66
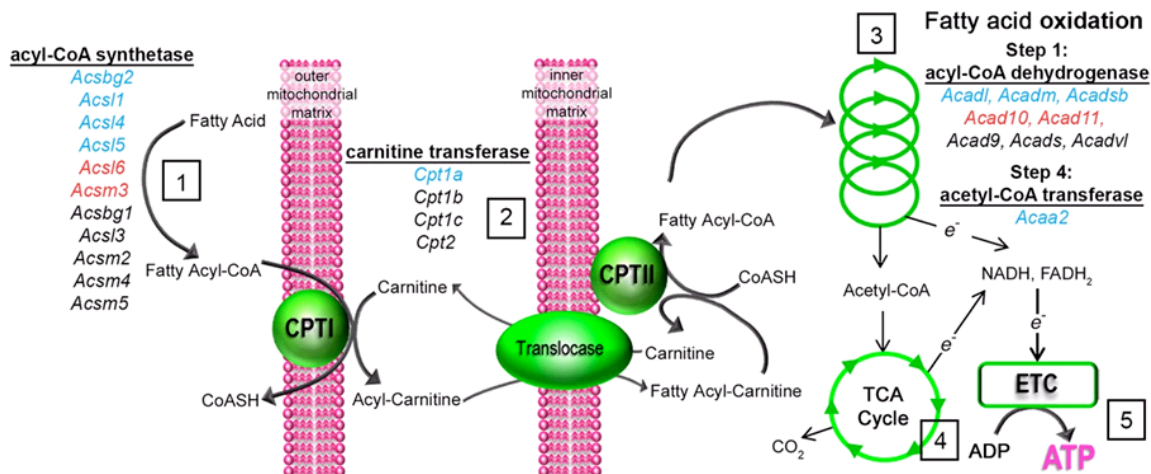
Figure 2.16 PPARα Regulates Fatty Acid β-Oxidation. Fatty acid β-oxidation is the process by which fatty acids are broken down to produce energy. PPARα regulates expression of a number of genes involved in various steps of the β-Oxidation pathway. Examples of proteins involved in fatty acid β-oxidation that are transcriptionally regulated by the PPARs are shown in blue. Fatty acids primarily enter a cell via fatty acid protein transporters on the cell surface. Once inside, FACS adds a CoA group to the fatty acid. CPT1 then converts the long chain acyl-CoA to long chain acylcarnitine. The fatty acid moiety is transported by CAT across the inner mitochondrial membrane. CPT2 then converts the long chain acylcarnitine back to long chain acyl-CoA. The long chain acyl-CoA can then enter the fatty acid β-oxidation pathway, resulting in the production of one acetyl-CoA from each cycle of β-oxidation. The acetyl-CoA, the end product of each round of β-oxidation, then enters the TCA cycle, where it is further oxidized to CO2 with the concomitant generation of three moles of NADH, one mole of FADH2 and one mole of ATP. This acetyl-CoA then enters the TCA cycle. The NADH and FADH2 generated during the fat oxidation and acetyl-CoA oxidation in the TCA cycle then can enter the respiratory pathway for the production of ATP via oxidative phosphorylation. The NADH and FADH2 produced by both β-oxidation and the TCA cycle are used by the electron transport chain to produce ATP.

Figure 2.17 β-Oxidation Decreases Intestinal Absorption. Cholesterol is transported in the plasma predominantly as cholesteryl esters associated with lipoproteins. Dietary cholesterol is transported from the small intestine to the liver within chylomicrons. Cholesterol synthesized by the liver, as well as any dietary cholesterol in the liver that exceeds hepatic needs, is transported in the serum within LDLs. The liver synthesizes VLDLs and these are converted to LDLs through the action of endothelial cell-associated lipoprotein lipase. Cholesterol found in plas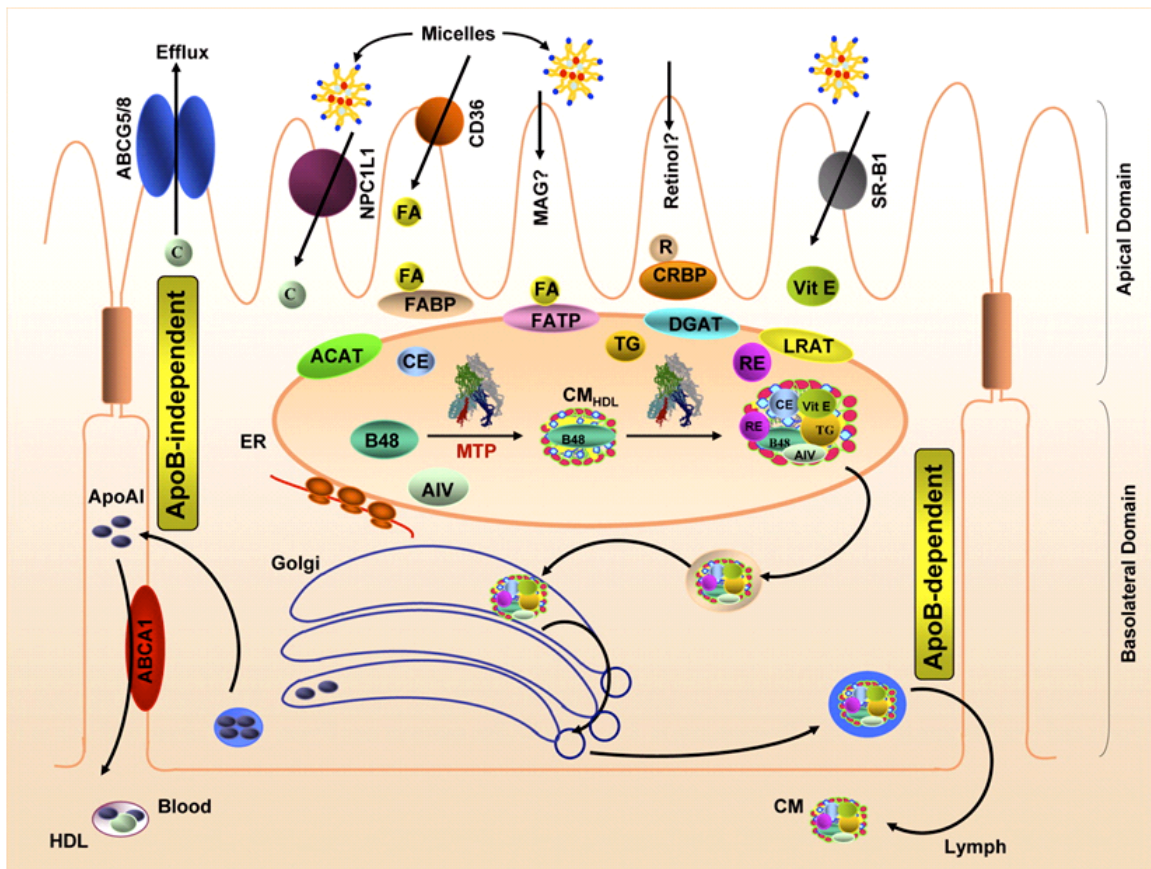ma membranes can be extracted by HDLs and esterified by the HDL-associated enzyme. The cholesterol acquired from peripheral tissues by HDLs can then be transferred to VLDLs and LDLs via the action of cholesteryl ester transfer protein (apo-D) which is associated with HDLs. Reverse cholesterol transport allows peripheral cholesterol to be returned to the liver in LDLs. Ultimately, cholesterol is excreted in the bile as free cholesterol or as bile salts following conversion to bile acids in the liver. Chylomicrons are assembled in the intestinal mucosa as a means to transport dietary cholesterol and triglycerides to the rest of the body. Chylomicrons are, therefore, the molecules formed to mobilize dietary (exogenous) lipids. The predominant lipids of chylomicrons are triglycerides. The apolipoproteins that predominate before the chylomicrons enter the circulation include apoB-48 and apoA-I, apoA-II and apoA-IV. ApoB-48 combines only with chylomicrons. Chylomicrons leave the intestine via the lymphatic system and enter the circulation. In the bloodstream, chylomicrons acquire apoC-II and apoE from plasma HDLs. HDL begins as protein-rich discoidal structures, composed primarily of apoA-I, produced by the liver and intestines. Within the vasculature apoA-I interacts with the ATP-binding cassette transporter, ABCA1 and extracts cholesterol from cells. Through the action of LCAT the apoA-I-associated cholesterol is esterified forming cholesterol esters. This process results in the generation of HDL_3 particles. As the HDL_3 particles continue through the circulation they pick up more cholesterol and through the action of LCAT, generate more cholesterol esters. As HDL migrates through the vasculature there is an interaction between them and IDL and LDL. This interaction occurs through the action of CETP, which exchanges the cholesterol esters in the HDL for triglycerides from LDL. This interaction results in the conversion of HDL_3 particles to HDL_2. HDL is then removed from the circulation by the liver through binding of the HDL to hepatic scavanger receptor SR-B1. Within the vasculature the generation of ROS results in oxidation of lipid components of LDL generating oxidized LDL, which is taken up by macrophages via the scavenger receptor, FAT/CD36.
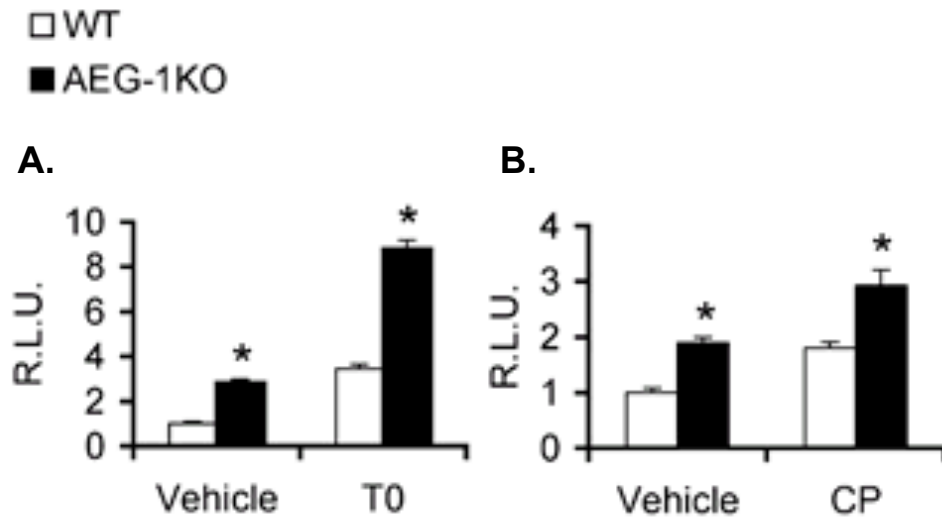
Figure 2.18 LXR and PPARα are activated in the intestine of AEG-1KO mice. LXRE (A) and PPARE (B) luciferase activity was determined in WT and AEG-1KO hepatocytes upon treatment with LXR ligand, T0901317 (T0) (5 µM), and PPARα ligand, CP775146 (CP)(2.5 µM), respectively. R.L.U.: relative luciferase unit.

The next step was to evaluate the functional relevance of this mechanism in vivo. To do so WT and AEG-1KO mice were treated with T0901317. After 24 h the animals were sacrificed and livers were analyzed for recruitment of LXR, acetylated histone H3 (AHH3) and co-activator SRC-1 on the promoter region of LXR target gene Abca1 by chromatin immunoprecipitation (ChIP) (Fig. 2.19). A significant increase in recruitment of LXR, was observed in AEG-1KO livers *versus* WT livers. AHH3 and SRC-1activity were also elevated in AEG-1KO mice as compared to the WT indicating an increase in co activator activity and recruitment respectively. This in vivo analysis confirmed and validated our previous in vitro observations.
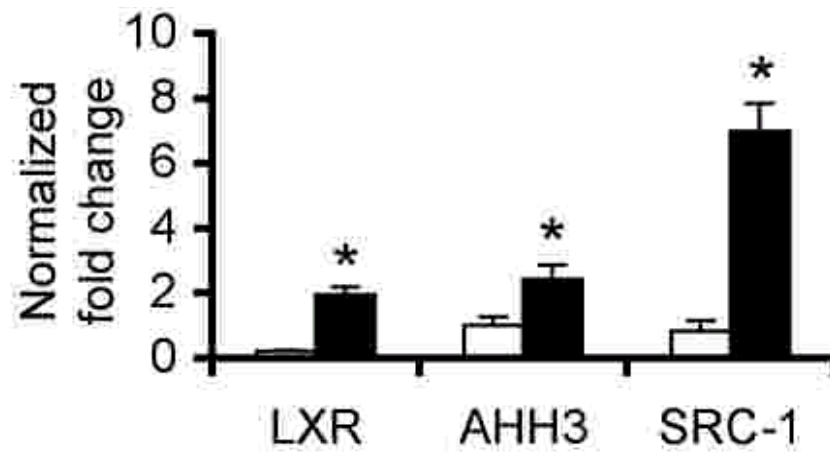
Figure 2.19 LXR is activated in AEG-1KO mice. ChIP assays were performed using anti-LXRα/β, anti-Acetyl Histone H3 (AHH3) and anti-SRC-1 antibodies using T0901317-treated WT and AEG-1KO livers and PCR primers amplifying promoter regions of Abca1 gene. Normal rabbit IgG was used as control and the data was normalized by results obtained using normal IgG.

Next we analyzed the expression of a number of LXR target genes in the small intestine of WT and AEG-1KO mice fed either regular chow or HFD. The basal expression level of Abca1 was markedly higher in chow fed-AEG-1KO mice compared to WT mice (Fig. 2.20A). With regular chow, the heterodimeric efflux pump Abcg5 and Abcg8 showed small but significant increase in AEG-1KO versus WT mice. Upon HFD treatment, the expression of all three genes was significantly induced in both WT and AEG-1KO mice. However, the magnitude of induction of these genes was significantly more robust in AEG-1KO mice compared to WT mice, particularly in the case of Abca1 (Fig. 2.20A). Conversely, the basal expression level of the cholesterol transporter Npc1l1 was significantly lower in AEG-1KO mice versus WT mice and upon HFD treatment levels were further depressed (Fig. 2.20B). It can be reasoned that the increased levels of the cholesterol efflux pumps and decrease in the cholesterol transporter (Npc1l1) explains the inhibition of intestinal cholesterol absorption in AEG-1KO mice. Even more compelling is the fact that these effects were further intensified when the animals were challenged with HFD, which provides ligands to LXR, functionally activating LXR and augmenting its activity.

A.

B.
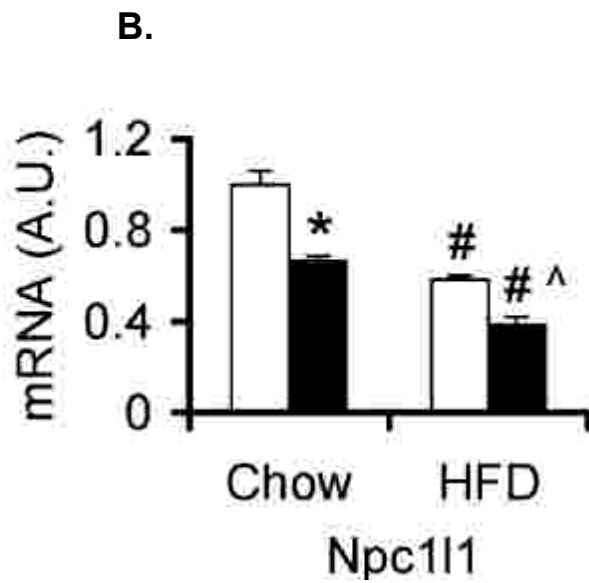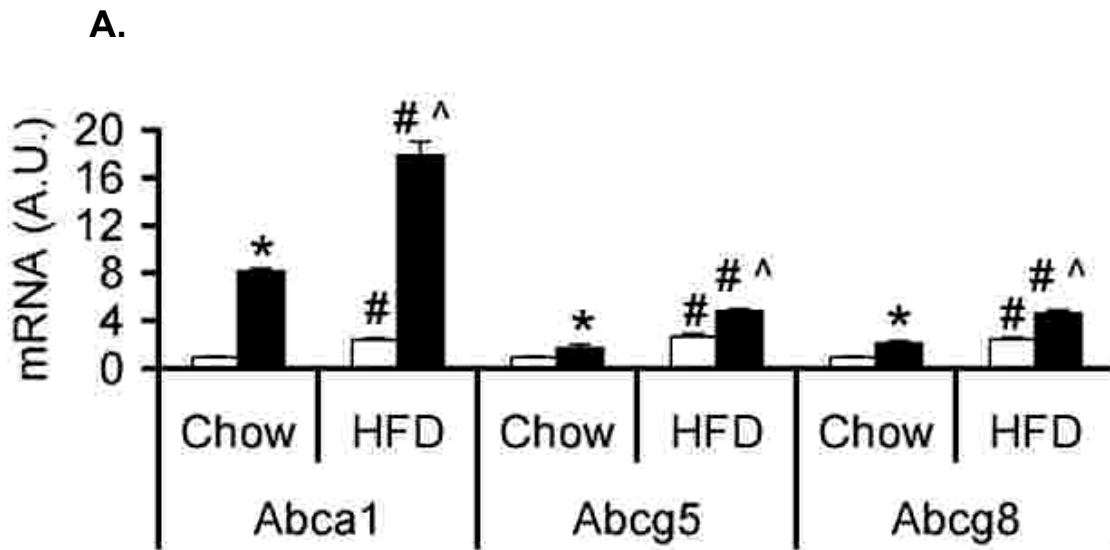
Figure 2.20 LXR is activated in the intestine of AEG-1KO mice. Expression of the indicated genes by Taqman Q-RT-PCR in small intestine of chow- and HFD-fed mice. The data represent mean ± SEM. *: p<0.05 versus corresponding data point in WT mice; #: p<0.05 chow versus HFD in WT mice; ^: p<0.05 chow versus HFD in AEG-1KO mice.

A number of PPARα target genes that are known regulators of β-oxidation of fatty acids in the small intestine and liver. We analyzed the expression levels of several of the key genes involved in this process, however no significant difference was observed in the enterocyte expression levels of fatty acid transporters, FABPpm/Got2, FAT/Cd36 and FATP4/Slc27a4 in WT and AEG-1KO mice (Fig. 2.21A) with regular chow or HFD. This indicated that fatty acid transport from the lumen to the enterocytes was not dysregulated in the KO animals and that enhanced β-oxidation may be responsible for the observed decreased absorption to the plasma. Fatty acid degradation in most organisms occurs primarily via the β-oxidation cycle. The major degradative pathway for fatty acid esters is β-oxidation. In mammals, β-oxidation occurs in both mitochondria and peroxisomes thus we analyzed components of both organelles. For the mitochondrial β-oxidation pathway, Cpt1a, the rate-limiting enzyme in the carnitine-dependent transport of fatty acids across the mitochondrial membrane was analyzed as well as Acadl and Acadm, which catalyze the initial steps of fatty acid β-oxidation [73]. For peroxisomal β-oxidation, we analyzed Acox1, the first enzyme in this pathway [73]. In standard chow fed mice, Cpt1a and Acadl expression levels were significantly higher in the small intestine (Fig. 2.21B), and Cpt1a, Acadl and Acadm levels were significantly higher in the liver of AEG-1KO mice versus WT mice (Fig. 2.21B). There were no significant differences in the Acox1 levels between AEG-1KO and WT mice in either organ. Interestingly however, a significant induction of all four genes was observed in both the small intestine and liver of WT mice following exposure to a HFD. In the small intestine

of AEG-1KO mice, HFD treatment resulted in a significant induction of all four genes, which was substantially more pronounced than the induction seen in WT mice (Fig. 2.21B-C). However, HFD treatment did not result in further induction of these genes in the liver of AEG-1KO mice (Fig. 2.21C).

A.

WT
AEG-1KO

Got2   Cd36   Slc27a4

B. S. I.

Acox1   Cpt1a   Acadm   Acadl

C. Liver

Acox1   Cpt1a   Acadm   Acadl
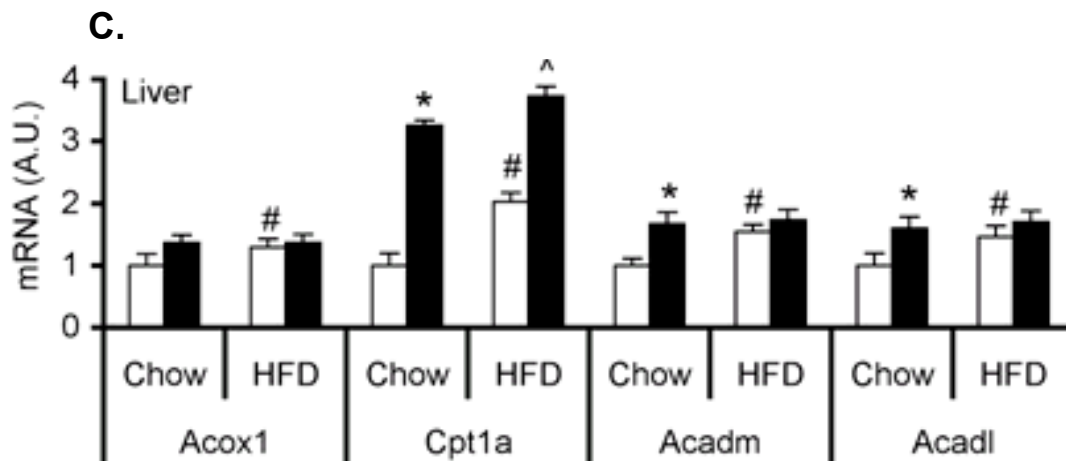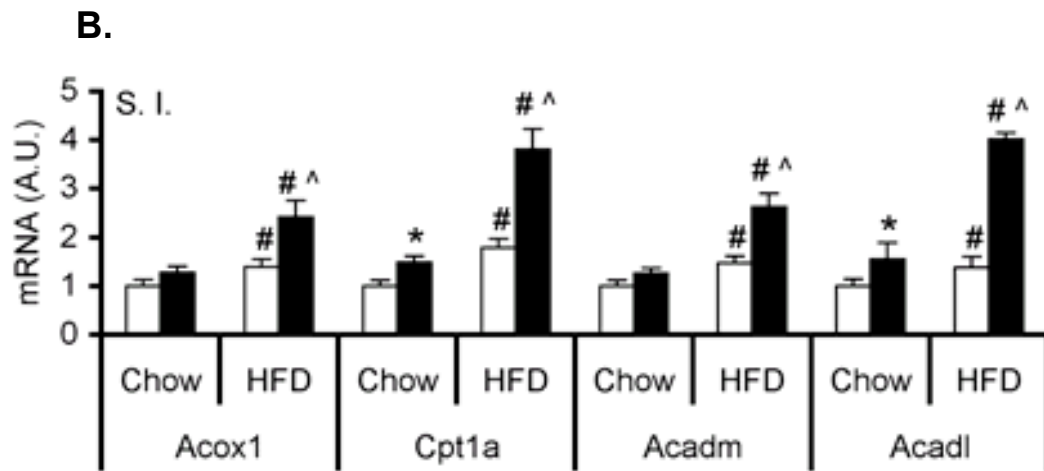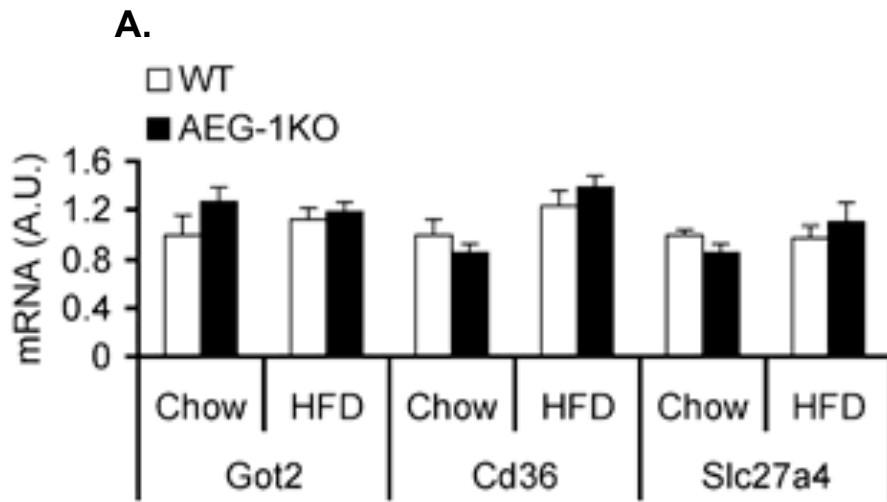
Figure 2.21 Expression of fatty acid transporters and PPARα target genes. Expression of the indicated genes by Taqman Q-RT-PCR in chow- and HFD-fed small intestine (A & B) and chow- and HFD-fed liver (C). The data represent mean ± SEM. *: $p < 0.05$ versus corresponding data point in WT mice; #: $p < 0.05$ chow versus HFD in WT mice; ^: $p < 0.05$ chow versus HFD in AEG-1KO mice.

We also directly assessed the levels of Ppara in these animals and found that the basal Ppara level was also significantly higher in the small intestine (Fig. 2.22A) and liver (Fig. 2.22B) of AEG-1KO mice as compared to WT mice. HFD treatment resulted in induction of Ppara in both WT and AEG-1KO liver and small intestine. However, here again we saw that the magnitude of induction was much more pronounced in the small intestine of AEG-1KO mice than in the WT (Fig. 2.22A-B). Intriguingly we also observed that the HFD-mediated induction of Ppara was more robust in the small intestine than in the liver of the AEG-1KO mice, (Fig. 2.22A-B). No significant differences were observed in the levels of Pparg or of Ppargc1, the co-activator for PPAR (Fig. 2.22A-B).
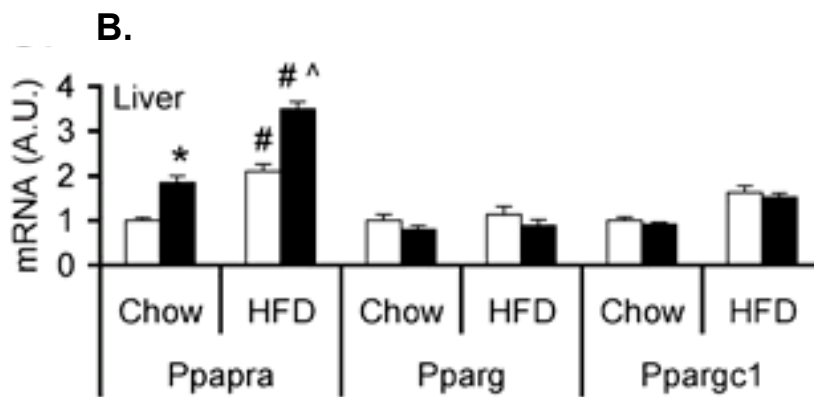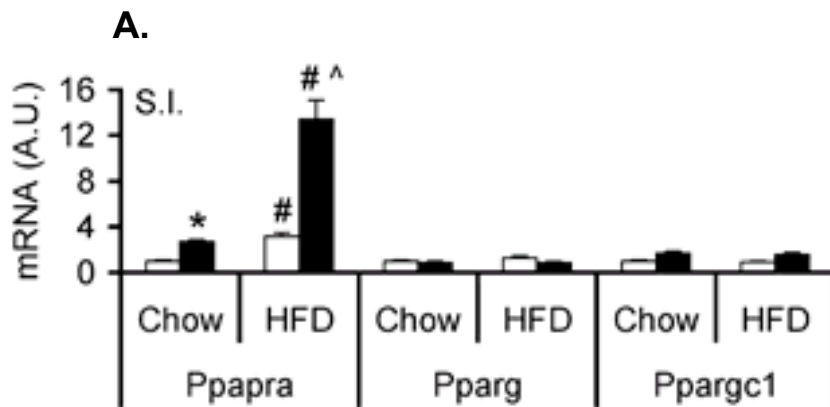
Figure 2.22 PPAR Expression. Expression of the indicated genes by Taqman Q-RT-PCR in chow- and HFD-fed small intestine (S.I.) (A) and chow- and HFD-fed liver (B). The data represent mean ± SEM. *: p<0.05 versus corresponding data point in WT mice; #: p<0.05 chow versus HFD in WT mice; ^: p<0.05 chow versus HFD in AEG-1KO mice.

Collectively these findings suggest that under basal conditions higher levels of PPARα and its target genes in the small intestine of AEG-1KO mice confer increased fatty acid β-oxidation in the enterocytes, resulting in decreased fatty acid absorption. This effect is heightened upon HFD treatment that provides ligands to PPARα, thus augmenting levels of both Ppara and its target genes. The lack of absorption of fatty acids from the intestines upon HFD treatment results in decreased delivery of PPARα ligands to the liver, so that there was no further induction by HFD compared to chow diet. The mitochondrial FA β-oxidation pathway is a major contributor to cellular energy production and homeostasis. To directly evaluate and quantify the rate of β-oxidation in vivo, products of fatty acid β-oxidation were measured in fresh liver and small intestine homogenates using 14C-palmitate. Acetyl-CoA, generated by β-oxidation, enters TCA cycle to generate CO_2. 14C-palmitate that does not get oxidized forms acid-soluble metabolites (ASM). Fatty acid β-oxidation was significantly increased in the liver and small intestine of AEG-1KO mouse versus WT (Fig. 2.23).
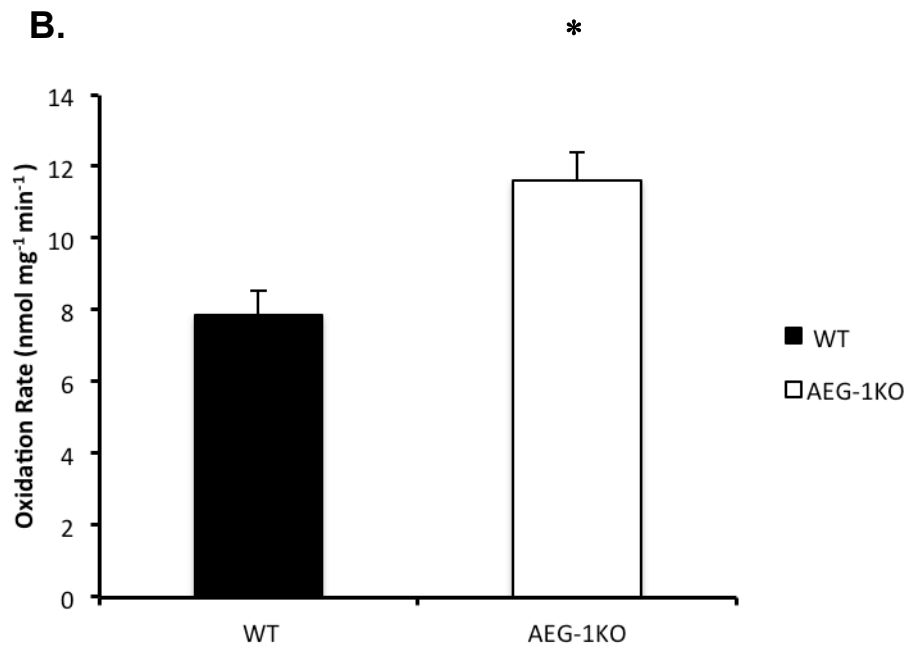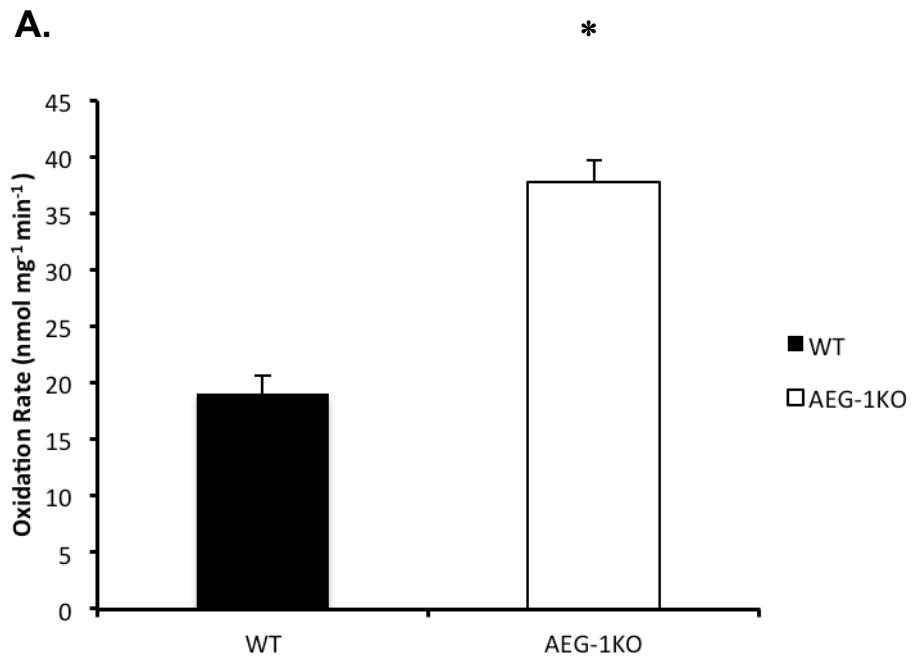
Figure 2.23 Fatty acid β-oxidation is increased in AEG-1KO mice. A. Fresh liver and B. small intestine homogenates were used with 14C-palmitate as substrate. The data represent mean ± SEM of 3 independent experiments. *: p<0.01.

IV. Discussion

Knockout of AEG-1 confers a lean phenotype marked by increased overall longevity in mice. In this study we systematically assessed many of the major known contributors to metabolic homeostasis. We were unable to identify any impairment in triglyceride synthesis in AEG-1KO mice. Similarly, calorimetric analysis did not provide evidence of increased energy expenditure in AEG-1KO mice nor did differences exist in glucose tolerance indicating that the lack of excess body fat and overall lean phenotype observed in AEG-1KO mice was not owed to aberrant fat production, increased energy expenditure or differential glucose management. A significant decrease in serum total triglyceride (TG) and cholesterol levels was observed in AEG-1KO mice as compared to WT. Our studies revealed a dramatic reduction in both cholesterol and fatty acid absorption in the intestine of AEG-1KO mice. The phenotypes observed in AEG-1KO mice may be explained by hyperactivity of RXR heterodimer partners LXR and PPAR-α. In enterocytes, activation of LXR inhibits cholesterol absorption and activation of PPAR-α promotes β-oxidation of fatty acids resulting in inhibition of fatty acid absorption. When fed a regular chow diet basal intestinal expression of LXR target genes, Abca1, Abcg5 and Abcg8 were elevated and Npc1l1 levels were reduced in the intestines of AEG-1KO mice as compared to WT. This difference was dramatically amplified upon feeding a HFD which provide ligands. Similar findings were also observed for PPAR-α target genes involved in fatty acid β-oxidation such as Cpt1a, Acox1, Fabp1, Acadl and Acadm. Cholesterol and fatty acid absorption from the intestine is a complicated process involving specific transporters and efflux pumps, the expression of which is regulated by

nuclear receptors, such as LXR and PPAR-α [62, 74]. In addition, metabolism of cholesterol and fatty acids in enterocytes determine their absorption into the lymph and blood and availability to other organs. Unesterified free cholesterol is taken up into the enterocytes by the cholesterol transporter NPC1L1 which can have three fates [62]. Free cholesterol can be transported to the ER where it is esterified by Acyl-CoA:cholesterol acyltransferase 2 (ACAT2) enzyme and then conjugated with ApoB48 to form chylomicrons which enter into the lymphatic system. Unesterified free cholesterol can be transported back to the intestinal lumen by apically located cholesterol pump ABCG5/ABCG8 heterodimer. Free cholesterol can also be transported into the circulation as a constituent of HDL via ABCA1 located on the basolateral membrane of the enterocytes. When cellular oxysterols accumulate as a result of increasing concentrations of cholesterol, LXR activation, by cholesterol metabolites such as oxysterols [60], causes a net loss of cholesterol through downregulation of NPC1L1 and reduction of ACAT2 enzyme activity as well as induction of ABCG5/ABCG8 and ABCA1 [75-77].

Important intestinal fatty acid transporters include: (1) Fatty acid binding protein, plasma membrane (FABPpm/Got2), located peripherally on the plasma membrane; (2) Fatty acid translocase (FAT/CD36), an integral membrane glycoprotein; and (3) Fatty acid transport protein subtype 4 (FATP4/Slc27a4), an integral membrane protein [78]. In the intestinal lumen triglycerides are broken down into free fatty acids by lipases. Once fatty acids enter into the enterocytes cytoplasmic fatty acid binding protein (FABPc) may transport them to the

mitochondria for β-oxidation [79]. The majority of fatty acids are re-esterified into TG and excreted into chylomicrons. In the enterocytes, PPAR-α promotes β-oxidation of fatty acids thereby decreasing fatty acid absorption in the circulation [64, 74]. This work provides a conceptual framework for understanding the role of AEG-1 in normal physiology. Up until now AEG-1 has been known only for its role in tumorigenesis. Here for the first time we show that the lack of AEG-1 in mice augments LXR and PPARα activity, thereby preventing fat absorption from the intestine. Taken together these findings provide evidence that AEG-1 plays an essential role in maintaining homeostasis in lipid metabolism. These findings have important implications for a number of different pathological conditions, including obesity and non-alcoholic fatty liver disease (NAFLD), where AEG-1 overexpression may facilitate increased fat availability, and may contribute to fat accumulation and ultimately cirrhosis of the liver and obesity-associated cancers. These findings highlight AEG-1 as a new potential target to therapeutic intervention of obesity-associated illnesses.

Chapter Three-The role of Astrocyte Elevated Gene-1 in the Onset and Progression of Hepatocellular Carcinoma

I. Summary

AEG-1 plays a key role in carcinogenesis. Activation of NF-κB in liver macrophages is pivotal for N-nitrosodiethylamine (DEN)-induced HCC initiation. We previously documented that AEG-1 is an essential component of NF-κB activation. In the present studies we interrogated the role of AEG-1 in hepatocarcinogenesis using an AEG-1 knockout mouse (AEG-1KO) model. AEG-1KO mice showed profound resistance to DEN- as well as DEN- and phenobarbital (PB)-induced HCC and lung metastasis. No differential signaling in response to growth factors was observed in AEG-1KO mouse hepatocytes compared to those of the Wild Type (WT) nor did we identify any differences in activation of the Akt, ERK or β-catenin pathways which are known to be activated by AEG-1 overexpression. Profound inhibition of NF-κB activation was observed in AEG-1KO hepatocytes and macrophages as compared to the WT. A marked inhibition in IL-6 production and in STAT-3 activation, key mediators of HCC development, was also observed in DEN-treated AEG-1KO mice. Conditioned media from hepatocytes failed to induce IL-6 expression in macrophages in AEG-1KO, but not in WT. Inhibition of myeloid cell migrations and inhibition of activation of granulocytes were the key functional consequences gleaned by analyzing global gene expression changes in AEG-1KO mice *versus* WT. These findings suggest that AEG-1 is essential for NF-κB activation and inhibition of this activation in macrophages and hepatocytes might confer protection to AEG-1KO

mice from hepatocarcinogenesis. Our studies, for the first time, unravel a unique

role of AEG-1 in tumor microenvironment that is critical for initial development of

HCC upon DEN-induced mutagenesis.

II. Hepatocellular Carcinoma

Hepatocellular carcinoma (HCC) is defined as malignant transformation of

hepatocytes, the primary and most abundant cell type in the liver. Chronic liver

diseases contribute to most cases of HCC, most frequently as a consequence of

viral hepatitis B (HBV) infection [80]. HCC has a high prevalence in Asian

countries because of endemic HBV infection. However, the incidence of HCC

has been rising in Western countries over the past 20 years due to increasing

rates of viral hepatitis C (HCV) infection and chronic alcoholism [81]. In addition

to HBV and HCV infection, heavy alcohol intake, toxic exposures, non alcoholic

fatty liver disease (NAFLD), nonalcoholic steatohepatitis (NASH), obesity and

diabetes through the development of NAFLD and NASH are also well

documented risk factors leading to hepatocarcinogenesis [80]. It is important to

note that the majority of documented risk factors result in cirrhotic liver damage

as HCC onset is almost exclusively seen in patients suffering from long term liver

inflammation or cirrhosis. HCC in the United States is characterized by significant

variations in incidence by age, gender and race [81]. HCC is rare before age 40,

rises in incidence progressively thereafter peaking between the ages of 70–75

with a mean diagnosis age of approximately 65 years [80]. The racial distribution

of patients is 48% Caucasian, 15% Hispanic, 13% African American, and 24%

other (predominantly Asian) [80]. At all ages and in all racial/ethnic groups in the US, HCC is 3–4 times more common in men than in women with an astounding 74% of cases occurring in men [80]. Higher levels of testosterone, higher body mass index, and higher rates of liver disease are proposed explanations for this significantly increased risk in men [81]. By and large HCC, particularly in the early stages is asymptomatic, going unnoticed until the disease has reached intermediate or advanced stages when conventional therapies are less effective [82]. Treatment options for HCC depend upon the stages, grades and localization of the disease [83]. Standard treatment options for patients afflicted with localized forms of the disease include surgical resection, liver transplantation, radiofrequency ablation, and chemoembolization [84] [85]. Unfortunately, the majority of HCC cases involve advanced tumors with underlying cirrhotic changes wherein surgical resection or transplantation are not viable options [56]. If tumors are not removed, patients generally survive between 3-6 months. Only 10 - 20% of HCC's can be removed completely by surgical [86]. Even after surgical resection, HCC recurrence rate is extremely high culminating into an overall high mortality rate for this disease. One of the primary reasons for such high mortality rates amongst HCC patients is the lack of effective treatment options, especially for those in the more advanced stages of the disease. Although surgery and percutaneous ablation has been shown to achieve long-term control in some early HCC cases, it reappears in close to 50% of such cases after approximately 3 years [86]. Due to the asymptomatic nature of early HCC, the lack of awareness and poorly defined screening strategies, close to

80% of patients present with advanced or unresectable disease [86]. These

patients generally have a very poor prognosis thus treatment options are mainly

palliative [86]. Studies have explored the use of transarterial chemoembolization

(TACE) and systemic therapy with doxorubicin alone or a combination of

cisplatin, IFN, doxorubicin, and 5-fluorouracil (5-FU) as options for patients

ineligible for liver resection, ablation or transplantation [87] [88]. However, clinical

trials incorporating these therapies yielded disappointing results as patients

showed only moderate improvements in survival time [87] [88] This lack of

response to such treatments suggests that chemoresistance may be an inherent

trait of HCC and there are currently no systemic therapies available for the

metastatic disease [89]. Cancer has been described as a DNA disease caused

by the accumulation of alterations in genes in a process of confounding genetic

and epigenetic alterations [90]. It is clear that this theory holds true for

hepatocarcinogenesis. In most cases HCC is a progression from chronic

hepatitis, to cirrhosis, to dysplastic nodules, to malignant tumors. However; clear

and specific sequences of genetic events have yet to be elucidated in the

progression of HCC. The fact that no consistent genomic abnormalities have

been identified in the disease may be largely due to the numerous etiologies

linked to HCC. It is clear that identification of integral molecules involved in the

genetic and subsequent pathway dysregulation is a critical step in the

development of effective therapeutics for the treatment of HCCNF-κB is a key

transcriptional regulator of the inflammatory response and plays an essential role

in regulating inflammatory signaling in the liver [91, 92]. NF-κB activation is a

frequent and early event in human HCC of viral and non-viral etiologies and has been attributed to the acquisition of transformed phenotype during hepatocarcinogenesis [93-97]. Both HBV X protein (HBX) and HCV core protein have been shown to activate NF-κB by multiple mechanisms [95, 98, 99]. Many patients with advanced liver disease present with increased levels of LPS, resulting in activation of NF-κB in the liver [100]. Fatty acids may also activate NF-κB in NAFLD patients [101].

The role of NF-κB in HCC development and progression has been interrogated in several mouse models. Mdr2-/- mice develop spontaneous cholestatic hepatitis and HCC [91]. Overexpression of a non-degradable mutant I IκBα that blocks NF-κB activation significantly inhibited HCC progression in this model [91]. Knockout of IKKβ in hepatocytes abrogated HCC development in a transgenic mouse model overexpressing lymphotoxin α and/or β [102]. These findings indicate that NF-κB activation in hepatocytes is necessary in inflammation-induced HCC. In contrast, hepatocyte-specific knockout IKKβ promoted HCC development in N-nitrosodiethylamine (DEN)-initiation model and hepatocyte-specific knockout of IKKγ (NEMO) resulted in spontaneous development of HCC [103, 104]. ROS-induced JNK and STAT3 activation has been suggested to promote HCC in IKKβ knockout model and IKKβ has been suggested to inhibit both hepatic injury and proliferation [105]. However, deletion of IKKβ in macrophages significantly abrogated DEN-induced HCC [103]. Additionally genetic deletion of IL-6 or inhibition of inflammatory cytokines, such as TNF-α, provided a significant reduction in tumor load [106].

Injury to hepatocytes, such as those caused by DEN, leads to release of IL-1α that activates NF-κB in liver macrophages (Kupffer cells) with subsequent release of cytokines, such as IL-6 [106-108]. IL-6 promotes proliferation and survival of hepatocytes by activating STAT-3 signaling [106]. Thus, NF-κB activation in the tumor microenvironment plays a fundamental role in hepatocarcinogenesis.

III. The Role of AEG-1 in Hepatocarcinogenesis

AEG-1, also known as Metadherin (MTDH) and LYRIC, is an oncogene that is overexpressed in all cancers [53]. AEG-1 overexpression is detected with the progression of cancer, especially in the aggressive metastatic stage, and negatively correlates with poor survival and overall adverse prognosis [53]. *In vitro* studies and investigations using nude mice xenograft and metastatic models with diverse cancer cell lines documented that AEG-1 overexpression induces an aggressive, angiogenic and metastatic phenotype whereas knockdown of AEG-1 inhibits proliferation and invasion and markedly abrogates tumor growth and metastasis [2, 9, 51, 52]. Conversely, siRNA inhibition of AEG-1 effectively inhibited the growth of cancer cells in nude mice xenograft and metastatic models further implicating AEG-1 as an integral component of cancer pathogenesis [51]. AEG-1 plays an important role in regulating hepatocarcinogenesis. Our group previously documented AEG-1 overexpression at both mRNA and protein levels in a high percentage (>90%) of HCC patients and a significant percentage of patients harbored genomic amplification of the

AEG-1 locus in chromosome 8q22 [51]. Immunohistochemical analysis of 109

human HCC patient samples detected variable levels of AEG-1 that directly

correlated with the stages of the disease with 94 percent efficiency, based on the

Barcelona Clinic Liver Cancer (BCLC) staging system (Figure 2A-H) [51]. These

data were further substantiated by gene expression, microarray analysis of 132

human samples. The analysis compared normal liver, cirrhotic liver, low-grade

dysplastic nodules, high-grade dysplastic nodules and HCV-related HCC tissue

samples (Figure 3). AEG-1 expression is significantly increased in HCC as

compared to the normal liver and cirrhotic tissue samples [51]. Microarray

analysis has identified that overexpression of AEG-1 in human HCC cells results

in profound modulation of expression in genes regulating chemoresistance,

senescence, metastasis, angiogenesis and invasion [89]. These same cell lines

also exhibit an AEG-1 mediated upregulation of several cell proliferation and

prosurvival signaling cascades [109] [110] [111] [112]. These findings suggest

that a direct relationship exists between the level of AEG-1 expression and the

stage of the disease. AEG-1 is transcriptionally regulated by c-Myc [15], an

oncogene frequently upregulated in HCC [113]. The tumor suppressor miRNA

miR-375, which is downregulated in HCC patients, targets AEG-1 [21]. Thus

AEG-1 overexpression occurs by multiple mechanisms in HCC patients. HCC

with more microvascular invasion or pathologic satellites, poorer differentiation,

and TNM stages II to III are prone to exhibit higher AEG-1 expression [114]. HCC

patients with high AEG-1 expression documented higher recurrence and poor

overall survival [114, 115]. Overexpression of AEG-1 in a poorly aggressive HCC

cell line HepG3, which expresses low level of AEG-1, significantly increases *in vitro* proliferation, invasion and anchorage-independent growth and *in vivo* tumorigenesis, angiogenesis and metastasis in nude mice [51]. Conversely, knockdown of AEG-1 in highly aggressive QGY-7703 cells, expressing high levels of AEG-1, significantly abrogates *in vivo* tumorigenesis [51, 55]. We have shown that transgenic mice with hepatocyte-specific overexpression of AEG-1 (Alb/AEG-1) do not show spontaneous HCC but develop highly aggressive angiogenic HCC with significantly accelerated kinetics upon treatment with DEN when compared to their WT counterparts [54]. AEG-1 overexpression profoundly modulates expression of genes associated with proliferation, invasion, chemoresistance, angiogenesis and metastasis in both human HCC cell lines and Alb/AEG-1 hepatocytes [51, 54].

Multiple pro-survival signaling pathways, such as NF-κB, PI3K/Akt, Wnt/β-catenin and MEK/ERK, become activated upon overexpression of AEG-1 in human cancer cells and Alb/AEG-1 hepatocytes [51, 54]. Pharmacological and genetic inhibition studies have elucidated the importance of all these signaling pathways in mediating AEG-1-induced oncogenesis [51]. However, apart from NF-κB, the molecular mechanism by which AEG-1 activates these signaling pathways is not known. More importantly, whether AEG-1 is required for activation of these pathways under physiological conditions has not been investigated. We have documented that AEG-1 directly interacts with the p65 subunit of NF-κB and CBP thereby functioning as a bridging factor between NF-κB and basal transcriptional machinery promoting NF-κB-induced transcription

[11, 12]. A recent study has documented that AEG-1, anchored on the ER membrane, associates with upstream ubiquitinated activators of NF-κB, such as RIP1 and TRAF2, facilitating their accumulation and subsequent NF-κB activation [116].

In this chapter, the response of AEG-1 knock-out (AEG-1KO) mouse to DEN-induced HCC development and progression is analyzed. The experiments described here unravel a fundamental role of AEG-1 in regulating NF-κB activation, especially in the tumor microenvironment, thereby rendering AEG-1KO mice to be significantly resistant to initiation and progression of HCC.

IV. Materials and methods
Mouse model:

AEG-1KO mouse was generated in C57BL/6:129/Sv background and the procedure is described in detail in the supplement. We have backcrossed the line to C57BL/6 for 10 generations and obtained similar results for both the WT and AEG-1KO mice on the C57BL/6 background as on the C57BL/6:129/Sv background. AEG-1KO mice were viable and fertile, although litter sizes were very small (1-2 pups per litter). Further, even litters generated by crossing AEG-1+/- breeding pairs were very small (2-3 pups per litter), which precluded generating large numbers of WT and AEG-1KO mice as littermates. Therefore, the majority of the experiments were carried out with age-matched mice generated by breeding WT and AEG-1KO mice separately. However, it should be noted that the same phenotypes were observed in AEG-1KO mice generated from AEG-1+/- X AEG-1+/- mating as from AEG-1KO X AEG-1KO mating. Thus our findings are not restricted to strains or littermates. All animal studies were approved by the Institutional Animal Care and Use Committee at Virginia Commonwealth University, and were conducted in accordance with the Animal Welfare Act, the PHS Policy on Humane Care and Use of Laboratory Animals, and the U.S. Government Principles for the Utilization and Care of Vertebrate Animals Used in Testing, Research, and Training.

Cell culture:

Primary mouse hepatocytes were isolated as described [54] and were cultured in Williams E medium containing $NaHCO_3$, L-glutamine, insulin (1.5 uM) and dexamethasone (0.1 uM) at 37°C and in 5% CO_2. For isolating primary perinoeal macrophages, mice were injected i.p. with 4% thioglycollate and 4 days later macrophages were harvested in PBS via i.p. injection. Macrophages were cultured in Dulbecco's Modified Eagle's Medium with 10% fetal calf serum at 37°C and in 5% CO_2.

Transient transfection and luciferase assay:

For transfections, 1×10^5 hepatocytes were plated in 24-well collagen coated plates and the next day transfected using Promofectin-Hepatocyte transfection reagent in 9:1 ratio of NF-κB luciferase reporter plasmid and renilla luciferase reporter plasmid. After 48 hours, cells were treated with LPS (200 ng/ml) for 24 h. Luciferase assays were measured using Dual Luciferase Reporter Assay kit (Promega) following manufacturer's protocol and firefly luciferase activity was normalized by renilla luciferase activity. Each experiment was performed in triplicates and three times to calculate means and standard errors.

Total RNA extraction, cDNA preparation and Real time PCR:

Total RNA was extracted from hepatocytes, macrophages or mouse tissues using the QIAGEN miRNAeasy Mini Kit (QIAGEN, Valencia, CA). cDNA preparation was done using ABI cDNA synthesis kit (Applied Biosystems, Foster

City, CA). Real-time polymerase chain reaction (RT-PCR) was performed using an ABI ViiA7 fast real-time PCR system and Taqman gene expression assays according to the manufacturer's protocol (Applied Biosystems, Foster City, CA).

RNA sequencing (RNA-Seq):

Total RNA, extracted using Qiagen miRNAeasy mini kit (Qiagen, Valencia, CA) from livers of 3 adult mice per group, was employed for RNA sequencing. RNA-Seq library was prepared using Illumina TruSeq RNA sample preparation kit and sequenced on Illumina HiSeq2000 platform. RNA-Seq libraries were pooled together to aim about 25-40M read passed filtered reads per sample. All sequencing reads were aligned with their reference genome (UCSC mouse genome build mm9) using TopHat2 and the Bam files from alignment were processed using HTSeq-count to obtain the counts per gene in all samples. The counts were read into R software using DESeq package and plot distributions were analyzed using Reads Per Kilobase Million (RPKM) values. Data were filtered based on low count or low RPKM value (<40 percentile). Pairwise tests were performed between each group using the functions in DESeq. Genes showing log2 fold-change of >1.5 or <-1.5, FDR of <0.1 and p-value of <0.01 were selected.

Statistical analysis:

Data were represented as the mean ± Standard Error of Mean (S.E.M) and

analyzed for statistical significance using one-way analysis of variance (ANOVA)

followed by Newman-Keuls test as a post hoc test.

V. Results

A. AEG-1KO Mice are Resistant to Age Associated Spontaneous Tumor Formation

No histological difference was observed in the internal organs of young adult AEG-1KO (8-12 weeks old) mice when compared to WT littermates or age-matched WT mice (Fig. 3.1A). Analysis of bone marrow, peripheral blood cells and spleen cell composition at this age also showed no difference (Table 3.1, Table 3.2 and Fig. 3.2). However, when aged (16 months), spontaneous age associated-tumorigenesis was observed in multiple organs a number of WT mice, however this phenomenon was completely absent in the AEG-1KO mice (n = 20) (Fig. 3.1A and 3.1B). Age-associated lymphoma and adenocarcinoma were observed in the liver, adenocarcinoma and carcinoid tumors were observed in the lungs and myxoma was observed in the heart of the aged WT mice.

A.

AEG-1KO

100x   400x

Liver

Lung

Spleen

Kidney

Heart

B.

WT

100x   400x

Liver Lymphoma

Liver Adenoca

Lung Adenoca

Lung Carcinoid

Heart Myxoma

C.

100x   400x

WT

D.
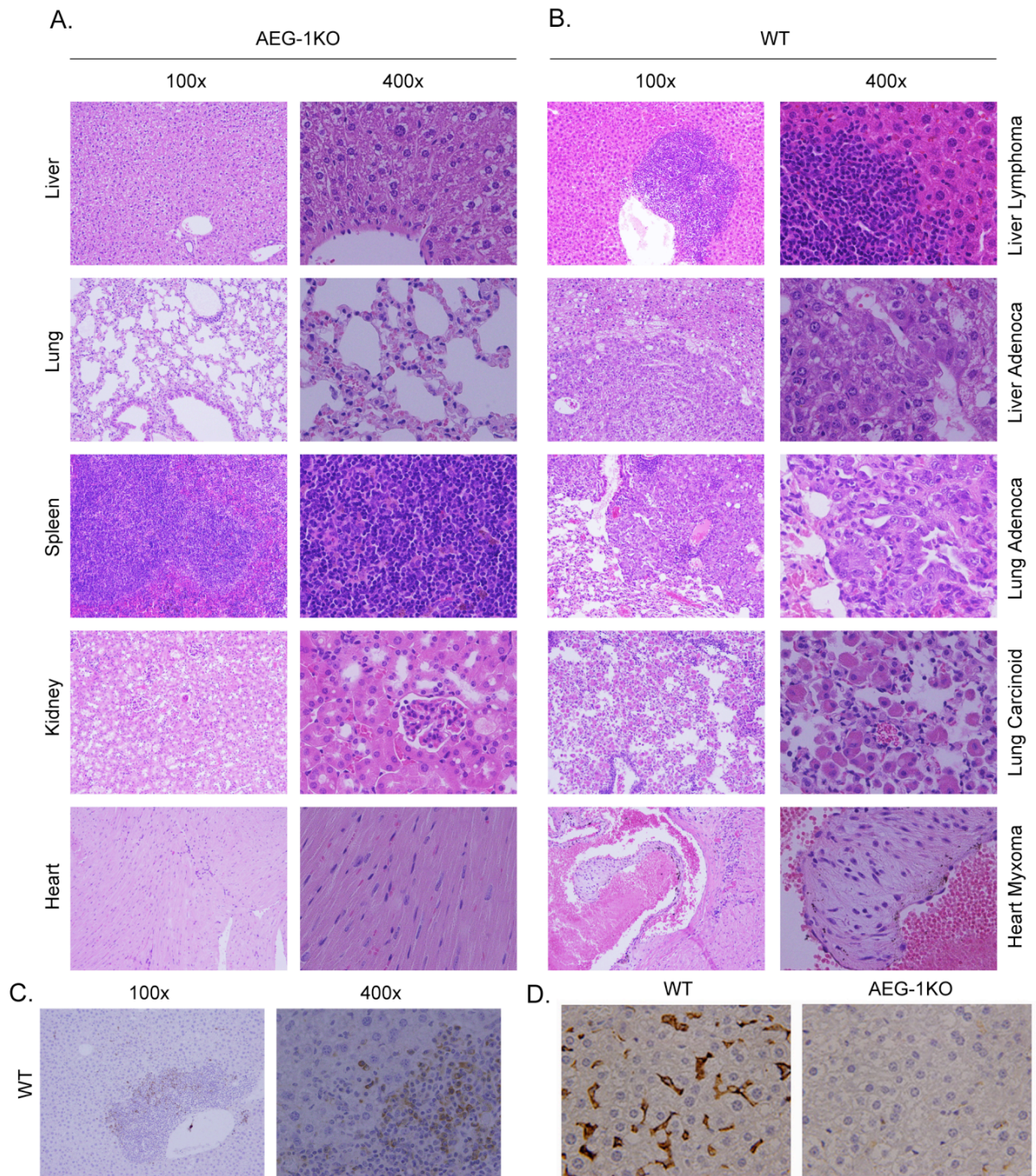
WT   AEG-1KO

Figure 3.1 AEG-1KO mice are resistant to age-associated spontaneous tumorigenesis.
A. H & E staining of the indicated tissue sections of aged (16 m) AEG-1KO mouse
demonstrating maintenance of normal histology and architecture. B. H & E staining of
sections of liver, lung and heart of aged (16 m) WT mouse showing tumors. C.
Immunohistochemical staining for AEG-1 in liver lymphoma of WT mouse. D. F4/80
staining for macrophages in liver sections of aged (16 m) WT and AEG-1KO mouse.

Table 3.1. Differential count of bone marrow cells of adult WT and AEG-1KO mice.
Bone marrow was collected from 8 weeks old WT and AEG-1KO mice. Bone marrow smear was made and stained. Two hundred cells were counted to obtain differential count.

Differential count	WT	AEG-1KO
Myeloblasts	0	0
Promyelocytes	1	1
Myelocytes	2	2
Metamyelocytes	4	6
Bands/Segs	49	46
Eosinophils	2	1
Basophils	0	0
Lymphocytes	11	7
Plasma cells	1	1
Monocytes	2	3
Erythroids	28	33

Table 3.2. Complete blood count of peripheral blood in WT and AEG-1KO mice.
Peripheral blood was collected from WT and AEG-1KO mice and analyzed for complete blood count. WBC: white blood cells; RBC: red blood cells; HCT: hematocrit; MCV: mean corpuscular volume.

Parameter	WT	AEG-1KO
Total WBCs ($\times 10^3/\mu l$)	20	20
RBCs ($\times 10^6/\mu l$)	9.96	9.83
Platelets ($\times 10^3/\mu l$)	1,072	1,021
Hemoglobin (g/dL)	13.9	13.9
HCT (%)	49.9	49.8
MCV (fL)	49.5	50.7
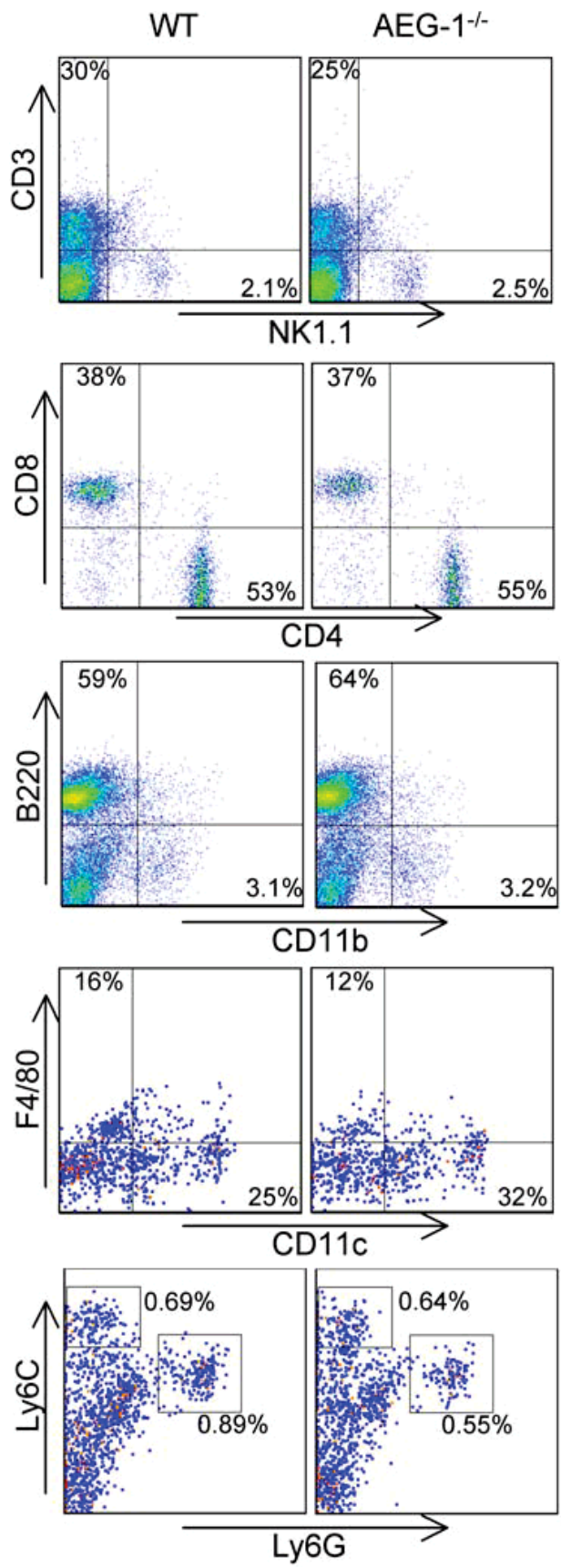
Figure 3.2. Analysis of spleen cells of adult WT and AEG-1KO mice. Spleen leukocyte as analyzed by flow cytometry show no significant differences between wild-type and AEG-1KO mice in: the frequency of NK1.1+CD3- natural killer cell, CD3+ T cell or their subsets (i.e., CD4+CD3+, CD8+CD3+), B220+ B cell, CD11b+ myeloid cell or their subsets, including macrophage (CD11b+F4/80+), dendritic cell (CD11b+CD11c+), monocyte (CD11b+Ly6C^{high}Ly6G-), or neutrophils (CD11b+Ly6C^{low}Ly6G+).

Interestingly the spontaneous tumors developing in the livers of WT mice stained strongly for AEG-1, especially those cells invading into the surrounding liver parenchyma, further confirming the essential role of AEG-1 in regulating tumor invasion (Fig. 3.1C). Marked infiltration of macrophages, evidenced by staining for macrophage marker F4/80, was observed in the aged (16 m old) WT liver but not in AEG-KO liver (Fig. 3.1D). No difference in infiltration of neutrophils was observed between aged WT and AEG-1KO mice, as evidenced by absence of Ly6G staining (Fig. 3.3). This data suggests that aging-associated chronic inflammatory responses are blunted in AEG-1KO mice.
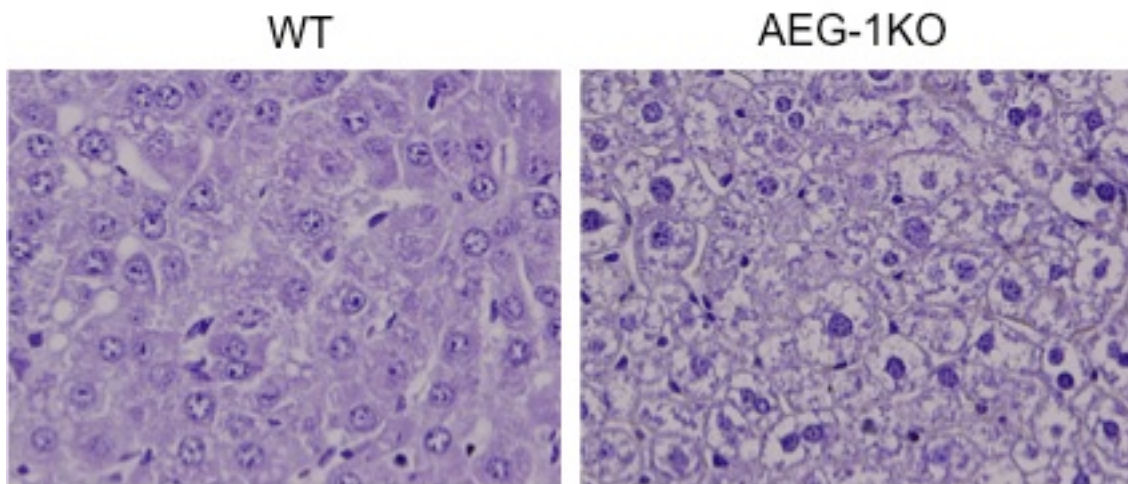
Figure 3.3. Ly6G staining for neutrophils in liver sections of aged (16 m) WT and AEG-1KO mouse. Magnification: 400X.

B. AEG-1KO Mice are Resistant to Experimental Hepatocarcinogenesis

WT and AEG-1KO mice were given a single i.p. injection of DEN (30 ug/gm) and tumorigenesis was monitored at 32 weeks. Compared to WT mice, AEG-1KO mice showed profound resistance to DEN-induced HCC. AEG-1KO mice either resisted tumorigenesis altogether or developed very small nodules (<2mm) (Table 3.3 and Fig. 3.4A). WT livers presented with AFP-positive HCC with vascular invasion (arrow in Fig. 3.4B) and high AEG-1 expression, while the liver architecture was preserved in AEG-1KO mice (Fig. 3.4B). Serum levels of aspartate aminotransferase (AST), alanine aminotransferase (ALT) and alkaline phosphatase (Alk Phos) were significantly higher in WT mice as compared to AEG-1KO mice indicating liver damage (Fig. 3.4C).

A.

WT | AEG-1KO

B.

WT | AEG-1KO

H & E

AFP

AEG-1

C.
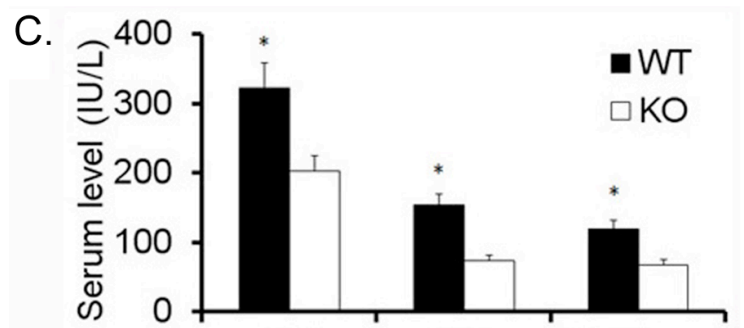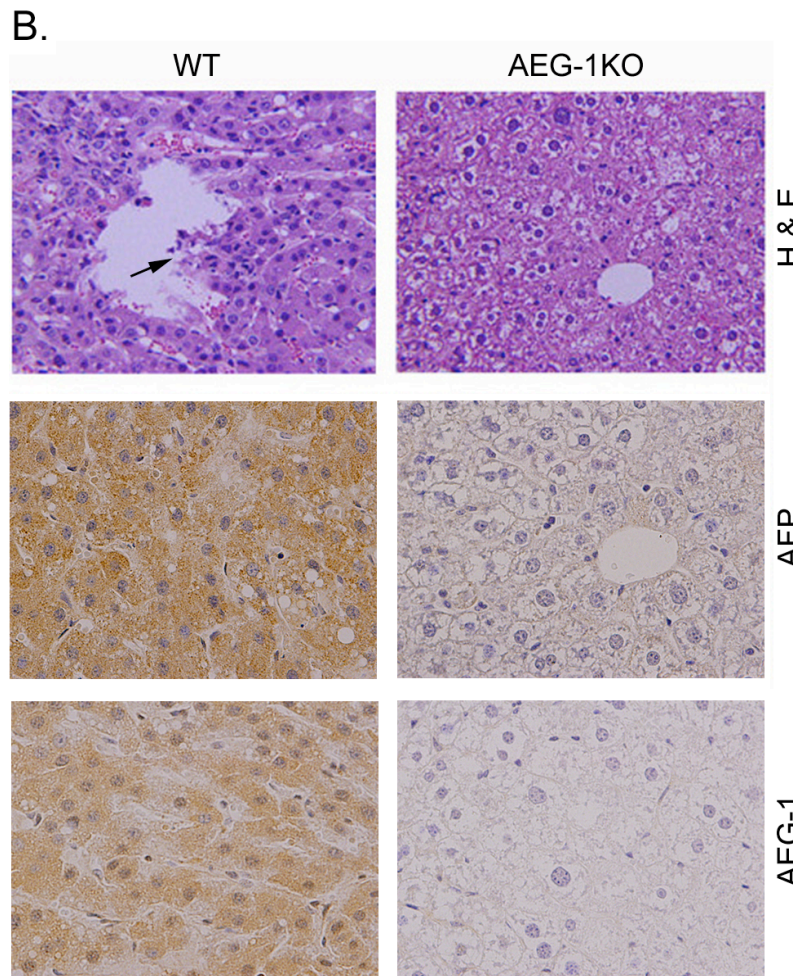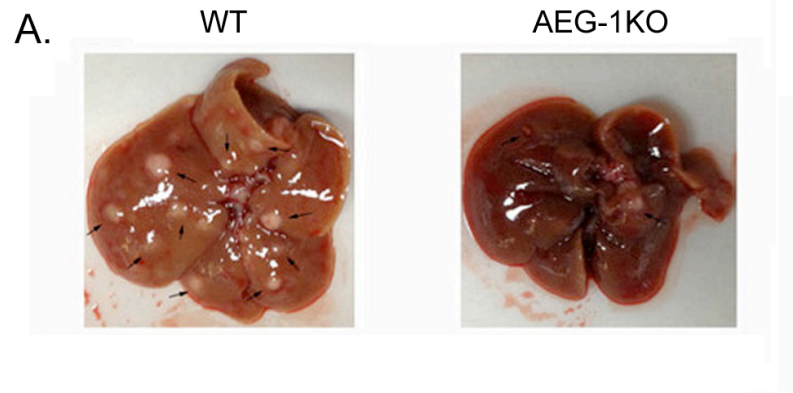
Figure 3.4. AEG-1KO mice are resistant to experimental hepatocarcinogenesis. A. Representative photograph of the livers of WT and AEG-1KO mice 32 weeks after DEN injection. B, top panel, H & E staining of liver sections; middle panel, AFP staining of the liver sections; bottom panel, AEG-1 staining of the liver sections. These samples were collected at 32 weeks after DEN injection. C. Serum levels of the indicated liver enzymes at the end of the study. AST: aspartate aminotransferase, ALT; alanine aminotransferase and Alk Phos: alkaline phosphatase. Data represent mean ± SEM. n = 12 for WT and n = 8 for AEG-1KO. *: p<0.01.

Table 3.3. Number of liver nodules in DEN-treated WT and AEG-1KO mice.

	ID#	Total no. of nodules	<1mm	1-2mm	3-5mm	6-8mm	>8mm
WT	1	12	0	12	0	0	0
	2	91	0	91	0	0	0
	3	92	0	0	75	15	2
	4	10	0	8	0	2	0
	5	49	0	46	0	3	0
	6	56	0	0	50	4	2
	7	8	0	6	2	0	0
	8	15	0	0	14	0	1
	9	10	0	0	8	0	2
	10	16	0	14	1	0	1
	11	14	0	0	13	0	1
	12	23	0	21	1	0	1
AEG-1KO	1	0	0	0	0	0	0
	2	5	5	0	0	0	0
	3	8	6	0	2	0	0
	4	0	0	0	0	0	0
	5	10	10	0	0	0	0
	6	0	0	0	0	0	0
	7	2	2	0	0	0	0
	8	2	2	0	0	0	0

One important aspect of AEG-1 is its ability to induce metastasis. We therefore tested a more aggressive experimental procedure where tumorigenesis was induced by injection of DEN (10 ug/gm) and then it was promoted by providing phenobarbital (PB; 0.05%) daily in drinking water. Tumorigenesis was monitored at 28 weeks. WT mice exhibited an intensified hepatocarcinogenic response evidenced by large necrotic liver tumors with a 52% rate of lung metastasis (Fig. 3.5A). AEG-1KO mice remained remarkably resistant even to this combinatorial treatment with no distant metastasis. Histological analysis of liver demonstrated HCC in WT mice (Fig. 3.5B). Although some level of dysplasia was observed in AEG-1KO mice, frank HCC was not detected. The metastatic nodules in the WT lung were positive for AFP indicating that the nodules originated in the liver (Fig. 3.5C).

A.

WT   AEG-1KO

B.

WT   AEG-1KO

Liver   H & E

C.

WT   AEG-1KO

Lung   H & E

AFP

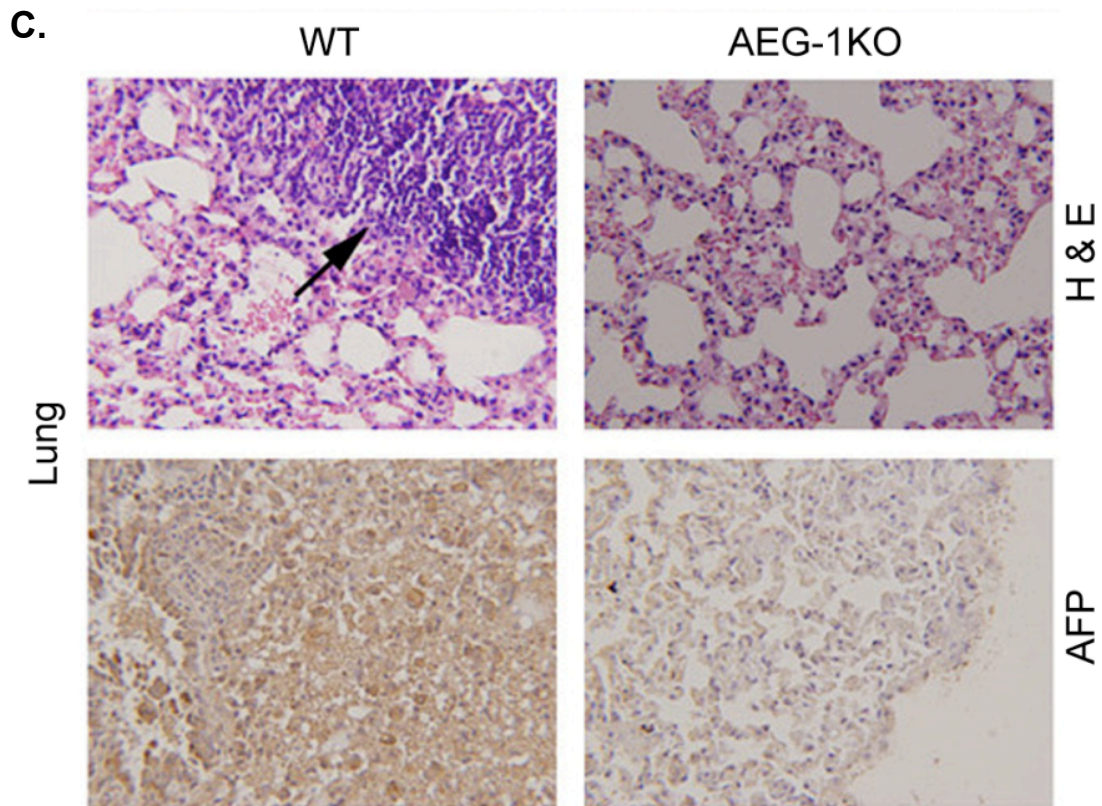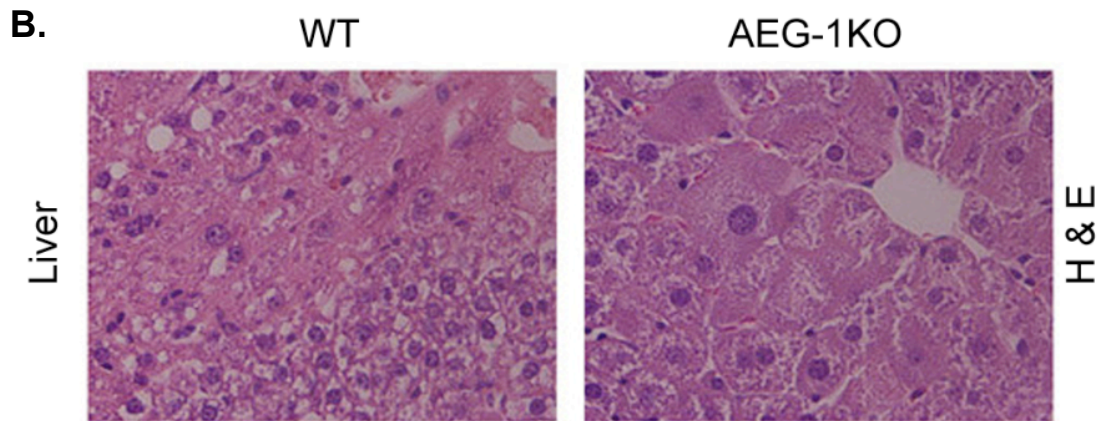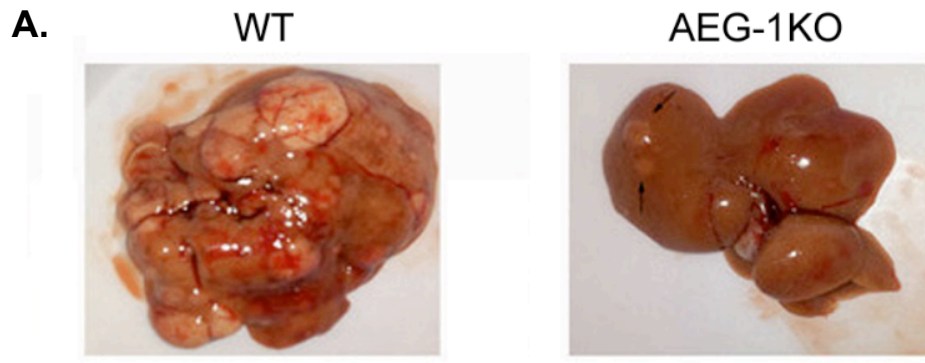**Figure 3.5 AEG-1KO mice are resistant to experimental hepatocarcinogenesis and metastasis.** A. Representative photograph of the livers of WT and AEG-1KO mice 28 weeks after initial DEN injection receiving PB in drinking water. B. H & E staining of liver sections at 28 weeks. C. top panel, H & E staining of the lungs showing lung metastasis in WT mouse; bottom panel, AFP staining of a metastatic lung tumor in WT mouse.

Staining for macrophage marker F4/80 showed significant infiltration of macrophages both in DEN- and DEN/PB-treated WT tumors but not in AEG-1KO livers (Fig. 3.6A). Quantification of macrophage infiltration is shown in (Fig. 3.6B). We stained DEN-treated WT and AEG-1KO liver for α-smooth muscle actin (α-SMA) as an indicator of activation of stellate cells and fibrogenic response. A substantial increase in α-SMA staining was observed in the tumor in WT mice when compared to non-tumor region (Fig. 3.6C). α-SMA staining in AEG-1KO liver was similar to that in the non-tumor region of WT liver.

A.

WT   AEG-1KO

DEN

DEN/PB

F4/80

B.

C.

WT   AEG-1KO

Tumor

Non-tumor

118
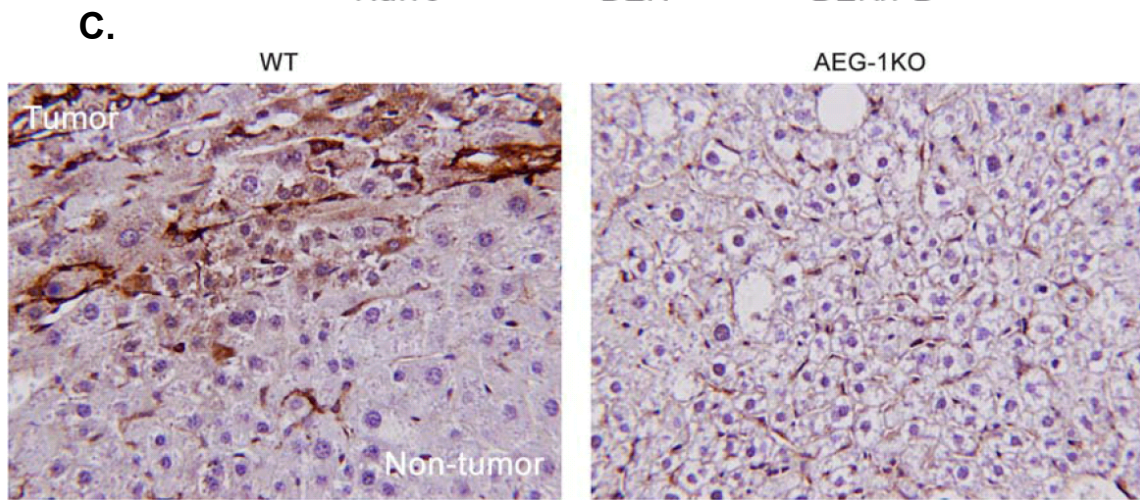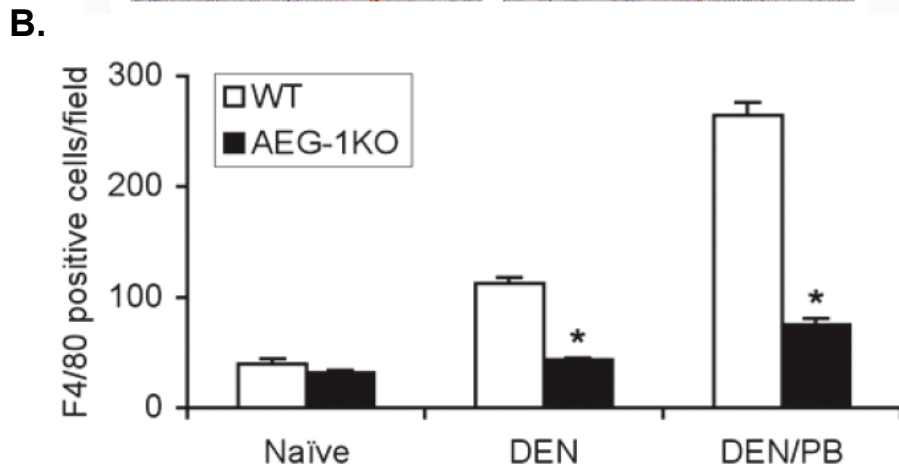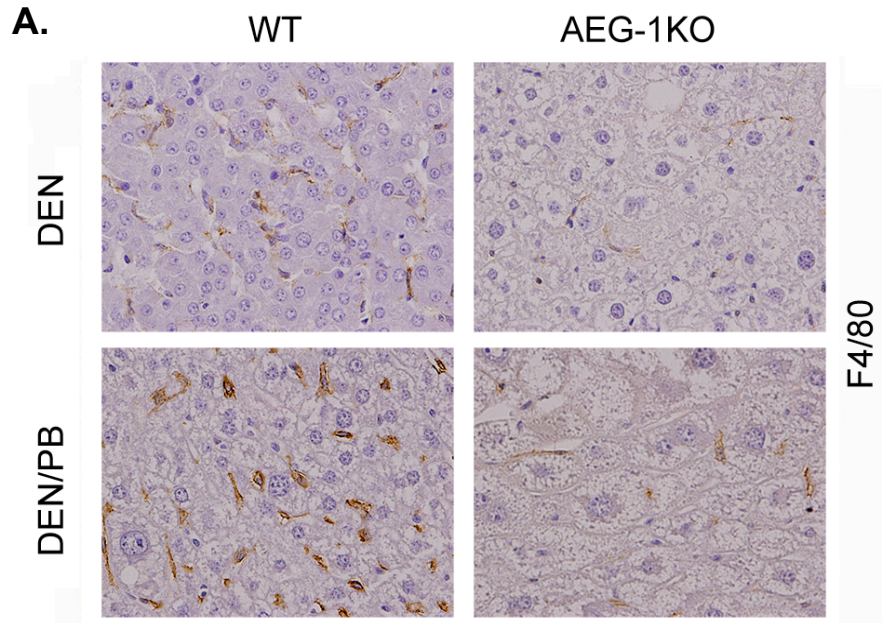
Figure 3.6 Macrophage and Stellate cell activity in the liver of AEG-1 and WT mice. A. F4/80 staining for macrophages in liver sections of WT and AEG-1KO mice treated with DEN alone (top panels) or DEN/PB (bottom panels). B. Graphical representation of quantification of F4/80 staining for macrophages in liver sections of WT and AEG-1KO mice either untreated (naïve) or treated with DEN or DEN/PB. N=3/group. At least 9 fields were counted for each mouse section. Data represent mean ± SEM. *: $p<0.01$. C. Stellate cells are activated in the tumor region of WT liver. DEN-treated liver sections from WT and AEG-1KO mice were stained for α-SMA. Note increased staining for α-SMA only in the tumor of WT mouse. Magnification 200X.

A possible cause of the pronounced resistance of AEG-1KO mice to DEN-induced HCC might be improper metabolism of DEN in these mice so that DEN is not capable of adequately damaging hepatocytes. To rule out this possibility we injected WT and AEG-1KO 2 wks old pups with DEN and then measured serum liver enzymes 48 h later. Both WT and AEG-1KO mice showed significant induction of liver enzymes indicating that DEN could damage both WT and AEG-1KO hepatocytes in a similar manner (Table 3.4).

Table 3.4. Liver enzyme levels in mouse sera 48 h after injection of DEN. Three WT and three AEG-1KO mice were used, 10 μg/gm of DEN was delivered by intra peritoneal injection.

	AST (IU/L)	ALT (IU/L)	Alk Phos (IU/L)
WT1	357	104	1116
WT2	143	80	792
WT3	1080	219	1380
AEG-1KO1	246	166	706
AEG-1KO2	198	98	571
AEG-1KO3	252	200	626

C. Growth Factor Signaling is not Altered in AEG-1KO Mice

Activation of pro-survival signaling pathways, such as PI3K/AKT, MEK/ERK and β-catenin, have been shown to play a role in mediating oncogenic effects of overexpressed AEG-1 in human HCC cells as well as in Alb/AEG-1 mice. We treated naïve primary WT and AEG-1KO hepatocytes with epidermal growth factor (EGF) (50 ng/mL) and analyzed temporal activation of EGFR, AKT and ERK1/2. Both WT and AEG-1KO hepatocytes showed similar kinetics and magnitude of activation suggesting that AEG-1 does not modulate growth factor signaling under physiological conditions (Fig. 3.7). Similarly no difference was observed in the activated (phosphorylated) forms of AKT, ERK1/2 and β-catenin in adult WT and AEG-1KO liver samples under normal basal conditions (Fig. 3.8A). These results indicate that AEG-1 is not required for physiological regulation of Akt, ERK1/2 and β-catenin. We next evaluated the activation of these signaling pathways in DEN-treated WT and AEG-1KO liver samples (Fig. 3.8B). No significant difference was observed in the activation of AKT, ERK1/2 and β-catenin in the two groups. In naïve mice, inhibition in activated STAT3 and p65 NF-κB, known regulators of HCC, was observed in AEG-1KO livers *versus* WT (Fig. 3.9A). DEN-treatment induced a robust activation of both p-p65 (NF-κB) and p-STAT3 in WT mice but not in AEG-1KO mice (Fig. 3.9A). These findings were confirmed by immunohistochemistry (IHC) in DEN-treated liver samples (Fig. 3.9B). In addition, DEN-treatment induced a significant increase in IL-6 protein level in liver homogenates of WT but not in AEG-1KO mice (Fig. 3.10).
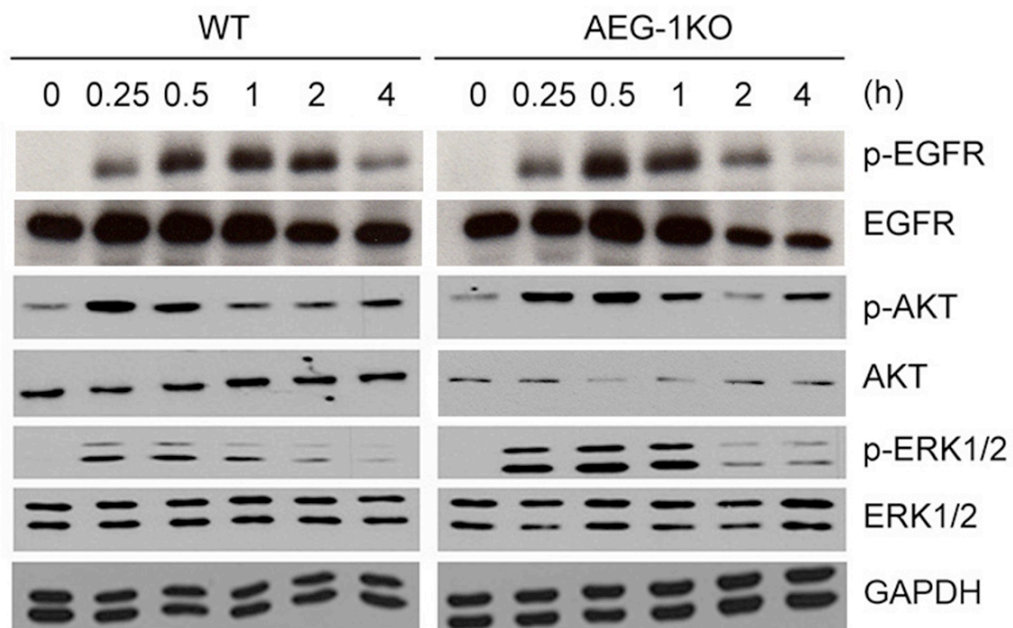
Figure 3.7 Knockout of AEG-1 does not affect hepatocyte response to growth factors
WT and AEG-1KO hepatocytes were treated with EGF (50 ng/mL) for the indicated time points and Western blotting was performed for the indicated proteins

Figure 3.8 Pathway activation in naïve and DEN treated livers. A. Western blot was performed for the indicated proteins using liver lysates from adult WT and AEG-1KO mice. B. Western blotting was performed for the indicated proteins using liver lysates from DEN-treated WT and AEG-1KO mice at the end of the study. Each lane represents one independent mouse.
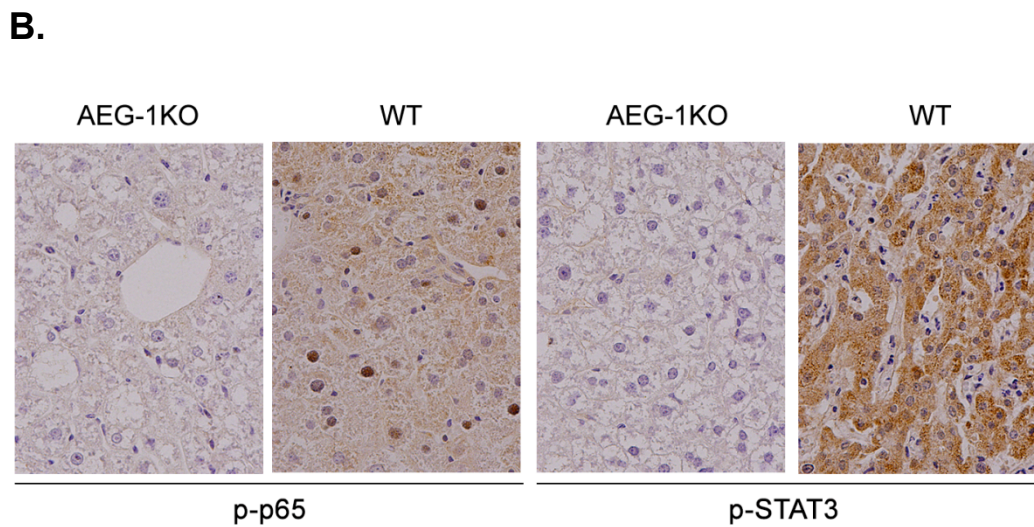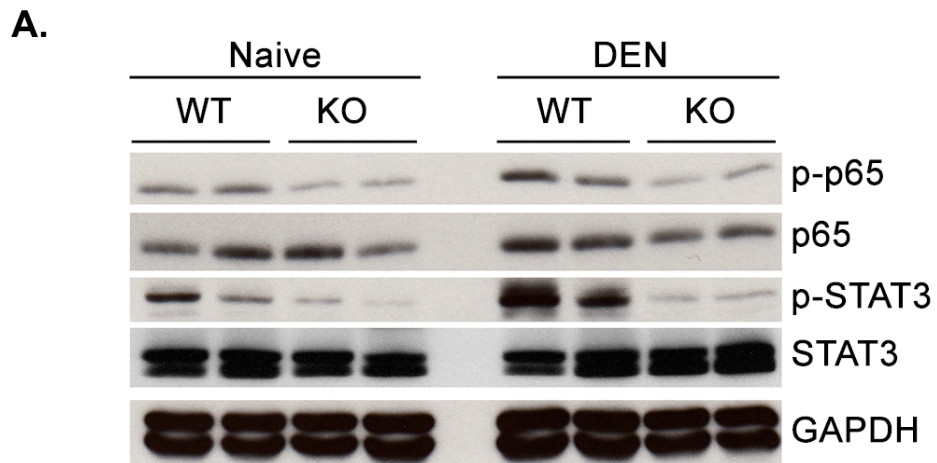
Figure 3.9 NF-κB and STAT3 activation is inhibited in AEG-1KO mice. A. Western blotting was performed for the indicated proteins using liver lysates from naïve and DEN-treated WT and AEG-1KO mice at the end of the study. Each lane represents one independent mouse. B. DEN-treated liver sections were stained for p-STAT3 and p-p65 NF-κB at the end of the study.
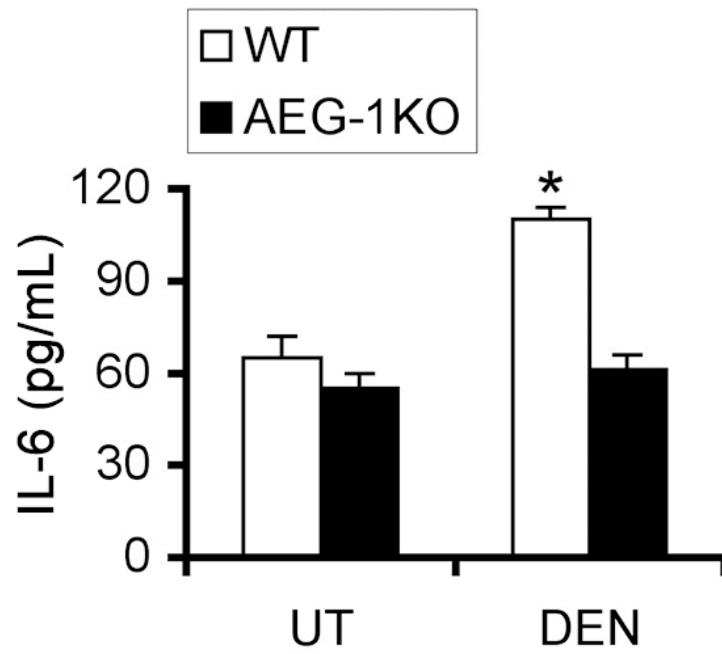
Figure 3.10 IL-6 protein level was measured in DEN-treated liver homogenates by ELISA. Data represent mean ± SEM. n = 5. *: p<0.01.

D. NF-κB Activation is Abrogated in AEG-1KO Mice

We measured NF-κB luciferase reporter activity in primary hepatocytes isolated from WT and AEG-1KO mice. Both basal and LPS-induced luciferase activity was significantly blunted in AEG-1KO hepatocytes when compared to WT hepatocytes (Fig. 3.11A). As a corollary LPS-induced phosphorylation (Fig. 3.11B) and nuclear translocation (Fig. 3.12) of the p65 subunit of NF-κB and induction of NF-κB-target genes IL-1β and IL-6 (Fig. 3.11C) were significantly abrogated in AEG-1KO hepatocytes versus WT hepatocytes. Since NF-κB activation in macrophages is crucial for HCC, we next analyzed peritoneal macrophages isolated from WT and AEG-1KO mice.
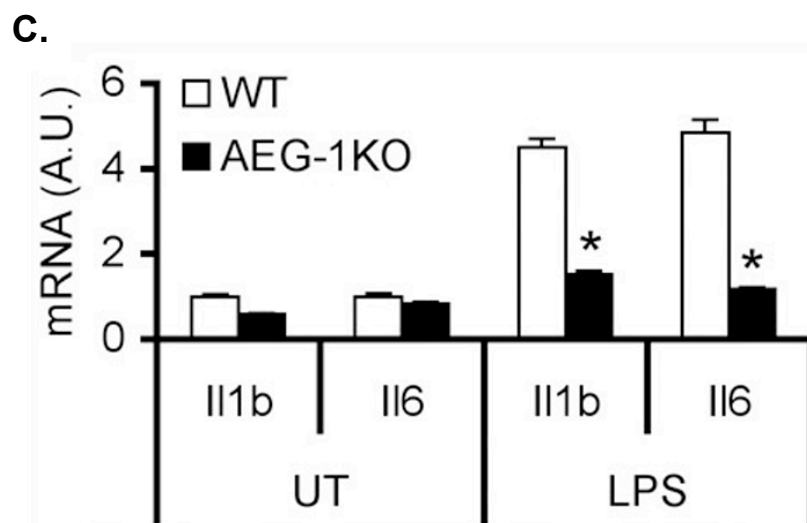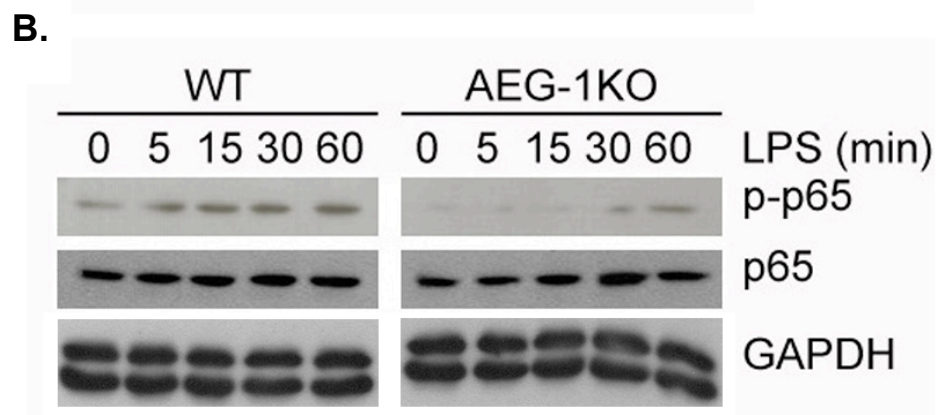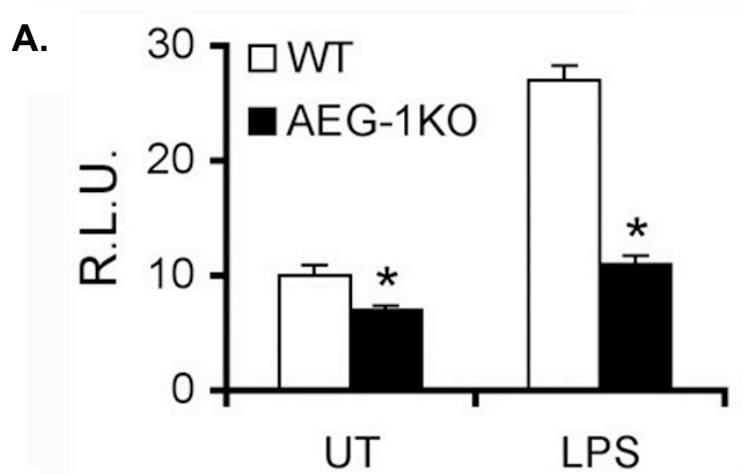
Figure 3.11 NF-κB activation is inhibited in AEG-1KO hepatocytes. A. NF-κB luciferase reporter activity was measured in WT and AEG-1KO hepatocytes. Firefly luciferase activity was normalized by Renilla luciferase activity. The activity of empty pGL3-basic vector was considered as 1. R.L.U.: Relative luciferase units. Data represent mean ± SEM of three independent experiments. *: p<0.01. B. WT and AEG-1KO hepatocytes were treated with LPS for the indicated time points a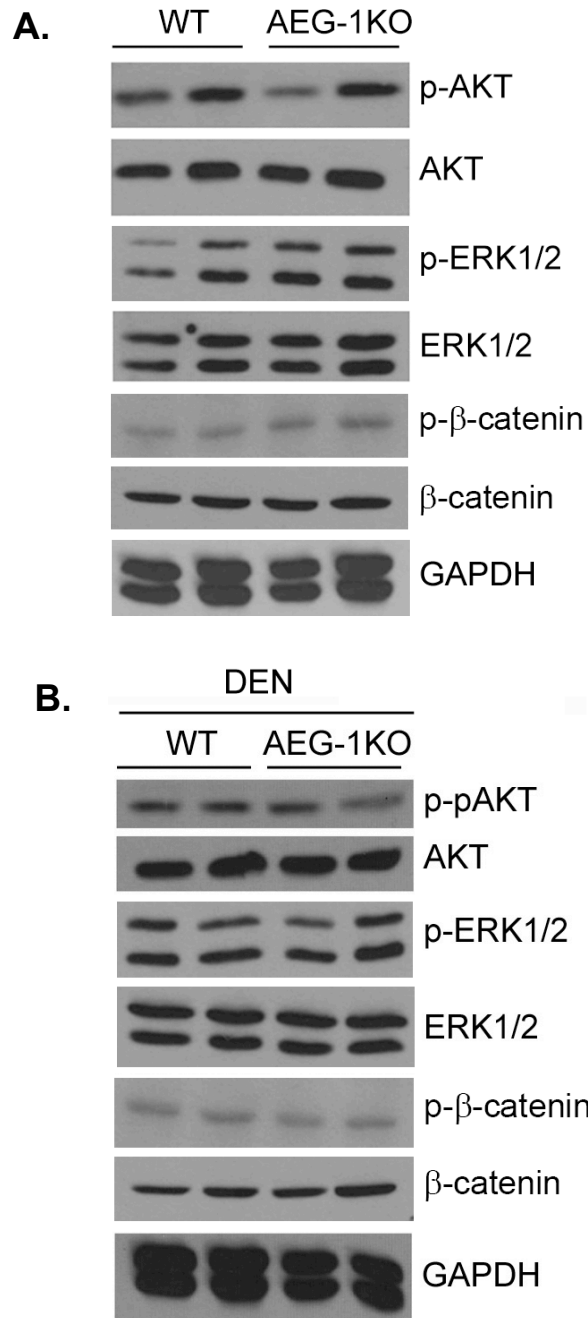nd Western blotting was performed for the indicated proteins. C. WT and AEG-1KO hepatocytes were treated with LPS for 4 h and the mRNA level of Il1b and Il6 was measured by Taqman Q-RT-PCR. Data represent mean ± SEM of three independent experiments. *: p<0.01.

DAPI   **p65**   **Merge**   **LPS**

WT

0 min

30 min
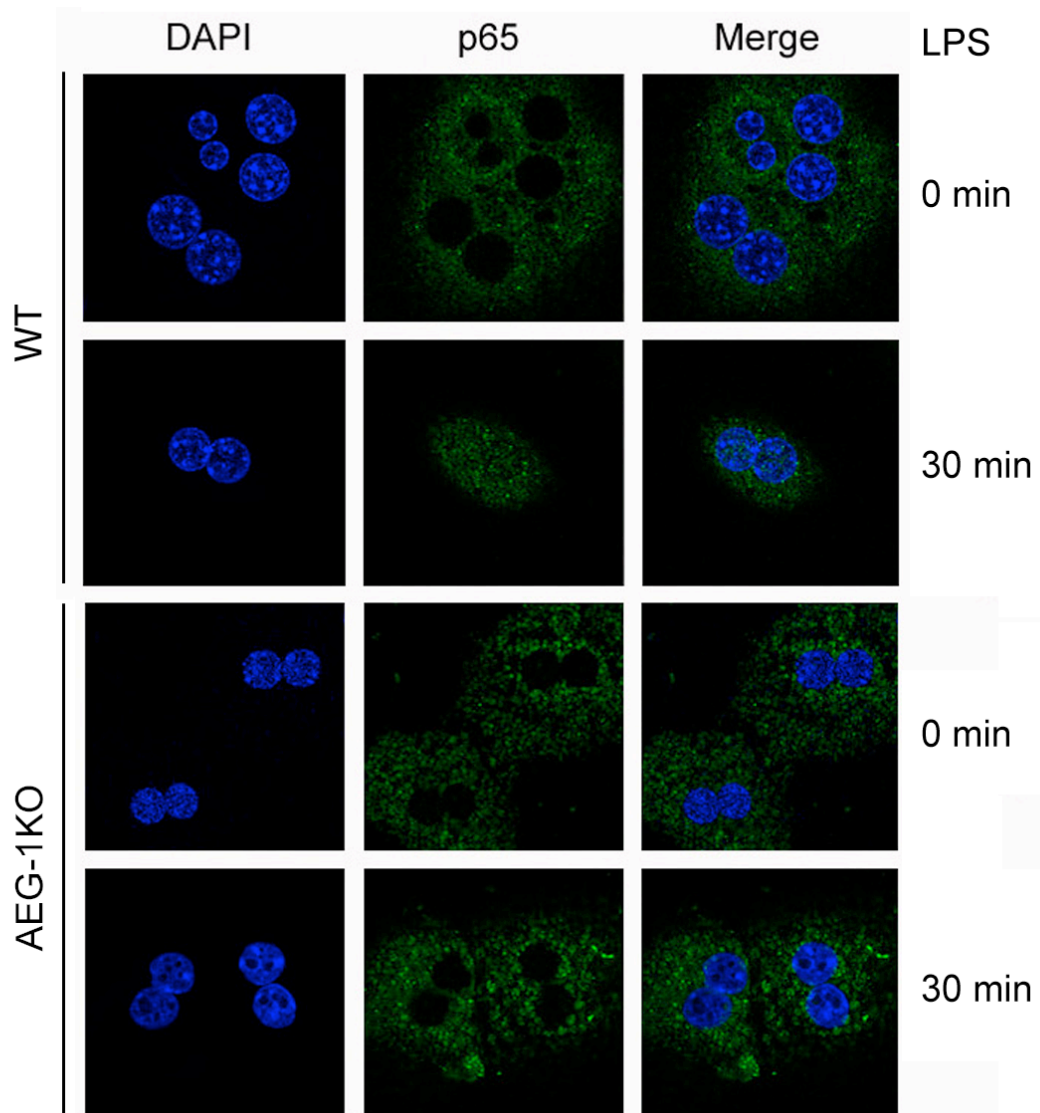
AEG-1KO

0 min

30 min

Figure 3.12 NF-κB localization is inhibited in AEG-1KO hepatocytes.
Immunofluorescence followed by confocal microscopy of WT and AEG-1KO hepatocytes after LPS treatment for 30 min showing p65 nuclear translocation.

AEG-1 mRNA expression in macrophages was significantly higher

compared to that in hepatocytes (Fig. 3.12). In primary hepatocytes AEG-1 is

localized predominantly in the nucleus while in macrophages it is located both in

the nucleus and in the cytoplasm (Fig. 3.13A). Upon LPS treatment nuclear

translocation of p65 NF-κB was substantially abrogated in AEG-1KO

macrophages compared to WT macrophages (Fig. 3.13B). LPS-mediated

induction of IL-6 and IL-1β was also markedly blunted in AEG-1KO peritoneal

macrophages versus WT (Fig. 3.14A-B). We collected conditioned media (CM)

from LPS-treated WT and AEG-1KO hepatocytes and treated WT and AEG-1KO

macrophages with the CM. CM from WT hepatocytes induced IL-6 mRNA

expression only in WT macrophages but not in AEG-1KO macrophages (Fig.

3.14C). Additionally CM from AEG-1KO hepatocytes failed to induce IL-6 mRNA

in either WT or AEG-1KO macrophages.
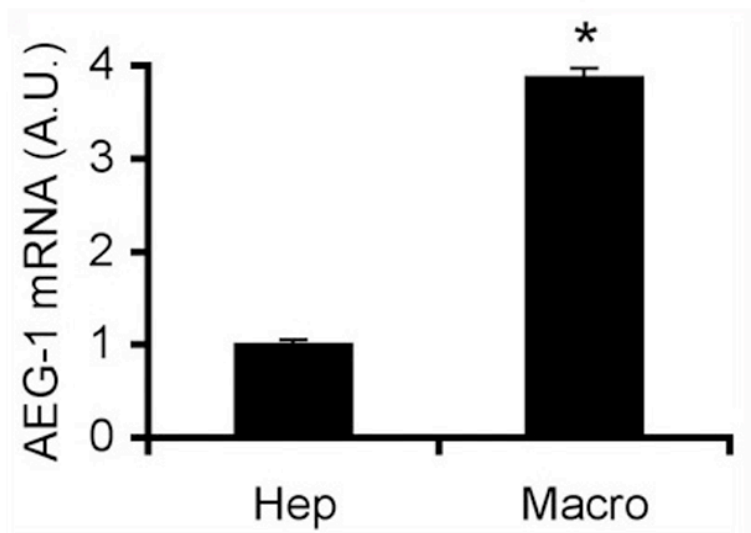
Figure 3.13 AEG-1 Expression in primary mouse hepatocytes and macrophages. mRNA level in hepatocytes and macrophages of WT mice measured by Taqman Q-RT-PCR. A.U.: arbitrary unit. Data represent mean ± SEM of three independent experiments. *: p<0.01.
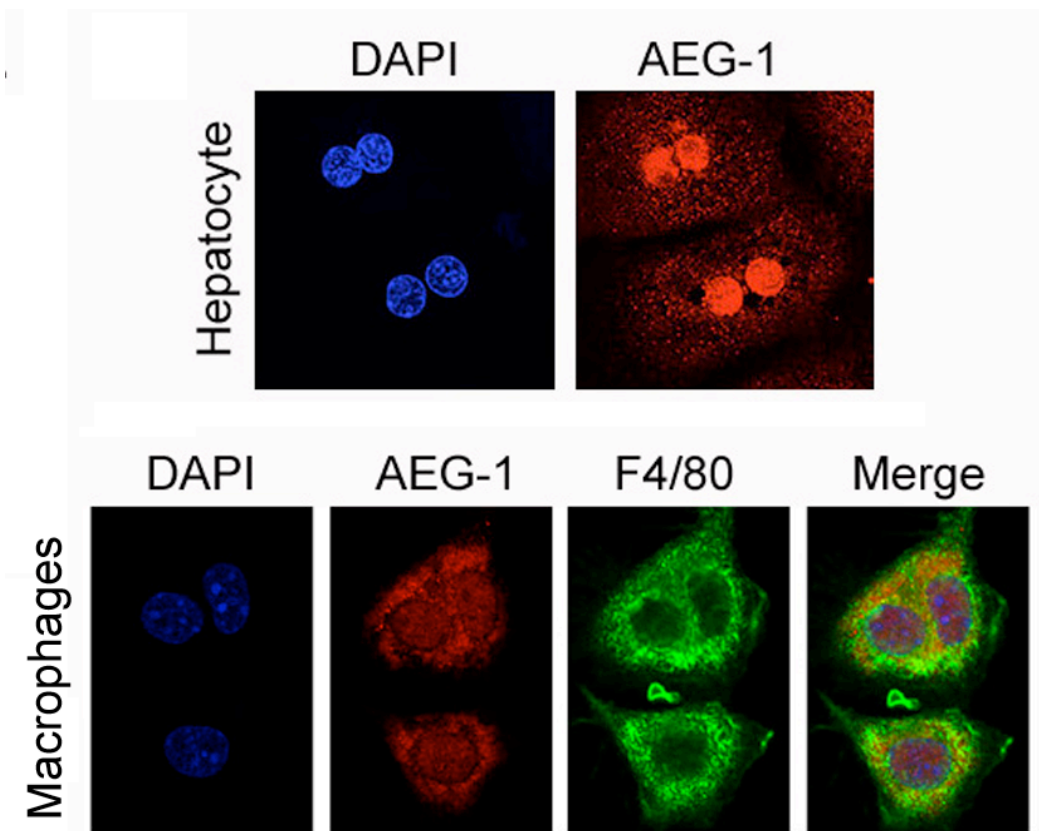
Figure 3.14 Subcellular localization of AEG-1 in WT hepatocytes and macrophages.
Immunofluorescence staining showing subcellular localization of AEG-1 in WT
hepatocytes and macrophages. F4/80 staining was performed in macrophages to
demonstrate authenticity of purification.
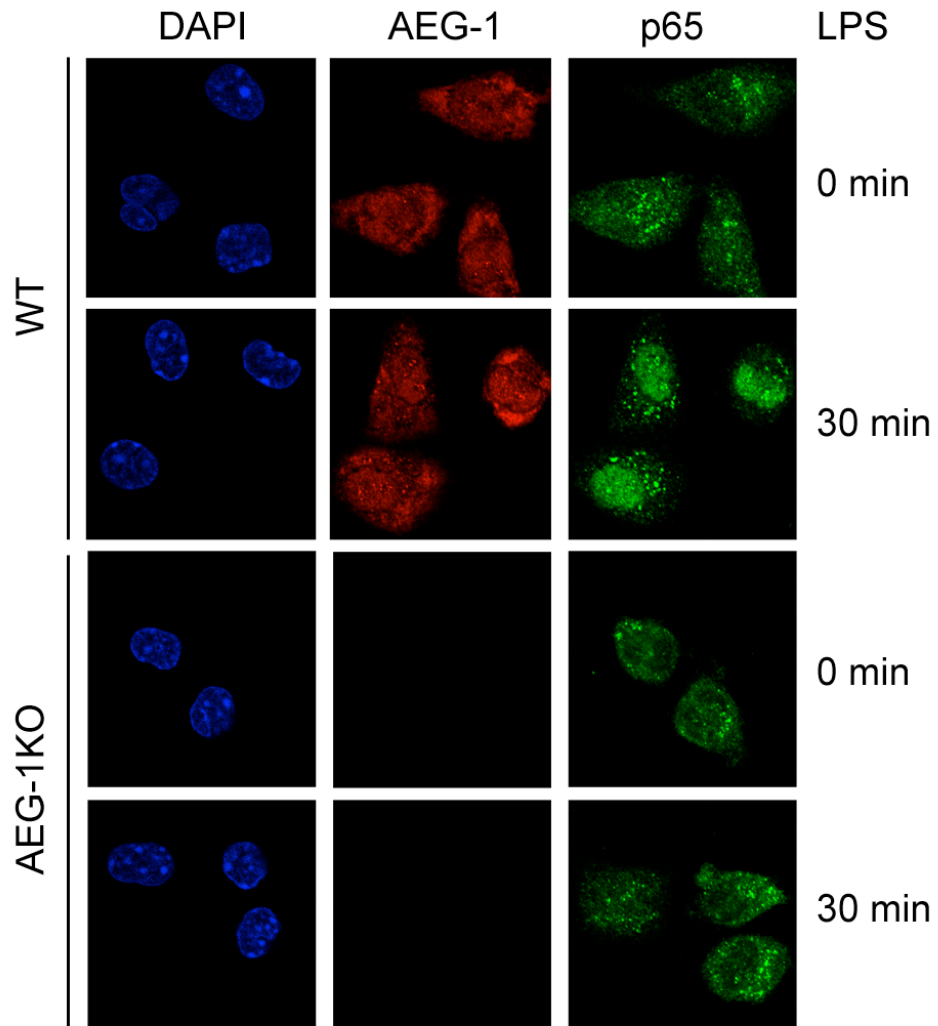
Figure 3.15 NF-κB translocation is abrogated in AEG-1KO macrophages.
Immunofluorescence followed by confocal microscopy of WT and AEG-1KO
macrophages after LPS treatment for 30 min showing p65 nuclear translocation.
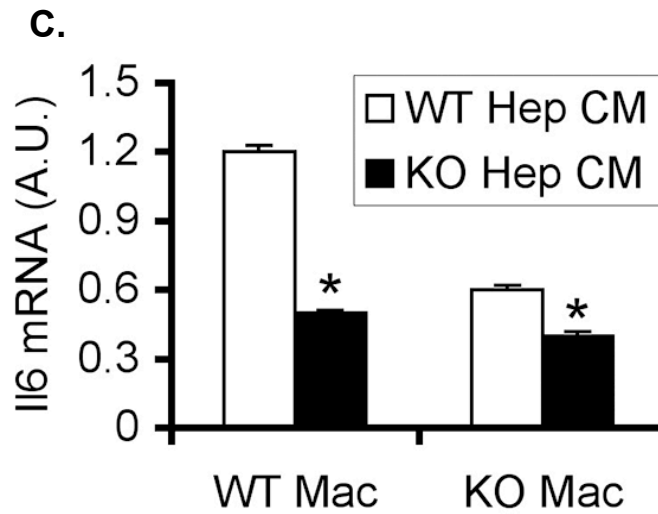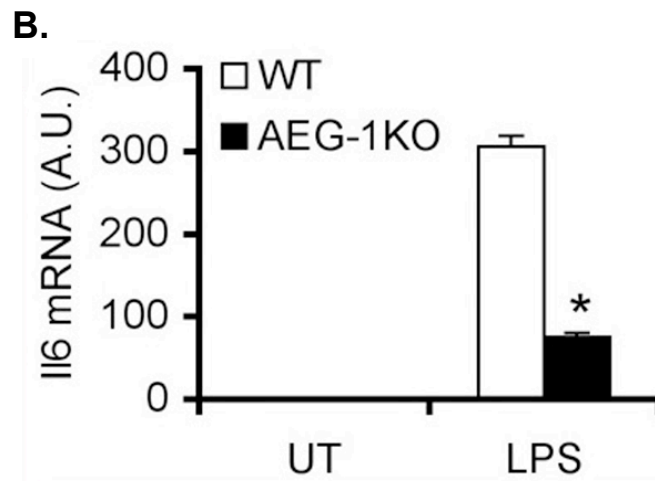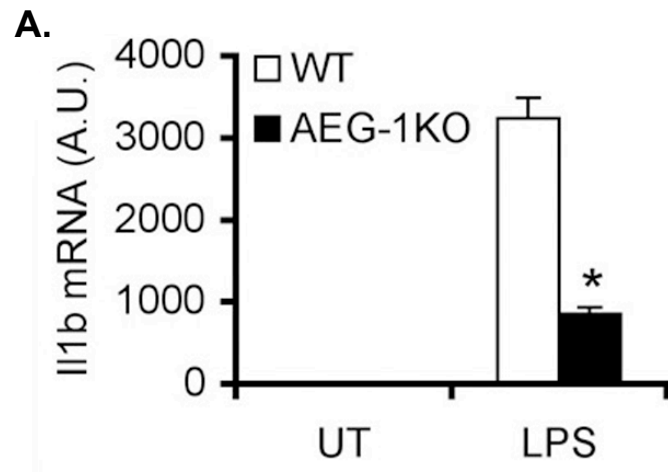
Figure 3.16 NF-κB signaling is inhibited between AEG-1KO hepatocytes and macrophages. WT and AEG-1KO macrophages were treated with LPS for 12 h and the mRNA levels of Il1b (A) and Il6 (B) were measured by Taqman Q-RT-PCR. C. WT and AEG-1KO macrophages were treated with conditioned media (CM) from LPS-treated WT and AEG-1KO hepatocytes and Il6 mRNA expression was measured by Taqman Q-RT-PCR 4 h later. For D-F, data represent mean ± SEM of three independent experiments. *: p<0.01.

To extend these observations further we performed RNA-sequencing analysis using liver samples from WT and AEG-1KO mice. Using cut-off of Log2 fold-change of 1.5 or -1.5, 597 genes showed differential change, out of which 247 genes were upregulated and 350 genes were downregulated in AEG-1KO liver *versus* WT liver. These differentially expressed genes were analyzed using Ingenuity pathway analysis software. The data were analyzed to identify the upstream regulators the activation or inhibition of which might lead to alterations in downstream genes. An activation z-score >2 indicates activation and a score of <-2 indicates inhibition. The most significant inhibition (p<0.02) was observed for genes downstream of IL-6, IL-1B, TNF family, IL17RA and NF-κB complex. These upstream regulators were analyzed for regulator effects to predict functional endpoints. It was observed that collective inhibition of these genes leads to suppression of movement of myeloid cells and decreased activation of granulocytes (Fig. 3.17). These analyses further support our hypothesis that inhibition of activation of myeloid cells is the major mechanism for resistance of AEG-1KO mice for developing HCC.
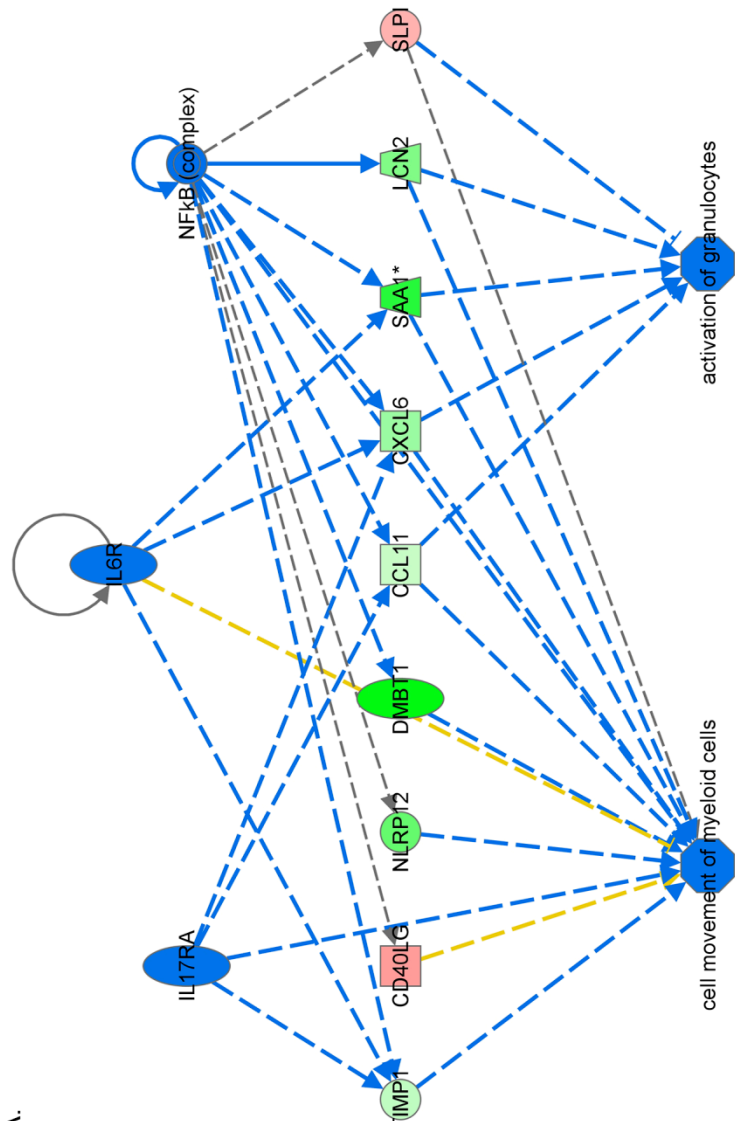
Figure 3.17 Molecular mechanisms rendering AEG-1KO mice resistant to HCC.
Functional end-points, analyzed by Ingenuity pathway analysis, that are inhibited in
AEG-1KO mice. Blue line: inhibition; red line: activation; yellow line: finding inconsistent
with state of downstream molecules; gray line: effect not predicted. Green color:
downregulation of expression; red color: upregulation of expression.
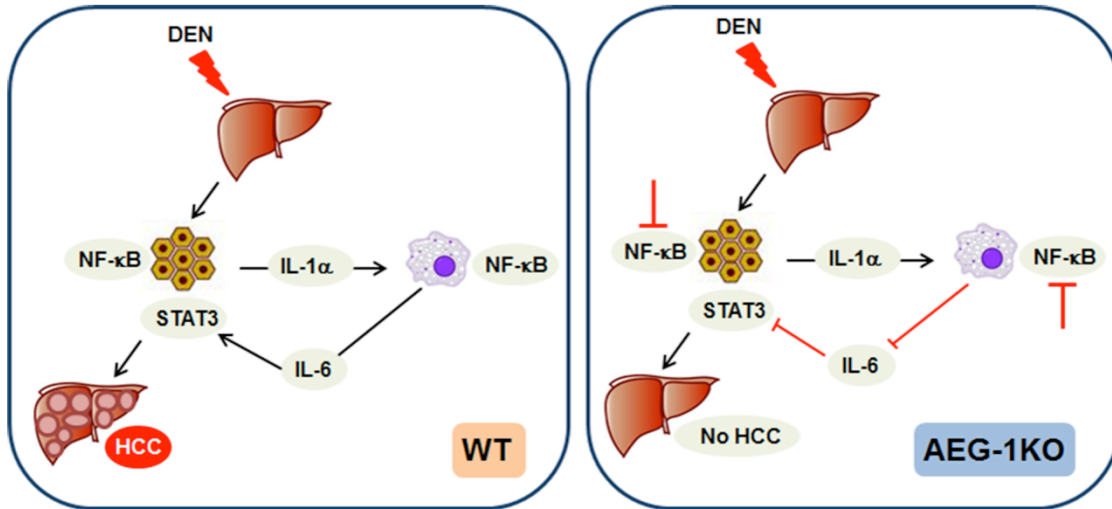
Figure 3.18 Schematic representation of the molecular mechanism of resistance of AEG-1KO mice to HCC. In WT mice DEN-induced hepatocyte injury leads to IL-1α production that activates NF-κB in the macrophages leading to production of IL-6. IL-6 activates STAT3 in hepatocytes facilitating proliferation of the mutated cells leading to HCC. In AEG-1KO mice NF-κB activation is inhibited in hepatocytes and macrophages thereby inhibiting IL-6 production and STAT3 activation. As a consequence, HCC development is significantly abrogated.

V. Discussion

The observation that Alb/AEG-1 mice do not develop spontaneous HCC [54] prompted us to hypothesize that AEG-1 is not able to transform hepatocytes, hence it is not required for initial development of HCC. In human HCC cells, overexpression of AEG-1 or knockdown of AEG-1 markedly affects invasion, angiogenesis and metastasis, and in comparison the effects on cell proliferation is significant but small [51]. In breast cancer cells modulation of AEG-1 does not affect proliferation at all, rather all phenotypes are reflected in more aggressive behavior, such as invasion and metastasis [2, 9]. These findings lead to the conclusion that the primary role of AEG-1 is to promote aggressive behavior and owing to its profound effect on metastasis, it was named Metadherin [2]. Our studies using AEG-1KO mice demonstrate for the first time that even after a mutagenic effect, such as by DEN, AEG-1 is required for initial development of the tumor, at least in the context of HCC. We document that abrogation of NF-κB signaling in hepatocytes and the tumor microenvironment cells, such as macrophages, might be the underlying mechanism that prevents paracrine signaling from macrophages to stimulate mutated hepatocytes to proliferate. Upon DEN treatment a significant decrease in activated NF-κB and STAT3 and IL-6 levels was observed in AEG-1KO livers *versus* WT providing supporting evidence for our hypothesis. In the short-term experiment DEN was able to cause liver damage to both WT and AEG-1KO mice indicating that the tumor-inhibitory effect observed in AEG-1KO mice is not because of ablation of DEN effect. Damaged hepatocytes release factors, such as IL-1β, that activate NF-κB in macrophages leading to secretion of IL-6 that stimulates STAT3 activation in

hepatocytes promoting their proliferation [107]. In AEG-1KO mice, inhibition of

NF-κB activation in macrophages stalls the subsequent processes, therefore,

profoundly abrogating initial development of the tumor (Fig. 3.18). This scenario

might be applicable to other cancers as well since chronic inflammation is a core

component of almost all cancers. Indeed, AEG-1KO mice show low basal level of

inflammation, which might protect them from spontaneous tumorigenesis as

observed in aged WT mice.

Multiple studies have documented the important roles of PI3K/AKT, MAPK

and Wnt/β-catenin signaling pathways in mediating oncogenic functions of

overexpressed AEG-1 [51, 52, 57]. However, AEG-1KO hepatocytes do not show

abrogated response upon EGF stimulation when compared to WT, and no

difference was observed in the activated status of AKT, ERK1/2 and β-catenin in

the livers of WT and AEG-1KO mice under basal condition or upon DEN

treatment. These observations might be explained by the localization of AEG-1 in

normal hepatocytes versus HCC cells. In normal hepatocytes AEG-1 is almost

exclusively located in the nucleus [54]. In cancer cells overexpressed AEG-1 is

monoubiquitinated, which facilitates its cytoplasmic accumulation [13, 54]e. In the

cytoplasm overexpressed AEG-1 might exert promiscuous interaction with other

signaling molecules leading to their activation, a function that is attributed to

oncogenic AEG-1 but not under physiological condition.

The observation that AEG-1 is required for NF-κB activation in

macrophages has profound implications in diverse physiological and pathological

states. Activation of NF-κB pathways in dendritic cells is essential for their

optimal functioning, including antigen processing and presentation [117]. Using

the human promonocytic cell line U937, it was documented that LPS induces

AEG-1 and this induction is required for subsequent NF-κB activation [16].

Additionally, NF-κB activation is required for LPS-induced AEG-1 induction thus

establishing a positive feedback loop between AEG-1 and NF-κB. NF-κB

activation is a key requirement for generating interferon-induced anti-viral

immunity. Thus AEG-1 might be a key component regulating immune function.

Additionally AEG-1 might be a key regulator of chronic inflammatory diseases.

In summary, our studies unravel a novel and important role of AEG-1 in

regulating inflammation and activation of cells in the tumor microenvironment.

AEG-1KO mice will be a valuable tool to interrogate in detail the role of AEG-1 in

physiological regulation of immunity and inflammation and diseases generated

from deregulation of these systems.

Chapter Four- Summary, Future Directions and Perspectives

Since the initial cloning of AEG-1, numerous research groups have focused on outlining the effects of AEG-1overexpression in cancer. The resultant body of work has soundly established the role of AEG-1 as a bona fide oncogene overexpressed in all cancers studied to date [54]. Similarly the pathway dysregulation, which characterizes AEG-1 overexpession, has been well described. However up until now, very few studies directly addressed the role of AEG-1 in normal physiology making it difficult to truly understand of broader implications of its dysregulation in the context of cancer. To address this gap in the literature we developed a germline AEG-1KO mouse. The insights gained from characterization of this novel mouse model have been presented here. In chapter two a novel function of AEG-1 as a modulator of lipid metabolism is described. Compared to WT, AEG-1KO mice were significantly leaner with markedly less body fat which. Our studies show that this was a result of decreased fat absorption from the intestines. AEG-1 interacts with RXR and inhibits RXR function. In enterocytes of AEG-1KO mice we observed increased activity of specific RXR heterodimer partners, LXR and PPAR-α, key inhibitors of intestinal fat absorption. Inhibition of fat absorption in AEG-1KO mice was further augmented when fed high fat diet (HFD) providing ligands to LXR and PPARα. Evidence of the mechanism conferring this phenotype was provided by functional assays. ChIP analysis and β-oxidation assays revealed increased activation of LXR target genes and FA oxidation respectively in AEG-1KO mice. These

studies reveal a novel role of AEG-1 in regulating nuclear receptors controlling lipid metabolism. AEG-1 might significantly modulate the effects of HFD, and thereby function as a unique determinant of obesity. Specific targeting of AEG-1 may be a viable therapeutic approach for the treatment of obesity.

Numerous epidemiological studies have correlated overweight and obesity to a substantial increase in cancer risk [118] [119] [120]. Obesity has also been consistently shown to increase rates of breast cancer in postmenopausal women by 30–50% [121] [122] [123]. Women with a BMI ≥ 40.0 have breast cancer death rates that are three times higher than very lean women (BMI < 20.5), this combined with mortality and survival studies demonstrate that excess body fat associates strongly with 1) reduced likelihood of survival and 2) increased likelihood of relapse regardless of menopausal status [124] [125]. Increased incidence of endometrial cancer in obese women has also been reported [126]. Studies show that even a modest elevation in BMI to the 25–30 range has been shown to significantly increase the risk of death due to pancreatic cancer, cancers of the gastrointestinal (GI) tract, kidney as well as HCC. Even more strikingly a recent study documented that a BMI of 35–40 is correlated to an astounding 4.5-fold increase in relative HCC risk in men [120]. HCC represents approximately 90% of primary liver cancers and is also marked by significant AEG-1 overexpression when compared to the normal liver [51]. Liver-specific AEG-1 transgenic mice also exhibit have an overweight phenotype with an increased propensity towards liver steatosis [54] . Taken together this data strongly suggests a link between dysregulation of AEG-1 and the increased risk

cancer associated with obesity, thus therapeutic targeting of AEG-1 in this context may be beneficial to both pathologies.

The implication of this research stretches beyond cancer. Nuclear receptors maintain cellular and organismal homeostasis by serving as ligand-activated transcription factors function. AEG-1 modulation of nuclear receptor function may also be important in maintaining homeostasis of hormone, vitamin and lipid signaling, inflammation, and myriad other biological and physiological processes. The highly conserved signature LXXLL sequence identified with in the AEG-1 protein has been demonstrated to a large number of mediate coactivator–nuclear receptor interactions including retinoic acid receptor (RAR), thyroid hormone receptor (TR) and vitamin D receptor (VDR). Additional studies are needed to analyze the specific impact of AEG-1 expression on the activation status of these and other nuclear receptors.

The link between inflammation and cancer has also been well described [127] [128, 129]. An estimated 15% of human cancers are associated with chronic infections and inflammation [130]. Among the infectious agents related to the pathogenesis of cancer we find bacteria such as *Helicobacter pylori* in gastric cancer and gastric mucosal lymphoma [134]. Proinflammatory conditions not related to microbial infections have also been linked to the increased cancer risk. Such are the cases of autoimmune diseases like inflammatory bowel disease, in which the severity of inflammation correlates with the risk of colorectal cancer, [135] chronic airway irritation and inflammation by tobacco smoke or airborne particles in lung carcinoma [136], or chronic inflammation of unknown origin in

148

the development of prostate cancer [137]. Indeed the majority of cases of HCC

also arise in a setting of chronic inflammation, such as infection with HBV or

HCV, alcoholism and non-alcoholic fatty liver disease (NAFLD) [131, 132]. In

chapter three we provide evidence that AEG-1 is required for the onset and

progression of DEN induced HCC. We also show that NF-κB and STAT3

signaling is abrogated in AEG-1KO hepatocytes and macrophages supporting

previous reports of an interaction between the two proteins [11, 12]. Previous

studies show that NF-κB activation in hepatocytes is necessary in inflammation-

induced HCC [102]. NF-κB-regulated expression of the STAT3-activating

cytokine IL-6 has recently been identified in viral hepatitis and in hepatosteatosis

[133]. Additionally, inhibition or genetic deletion of IL-6 has been shown to

provide a significant reduction in tumor load [106]. Injury to hepatocytes, such as

those caused by DEN, leads to release of IL-1α that activates NF-κB in liver

macrophages (Kupffer cells) with subsequent release of cytokines, such as IL-6

[106-108]. IL-6 promotes proliferation and survival of hepatocytes by activating

Stat3 signaling [106]. While the AEG-1KO mouse provided valuable insights

about the role of AEG-1 in these signaling cascades there were limitations to

studying this genome wide knockout. For instance, it was difficult to identify the

specific role of AEG-1 expression in each cell type of the tumor

microenvironment. To better understand where AEG-1 fits into this cascade we

have also generated liver-specific and macrophage-specific AEG-1KO mice.

These mice, particularly the macrophage-specific KOs will be useful not only to

the investigation of HCC but also to other inflammation-associated cancers. More

broadly, analysis of the macrophage-specific AEG-1KO mouse will be a useful tool to interrogate the role of AEG-1 in the immune response. We see that AEG-1KO mice have an impaired response to the inflammation-linked DEN carcinogenesis model leading us to question the integrity of their overall immune response. These and other questions will be addressed in forthcoming experiments.

Literature Cited

1. Su, ZZ, Kang, DC, Chen, Y, Pekarskaya, O, Chao, W, Volsky, DJ, and Fisher, PB, Identification and cloning of human astrocyte genes displaying elevated expression after infection with HIV-1 or exposure to HIV-1 envelope glycoprotein by rapid subtraction hybridization, RaSH. Oncogene, 2002. 21(22): p. 3592-3602.

2. Brown, DM and Ruoslahti, E, Metadherin, a cell surface protein in breast tumors that mediates lung metastasis. Cancer Cell, 2004. 5(4): p. 365-374.

3. Sutherland, HG, Lam, YW, Briers, S, Lamond, AI, and Bickmore, WA, 3D3/lyric: a novel transmembrane protein of the endoplasmic reticulum and nuclear envelope, which is also present in the nucleolus. Exp Cell Res, 2004. 294(1): p. 94-105.

4. Britt, DE, Yang, DF, Yang, DQ, Flanagan, D, Callanan, H, Lim, YP, Lin, SH, and Hixson, DC, Identification of a novel protein, LYRIC, localized to tight junctions of polarized epithelial cells. Exp Cell Res, 2004. 300(1): p. 134-148.

5. Lee, SG, Kang, DC, Desalle, R, Sarkar, D, and Fisher, PB, AEG-1/MTDH/LYRIC, the Beginning: Initial Cloning, Structure, Expression Profile, and Regulation of Expression. Adv Cancer Res, 2013. 120: p. 1-38.

6.   Kang, DC, Su, ZZ, Sarkar, D, Emdad, L, Volsky, DJ, and Fisher, PB, Cloning and characterization of HIV-1-inducible astrocyte elevated gene-1, AEG-1. Gene, 2005. 353(1): p. 8-15.

7.   Bergamaschi, W, Rapone, L, and Sorda, E, New national healthcare information system. Clin Chem Lab Med, 2006. 44(6): p. 708-711.

8.   Poon, JK, Zhu, L, DeRose, GA, and Yariv, A, Transmission and group delay of microring coupled-resonator optical waveguides. Opt Lett, 2006. 31(4): p. 456-458.

9.   Hu, G, Chong, RA, Yang, Q, Wei, Y, Blanco, MA, Li, F, Reiss, M, Au, JL, Haffty, BG, and Kang, Y, MTDH activation by 8q22 genomic gain promotes chemoresistance and metastasis of poor-prognosis breast cancer. Cancer Cell, 2009. 15(1): p. 9-20.

10.   Li, J, Zhang, N, Song, LB, Liao, WT, Jiang, LL, Gong, LY, Wu, J, Yuan, J, Zhang, HZ, Zeng, MS, and Li, M, Astrocyte elevated gene-1 is a novel prognostic marker for breast cancer progression and overall patient survival. Clin Cancer Res, 2008. 14(11): p. 3319-3326.

11.   Sarkar, D, Park, ES, Emdad, L, Lee, SG, Su, ZZ, and Fisher, PB, Molecular basis of nuclear factor-kappaB activation by astrocyte elevated gene-1. Cancer Res, 2008. 68(5): p. 1478-1484.

12.   Emdad, L, Sarkar, D, Su, ZZ, Randolph, A, Boukerche, H, Valerie, K, and Fisher, PB, Activation of the nuclear factor kappaB pathway by astrocyte elevated gene-1: implications for tumor progression and metastasis. Cancer Res, 2006. 66(3): p. 1509-1516.

13. Thirkettle, HJ, Girling, J, Warren, AY, Mills, IG, Sahadevan, K, Leung, H, Hamdy, F, Whitaker, HC, and Neal, DE, LYRIC/AEG-1 is targeted to different subcellular compartments by ubiquitinylation and intrinsic nuclear localization signals. Clin Cancer Res, 2009. 15(9): p. 3003-3013.

14. Jeon, HY, Choi, M, Howlett, EL, Vozhilla, N, Yoo, BK, Lloyd, JA, Sarkar, D, Lee, SG, and Fisher, PB, Expression patterns of astrocyte elevated gene-1 (AEG-1) during development of the mouse embryo. Gene Expr Patterns, 2010. 10(7-8): p. 361-367.

15. Lee, SG, Su, ZZ, Emdad, L, Sarkar, D, and Fisher, PB, Astrocyte elevated gene-1 (AEG-1) is a target gene of oncogenic Ha-ras requiring phosphatidylinositol 3-kinase and c-Myc. Proc Natl Acad Sci U S A, 2006. 103(46): p. 17390-17395.

16. Khuda, II, Koide, N, Noman, AS, Dagvadorj, J, Tumurkhuu, G, Naiki, Y, Komatsu, T, Yoshida, T, and Yokochi, T, Astrocyte elevated gene-1 (AEG-1) is induced by lipopolysaccharide as toll-like receptor 4 (TLR4) ligand and regulates TLR4 signalling. Immunology, 2009. 128(1 Suppl): p. e700-706.

17. Bartel, F, Pinkert, D, Fiedler, W, Kappler, M, Wurl, P, Schmidt, H, and Taubert, H, Expression of alternatively and aberrantly spliced transcripts of the MDM2 mRNA is not tumor-specific. Int J Oncol, 2004. 24(1): p. 143-151.

18. Krek, A, Grun, D, Poy, MN, Wolf, R, Rosenberg, L, Epstein, EJ, MacMenamin, P, da Piedade, I, Gunsalus, KC, Stoffel, M, and Rajewsky,

N, Combinatorial microRNA target predictions. Nat Genet, 2005. 37(5): p. 495-500.

19. Poy, MN, Eliasson, L, Krutzfeldt, J, Kuwajima, S, Ma, X, Macdonald, PE, Pfeffer, S, Tuschl, T, Rajewsky, N, Rorsman, P, and Stoffel, M, A pancreatic islet-specific microRNA regulates insulin secretion. Nature, 2004. 432(7014): p. 226-230.

20. Chen, B, Li, H, Zeng, X, Yang, P, Liu, X, Zhao, X, and Liang, S, Roles of microRNA on cancer cell metabolism. J Transl Med, 2012. 10: p. 228.

21. He, XX, Chang, Y, Meng, FY, Wang, MY, Xie, QH, Tang, F, Li, PY, Song, YH, and Lin, JS, MicroRNA-375 targets AEG-1 in hepatocellular carcinoma and suppresses liver cancer cell growth in vitro and in vivo. Oncogene, 2012. 31(28): p. 3357-3369.

22. Nohata, N, Hanazawa, T, Kikkawa, N, Sakurai, D, Fujimura, L, Chiyomaru, T, Kawakami, K, Yoshino, H, Enokida, H, Nakagawa, M, Katayama, A, Harabuchi, Y, Okamoto, Y, and Seki, N, Tumour suppressive microRNA-874 regulates novel cancer networks in maxillary sinus squamous cell carcinoma. Br J Cancer, 2011. 105(6): p. 833-841.

23. Ji, J, Shi, J, Budhu, A, Yu, Z, Forgues, M, Roessler, S, Ambs, S, Chen, Y, Meltzer, PS, Croce, CM, Qin, LX, Man, K, Lo, CM, Lee, J, Ng, IO, Fan, J, Tang, ZY, Sun, HC, and Wang, XW, MicroRNA expression, survival, and response to interferon in liver cancer. N Engl J Med, 2009. 361(15): p. 1437-1447.

24. Zhang, B, Liu, XX, He, JR, Zhou, CX, Guo, M, He, M, Li, MF, Chen, GQ, and Zhao, Q, Pathologically decreased miR-26a antagonizes apoptosis and facilitates carcinogenesis by targeting MTDH and EZH2 in breast cancer. Carcinogenesis, 2011. 32(1): p. 2-9.

25. Guo, J, Xia, B, Meng, F, and Lou, G, miR-137 suppresses cell growth in ovarian cancer by targeting AEG-1. Biochem Biophys Res Commun, 2013. 441(2): p. 357-363.

26. Yang, Y, Wu, J, Guan, H, Cai, J, Fang, L, Li, J, and Li, M, MiR-136 promotes apoptosis of glioma cells by targeting AEG-1 and Bcl-2. FEBS Lett, 2012. 586(20): p. 3608-3612.

27. Molica, S, Dattilo, A, Mannella, A, and Levato, D, Intercellular adhesion molecules (ICAMs) 2 and 3 are frequently expressed in B cell chronic lymphocytic leukemia. Leukemia, 1996. 10(5): p. 907-908.

28. Aruffo, A, Kanner, SB, Sgroi, D, Ledbetter, JA, and Stamenkovic, I, CD22-mediated stimulation of T cells regulates T-cell receptor/CD3-induced signaling. Proc Natl Acad Sci U S A, 1992. 89(21): p. 10242-10246.

29. Uner, A, Akcali, Z, and Unsal, D, Serum levels of soluble E-selectin in colorectal cancer. Neoplasma, 2004. 51(4): p. 269-274.

30. Huang, B, Zhao, J, Li, H, He, KL, Chen, Y, Chen, SH, Mayer, L, Unkeless, JC, and Xiong, H, Toll-like receptors on tumor cells facilitate evasion of immune surveillance. Cancer Res, 2005. 65(12): p. 5009-5014.

31. Thirkettle, HJ, Mills, IG, Whitaker, HC, and Neal, DE, Nuclear LYRIC/AEG-1 interacts with PLZF and relieves PLZF-mediated repression. Oncogene, 2009. 28(41): p. 3663-3670.

32. Shaknovich, R, Yeyati, PL, Ivins, S, Melnick, A, Lempert, C, Waxman, S, Zelent, A, and Licht, JD, The promyelocytic leukemia zinc finger protein affects myeloid cell growth, differentiation, and apoptosis. Mol Cell Biol, 1998. 18(9): p. 5533-5545.

33. Parrado, A, Robledo, M, Moya-Quiles, MR, Marin, LA, Chomienne, C, Padua, RA, and Alvarez-Lopez, MR, The promyelocytic leukemia zinc finger protein down-regulates apoptosis and expression of the proapoptotic BID protein in lymphocytes. Proc Natl Acad Sci U S A, 2004. 101(7): p. 1898-1903.

34. Wahlstrom, T and Henriksson, MA, Impact of MYC in regulation of tumor cell metabolism. Biochim Biophys Acta, 2014.

35. Wang, MJ and Gegenheimer, P, Substrate masking: binding of RNA by EGTA-inactivated micrococcal nuclease results in artifactual inhibition of RNA processing reactions. Nucleic Acids Res, 1990. 18(22): p. 6625-6631.

36. Yang, Y, Ballatori, N, and Smith, HC, Apolipoprotein B mRNA editing and the reduction in synthesis and secretion of the atherogenic risk factor, apolipoprotein B100 can be effectively targeted through TAT-mediated protein transduction. Mol Pharmacol, 2002. 61(2): p. 269-276.

37. Scadden, AD, The RISC subunit Tudor-SN binds to hyper-edited double-stranded RNA and promotes its cleavage. Nat Struct Mol Biol, 2005. 12(6): p. 489-496.

38. Yang, Q, Xu, J, Sun, Y, Li, Z, Li, Y, and Qian, X, Hydrolysis of plasmid DNA and RNA by amino alkyl naphthalimide as metal-free artificial nuclease. Bioorg Med Chem Lett, 2006. 16(4): p. 803-806.

39. Caudy, AA, Ketting, RF, Hammond, SM, Denli, AM, Bathoorn, AM, Tops, BB, Silva, JM, Myers, MM, Hannon, GJ, and Plasterk, RH, A micrococcal nuclease homologue in RNAi effector complexes. Nature, 2003. 425(6956): p. 411-414.

40. Yoo, BK, Santhekadur, PK, Gredler, R, Chen, D, Emdad, L, Bhutia, S, Pannell, L, Fisher, PB, and Sarkar, D, Increased RNA-induced silencing complex (RISC) activity contributes to hepatocellular carcinoma. Hepatology, 2011. 53(5): p. 1538-1548.

41. Blanco, MA, Aleckovic, M, Hua, Y, Li, T, Wei, Y, Xu, Z, Cristea, IM, and Kang, Y, Identification of staphylococcal nuclease domain-containing 1 (SND1) as a Metadherin-interacting protein with metastasis-promoting functions. J Biol Chem, 2011. 286(22): p. 19982-19992.

42. Shaw, N, Zhao, M, Cheng, C, Xu, H, Saarikettu, J, Li, Y, Da, Y, Yao, Z, Silvennoinen, O, Yang, J, Liu, ZJ, Wang, BC, and Rao, Z, The multifunctional human p100 protein 'hooks' methylated ligands. Nat Struct Mol Biol, 2007. 14(8): p. 779-784.

43. Yang, J, Valineva, T, Hong, J, Bu, T, Yao, Z, Jensen, ON, Frilander, MJ, and Silvennoinen, O, Transcriptional co-activator protein p100 interacts with snRNP proteins and facilitates the assembly of the spliceosome. Nucleic Acids Res, 2007. 35(13): p. 4485-4494.

44. Wan, L, Lu, X, Yuan, S, Wei, Y, Guo, F, Shen, M, Yuan, M, Chakrabarti, R, Hua, Y, Smith, HA, Blanco, MA, Chekmareva, M, Wu, H, Bronson, RT, Haffty, BG, Xing, Y, and Kang, Y, MTDH-SND1 interaction is crucial for expansion and activity of tumor-initiating cells in diverse oncogene- and carcinogen-induced mammary tumors. Cancer Cell, 2014. 26(1): p. 92-105.

45. Heery, DM, Kalkhoven, E, Hoare, S, and Parker, MG, A signature motif in transcriptional co-activators mediates binding to nuclear receptors. Nature, 1997. 387(6634): p. 733-736.

46. Torchia, J, Rose, DW, Inostroza, J, Kamei, Y, Westin, S, Glass, CK, and Rosenfeld, MG, The transcriptional co-activator p/CIP binds CBP and mediates nuclear-receptor function. Nature, 1997. 387(6634): p. 677-684.

47. Srivastava, J, Robertson, CL, Rajasekaran, D, Gredler, R, Siddiq, A, Emdad, L, Mukhopadhyay, ND, Ghosh, S, Hylemon, PB, Gil, G, Shah, K, Bhere, D, Subler, MA, Windle, JJ, Fisher, PB, and Sarkar, D, AEG-1 Regulates Retinoid X Receptor and Inhibits Retinoid Signaling. Cancer Res, 2014. 74(16): p. 4364-4377.

48. Hu, G, Wei, Y, and Kang, Y, The multifaceted role of MTDH/AEG-1 in cancer progression. Clin Cancer Res, 2009. 15(18): p. 5615-5620.

49. Hornbeck, PV, Kornhauser, JM, Tkachev, S, Zhang, B, Skrzypek, E, Murray, B, Latham, V, and Sullivan, M, PhosphoSitePlus: a comprehensive resource for investigating the structure and function of experimentally determined post-translational modifications in man and mouse. Nucleic Acids Res, 2012. 40(Database issue): p. D261-270.

50. Luxton, HJ, Barnouin, K, Kelly, G, Hanrahan, S, Totty, N, Neal, DE, and Whitaker, HC, Regulation of the localisation and function of the oncogene LYRIC/AEG-1 by ubiquitination at K486 and K491. Mol Oncol, 2014. 8(3): p. 633-641.

51. Yoo, BK, Emdad, L, Su, ZZ, Villanueva, A, Chiang, DY, Mukhopadhyay, ND, Mills, AS, Waxman, S, Fisher, RA, Llovet, JM, Fisher, PB, and Sarkar, D, Astrocyte elevated gene-1 regulates hepatocellular carcinoma development and progression. J Clin Invest, 2009. 119(3): p. 465-477.

52. Emdad, L, Lee, SG, Su, ZZ, Jeon, HY, Boukerche, H, Sarkar, D, and Fisher, PB, Astrocyte elevated gene-1 (AEG-1) functions as an oncogene and regulates angiogenesis. Proc Natl Acad Sci U S A, 2009. 106(50): p. 21300-21305.

53. Sarkar, D and Fisher, PB, AEG-1/MTDH/LYRIC: Clinical Significance. Adv Cancer Res, 2013. 120: p. 39-74.

54. Srivastava, J, Siddiq, A, Emdad, L, Santhekadur, P, Chen, D, Gredler, R, Shen, X-N, Robertson, CL, Dumur, CI, Hylemon, PB, Mukhopadhyay, ND, Bhere, D, Shah, K, Ahmad, R, Giashuddin, S, Stafflinger, J, Subler, MA, Windle, JJ, Fisher, PB, and Sarkar, D, Astrocyte elevated gene-1 (AEG-1)

promotes hepatocarcinogenesis: novel insights from a mouse model. Hepatology, 2012. 56: p. 1782-1791.

55.   Yoo, BK, Gredler, R, Vozhilla, N, Su, ZZ, Chen, D, Forcier, T, Shah, K, Saxena, U, Hansen, U, Fisher, PB, and Sarkar, D, Identification of genes conferring resistance to 5-fluorouracil. Proc Natl Acad Sci U S A, 2009. 106(31): p. 12938-12943.

56.   Yoo, BK, Chen, D, Su, Z-Z, Gredler, R, Yoo, J, Shah, K, Fisher, PB, and Sarkar, D, Molecular mechanism of chemoresistance by Astrocyte Elevated Gene-1 (AEG-1). Cancer Res, 2010. 70: p. 3249-3258.

57.   Lee, SG, Su, ZZ, Emdad, L, Sarkar, D, Franke, TF, and Fisher, PB, Astrocyte elevated gene-1 activates cell survival pathways through PI3K-Akt signaling. Oncogene, 2008. 27(8): p. 1114-1121.

58.   Mangelsdorf, DJ, Ong, ES, Dyck, JA, and Evans, RM, Nuclear receptor that identifies a novel retinoic acid response pathway. Nature, 1990. 345(6272): p. 224-229.

59.   Lefebvre, P, Benomar, Y, and Staels, B, Retinoid X receptors: common heterodimerization partners with distinct functions. Trends Endocrinol Metab, 2010. 21(11): p. 676-683.

60.   Janowski, BA, Willy, PJ, Devi, TR, Falck, JR, and Mangelsdorf, DJ, An oxysterol signalling pathway mediated by the nuclear receptor LXR alpha. Nature, 1996. 383(6602): p. 728-731.

61. Willy, PJ and Mangelsdorf, DJ, Unique requirements for retinoid-dependent transcriptional activation by the orphan receptor LXR. Genes Dev, 1997. 11(3): p. 289-298.

62. Bonamassa, B and Moschetta, A, Atherosclerosis: lessons from LXR and the intestine. Trends Endocrinol Metab, 2013. 24(3): p. 120-128.

63. Bugge, A, Siersbaek, M, Madsen, MS, Gondor, A, Rougier, C, and Mandrup, S, A novel intronic peroxisome proliferator-activated receptor gamma enhancer in the uncoupling protein (UCP) 3 gene as a regulator of both UCP2 and -3 expression in adipocytes. J Biol Chem, 2010. 285(23): p. 17310-17317.

64. Pyper, SR, Viswakarma, N, Yu, S, and Reddy, JK, PPARalpha: energy combustion, hypolipidemia, inflammation and cancer. Nucl Recept Signal, 2010. 8: p. e002.

65. Ferre, P, The biology of peroxisome proliferator-activated receptors: relationship with lipid metabolism and insulin sensitivity. Diabetes, 2004. 53 Suppl 1: p. S43-50.

66. Bederman, IR, Foy, S, Chandramouli, V, Alexander, JC, and Previs, SF, Triglyceride synthesis in epididymal adipose tissue: contribution of glucose and non-glucose carbon sources. J Biol Chem, 2009. 284(10): p. 6101-6108.

67. Lee, WN, Bassilian, S, Guo, Z, Schoeller, D, Edmond, J, Bergner, EA, and Byerley, LO, Measurement of fractional lipid synthesis using deuterated

water (2H2O) and mass isotopomer analysis. Am J Physiol, 1994. 266(3 Pt 1): p. E372-383.

68.   Diraison, F, Pachiaudi, C, and Beylot, M, Measuring lipogenesis and cholesterol synthesis in humans with deuterated water: use of simple gas chromatographic/mass spectrometric techniques. J Mass Spectrom, 1997. 32(1): p. 81-86.

69.   Turley, SD, Herndon, MW, and Dietschy, JM, Reevaluation and application of the dual-isotope plasma ratio method for the measurement of intestinal cholesterol absorption in the hamster. J Lipid Res, 1994. 35(2): p. 328-339.

70.   Clark, SB, Ekkers, TE, Singh, A, Balint, JA, Holt, PR, and Rodgers, JB, Jr., Fat absorption in essential fatty acid deficiency: a model experimental approach to studies of the mechanism of fat malabsorption of unknown etiology. J Lipid Res, 1973. 14(5): p. 581-588.

71.   Gao, X, Zhang, Q, Meng, D, Isaac, G, Zhao, R, Fillmore, TL, Chu, RK, Zhou, J, Tang, K, Hu, Z, Moore, RJ, Smith, RD, Katze, MG, and Metz, TO, A reversed-phase capillary ultra-performance liquid chromatography-mass spectrometry (UPLC-MS) method for comprehensive top-down/bottom-up lipid profiling. Anal Bioanal Chem, 2012. 402(9): p. 2923-2933.

72.   Huynh, FK, Green, MF, Koves, TR, and Hirschey, MD, Measurement of fatty acid oxidation rates in animal tissues and cell lines. Methods Enzymol, 2013. 542: p. 391-405.

73.   Houten, SM and Wanders, RJ, A general introduction to the biochemistry of mitochondrial fatty acid beta-oxidation. J Inherit Metab Dis, 2010. 33(5): p. 469-477.

74.   Wahli, W and Michalik, L, PPARs at the crossroads of lipid signaling and inflammation. Trends Endocrinol Metab, 2012. 23(7): p. 351-363.

75.   Venkateswaran, A, Laffitte, BA, Joseph, SB, Mak, PA, Wilpitz, DC, Edwards, PA, and Tontonoz, P, Control of cellular cholesterol efflux by the nuclear oxysterol receptor LXR alpha. Proc Natl Acad Sci U S A, 2000. 97(22): p. 12097-12102.

76.   Repa, JJ, Turley, SD, Lobaccaro, JA, Medina, J, Li, L, Lustig, K, Shan, B, Heyman, RA, Dietschy, JM, and Mangelsdorf, DJ, Regulation of absorption and ABC1-mediated efflux of cholesterol by RXR heterodimers. Science, 2000. 289(5484): p. 1524-1529.

77.   Repa, JJ, Berge, KE, Pomajzl, C, Richardson, JA, Hobbs, H, and Mangelsdorf, DJ, Regulation of ATP-binding cassette sterol transporters ABCG5 and ABCG8 by the liver X receptors alpha and beta. J Biol Chem, 2002. 277(21): p. 18793-18800.

78.   Masson, CJ, Plat, J, Mensink, RP, Namiot, A, Kisielewski, W, Namiot, Z, Fullekrug, J, Ehehalt, R, Glatz, JF, and Pelsers, MM, Fatty acid- and cholesterol transporter protein expression along the human intestinal tract. PLoS ONE, 2010. 5(4): p. e10380.

79. Glatz, JF and van der Vusse, GJ, Cellular fatty acid-binding proteins: their function and physiological significance. Prog Lipid Res, 1996. 35(3): p. 243-282.

80. El-Serag, HB and Rudolph, KL, Hepatocellular carcinoma: epidemiology and molecular carcinogenesis. Gastroenterology, 2007. 132(7): p. 2557-2576.

81. El-Serag, HB, Davila, JA, Petersen, NJ, and McGlynn, KA, The continuing increase in the incidence of hepatocellular carcinoma in the United States: an update. Ann Intern Med, 2003. 139(10): p. 817-823.

82. Llovet, JM, Burroughs, A, and Bruix, J, Hepatocellular carcinoma. Lancet, 2003. 362(9399): p. 1907-1917.

83. Llovet, JM, Bru, C, and Bruix, J, Prognosis of hepatocellular carcinoma: the BCLC staging classification. Semin Liver Dis, 1999. 19(3): p. 329-338.

84. O'Neil, BH and Venook, AP, Hepatocellular carcinoma: the role of the North American GI Steering Committee Hepatobiliary Task Force and the advent of effective drug therapy. Oncologist, 2007. 12(12): p. 1425-1432.

85. Georgiades, CS, Hong, K, and Geschwind, JF, Radiofrequency ablation and chemoembolization for hepatocellular carcinoma. Cancer J, 2008. 14(2): p. 117-122.

86. Whittaker, S, Marais, R, and Zhu, AX, The role of signaling pathways in the development and treatment of hepatocellular carcinoma. Oncogene, 2010. 29(36): p. 4989-5005.

87. Yeo, W, Mok, TS, Zee, B, Leung, TW, Lai, PB, Lau, WY, Koh, J, Mo, FK, Yu, SC, Chan, AT, Hui, P, Ma, B, Lam, KC, Ho, WM, Wong, HT, Tang, A, and Johnson, PJ, A randomized phase III study of doxorubicin versus cisplatin/interferon alpha-2b/doxorubicin/fluorouracil (PIAF) combination chemotherapy for unresectable hepatocellular carcinoma. J Natl Cancer Inst, 2005. 97(20): p. 1532-1538.

88. Llovet, JM and Bruix, J, Systematic review of randomized trials for unresectable hepatocellular carcinoma: Chemoembolization improves survival. Hepatology, 2003. 37(2): p. 429-442.

89. Yoo, BK, Chen, D, Su, ZZ, Gredler, R, Yoo, J, Shah, K, Fisher, PB, and Sarkar, D, Molecular mechanism of chemoresistance by astrocyte elevated gene-1. Cancer Res, 2010. 70(8): p. 3249-3258.

90. Vogelstein, B and Kinzler, KW, Cancer genes and the pathways they control. Nat Med, 2004. 10(8): p. 789-799.

91. Pikarsky, E, Porat, RM, Stein, I, Abramovitch, R, Amit, S, Kasem, S, Gutkovich-Pyest, E, Urieli-Shoval, S, Galun, E, and Ben-Neriah, Y, NF-kappaB functions as a tumour promoter in inflammation-associated cancer. Nature, 2004. 431(7007): p. 461-466.

92. Karin, M and Ben-Neriah, Y, Phosphorylation meets ubiquitination: the control of NF-[kappa]B activity. Annu Rev Immunol, 2000. 18: p. 621-663.

93. Liu, P, Kimmoun, E, Legrand, A, Sauvanet, A, Degott, C, Lardeux, B, and Bernuau, D, Activation of NF-kappa B, AP-1 and STAT transcription

factors is a frequent and early event in human hepatocellular carcinomas. J Hepatol, 2002. 37(1): p. 63-71.

94. Tai, DI, Tsai, SL, Chang, YH, Huang, SN, Chen, TC, Chang, KS, and Liaw, YF, Constitutive activation of nuclear factor kappaB in hepatocellular carcinoma. Cancer, 2000. 89(11): p. 2274-2281.

95. Tai, DI, Tsai, SL, Chen, YM, Chuang, YL, Peng, CY, Sheen, IS, Yeh, CT, Chang, KS, Huang, SN, Kuo, GC, and Liaw, YF, Activation of nuclear factor kappaB in hepatitis C virus infection: implications for pathogenesis and hepatocarcinogenesis. Hepatology, 2000. 31(3): p. 656-664.

96. Hosel, M, Quasdorff, M, Wiegmann, K, Webb, D, Zedler, U, Broxtermann, M, Tedjokusumo, R, Esser, K, Arzberger, S, Kirschning, CJ, Langenkamp, A, Falk, C, Buning, H, Rose-John, S, and Protzer, U, Not interferon, but interleukin-6 controls early gene expression in hepatitis B virus infection. Hepatology, 2009. 50(6): p. 1773-1782.

97. Mandrekar, P and Szabo, G, Signalling pathways in alcohol-induced liver inflammation. J Hepatol, 2009. 50(6): p. 1258-1266.

98. Kim, HR, Lee, SH, and Jung, G, The hepatitis B viral X protein activates NF-kappaB signaling pathway through the up-regulation of TBK1. FEBS Lett, 2010. 584(3): p. 525-530.

99. Lu, B, Guo, H, Zhao, J, Wang, C, Wu, G, Pang, M, Tong, X, Bu, F, Liang, A, Hou, S, Fan, X, Dai, J, Wang, H, and Guo, Y, Increased expression of iASPP, regulated by hepatitis B virus X protein-mediated NF-kappaB

activation, in hepatocellular carcinoma. Gastroenterology, 2010. 139(6): p. 2183-2194 e2185.

100. Schwabe, RF, Seki, E, and Brenner, DA, Toll-like receptor signaling in the liver. Gastroenterology, 2006. 130(6): p. 1886-1900.

101. Shi, H, Kokoeva, MV, Inouye, K, Tzameli, I, Yin, H, and Flier, JS, TLR4 links innate immunity and fatty acid-induced insulin resistance. J Clin Invest, 2006. 116(11): p. 3015-3025.

102. Haybaeck, J, Zeller, N, Wolf, MJ, Weber, A, Wagner, U, Kurrer, MO, Bremer, J, Iezzi, G, Graf, R, Clavien, PA, Thimme, R, Blum, H, Nedospasov, SA, Zatloukal, K, Ramzan, M, Ciesek, S, Pietschmann, T, Marche, PN, Karin, M, Kopf, M, Browning, JL, Aguzzi, A, and Heikenwalder, M, A lymphotoxin-driven pathway to hepatocellular carcinoma. Cancer Cell, 2009. 16(4): p. 295-308.

103. Maeda, S, Kamata, H, Luo, JL, Leffert, H, and Karin, M, IKKbeta couples hepatocyte death to cytokine-driven compensatory proliferation that promotes chemical hepatocarcinogenesis. Cell, 2005. 121(7): p. 977-990.

104. Luedde, T, Beraza, N, Kotsikoris, V, van Loo, G, Nenci, A, De Vos, R, Roskams, T, Trautwein, C, and Pasparakis, M, Deletion of NEMO/IKKgamma in liver parenchymal cells causes steatohepatitis and hepatocellular carcinoma. Cancer Cell, 2007. 11(2): p. 119-132.

105. He, G, Yu, GY, Temkin, V, Ogata, H, Kuntzen, C, Sakurai, T, Sieghart, W, Peck-Radosavljevic, M, Leffert, HL, and Karin, M, Hepatocyte IKKbeta/NF-

kappaB inhibits tumor promotion and progression by preventing oxidative stress-driven STAT3 activation. Cancer Cell, 2010. 17(3): p. 286-297.

106. Park, EJ, Lee, JH, Yu, GY, He, G, Ali, SR, Holzer, RG, Osterreicher, CH, Takahashi, H, and Karin, M, Dietary and genetic obesity promote liver inflammation and tumorigenesis by enhancing IL-6 and TNF expression. Cell, 2010. 140(2): p. 197-208.

107. Sakurai, T, He, G, Matsuzawa, A, Yu, GY, Maeda, S, Hardiman, G, and Karin, M, Hepatocyte necrosis induced by oxidative stress and IL-1 alpha release mediate carcinogen-induced compensatory proliferation and liver tumorigenesis. Cancer Cell, 2008. 14(2): p. 156-165.

108. Naugler, WE, Sakurai, T, Kim, S, Maeda, S, Kim, K, Elsharkawy, AM, and Karin, M, Gender disparity in liver cancer due to sex differences in MyD88-dependent IL-6 production. Science, 2007. 317(5834): p. 121-124.

109. Clevers, H, Wnt/beta-catenin signaling in development and disease. Cell, 2006. 127(3): p. 469-480.

110. Coutant, A, Rescan, C, Gilot, D, Loyer, P, Guguen-Guillouzo, C, and Baffet, G, PI3K-FRAP/mTOR pathway is critical for hepatocyte proliferation whereas MEK/ERK supports both proliferation and survival. Hepatology, 2002. 36(5): p. 1079-1088.

111. Thompson, MD and Monga, SP, WNT/beta-catenin signaling in liver health and disease. Hepatology, 2007. 45(5): p. 1298-1305.

112. Villanueva, A, Chiang, DY, Newell, P, Peix, J, Thung, S, Alsinet, C, Tovar, V, Roayaie, S, Minguez, B, Sole, M, Battiston, C, Van Laarhoven, S, Fiel,

MI, Di Feo, A, Hoshida, Y, Yea, S, Toffanin, S, Ramos, A, Martignetti, JA, Mazzaferro, V, Bruix, J, Waxman, S, Schwartz, M, Meyerson, M, Friedman, SL, and Llovet, JM, Pivotal role of mTOR signaling in hepatocellular carcinoma. Gastroenterology, 2008. 135(6): p. 1972-1983, 1983 e1971-1911.

113. Villanueva, A, Newell, P, Chiang, DY, Friedman, SL, and Llovet, JM, Genomics and signaling pathways in hepatocellular carcinoma. Semin Liver Dis, 2007. 27(1): p. 55-76.

114. Zhu, K, Dai, Z, Pan, Q, Wang, Z, Yang, GH, Yu, L, Ding, ZB, Shi, GM, Ke, AW, Yang, XR, Tao, ZH, Zhao, YM, Qin, Y, Zeng, HY, Tang, ZY, Fan, J, and Zhou, J, Metadherin Promotes Hepatocellular Carcinoma Metastasis through Induction of Epithelial-Mesenchymal Transition. Clin Cancer Res, 2011. 17: p. 7294-7302.

115. Gong, Z, Liu, W, You, N, Wang, T, Wang, X, Lu, P, Zhao, G, Yang, P, Wang, D, and Dou, K, Prognostic significance of metadherin overexpression in hepatitis B virus-related hepatocellular carcinoma. Oncol Rep, 2012. 27(6): p. 2073-2079.

116. Alexia, C, Poalas, K, Carvalho, G, Zemirli, N, Dwyer, J, Dubois, SM, Hatchi, EM, Cordeiro, N, Smith, SS, Castanier, C, Le Guelte, A, Wan, L, Kang, Y, Vazquez, A, Gavard, J, Arnoult, D, and Bidere, N, The endoplasmic reticulum acts as a platform for ubiquitylated components of nuclear factor kappaB signaling. Sci Signal, 2013. 6(291): p. ra79.

117. Andreakos, E, Williams, RO, Wales, J, Foxwell, BM, and Feldmann, M, Activation of NF-kappaB by the intracellular expression of NF-kappaB-inducing kinase acts as a powerful vaccine adjuvant. Proc Natl Acad Sci U S A, 2006. 103(39): p. 14459-14464.

118. Bianchini, F, Kaaks, R, and Vainio, H, Overweight, obesity, and cancer risk. Lancet Oncol, 2002. 3(9): p. 565-574.

119. Calle, EE and Kaaks, R, Overweight, obesity and cancer: epidemiological evidence and proposed mechanisms. Nat Rev Cancer, 2004. 4(8): p. 579-591.

120. Calle, EE, Rodriguez, C, Walker-Thurmond, K, and Thun, MJ, Overweight, obesity, and mortality from cancer in a prospectively studied cohort of U.S. adults. N Engl J Med, 2003. 348(17): p. 1625-1638.

121. Ballard-Barbash, R and Swanson, CA, Body weight: estimation of risk for breast and endometrial cancers. Am J Clin Nutr, 1996. 63(3 Suppl): p. 437S-441S.

122. Galanis, DJ, Kolonel, LN, Lee, J, and Le Marchand, L, Anthropometric predictors of breast cancer incidence and survival in a multi-ethnic cohort of female residents of Hawaii, United States. Cancer Causes Control, 1998. 9(2): p. 217-224.

123. Trentham-Dietz, A, Newcomb, PA, Storer, BE, Longnecker, MP, Baron, J, Greenberg, ER, and Willett, WC, Body size and risk of breast cancer. Am J Epidemiol, 1997. 145(11): p. 1011-1019.

124. Stephenson, GD and Rose, DP, Breast cancer and obesity: an update. Nutr Cancer, 2003. 45(1): p. 1-16.

125. Rock, CL and Demark-Wahnefried, W, Nutrition and survival after the diagnosis of breast cancer: a review of the evidence. J Clin Oncol, 2002. 20(15): p. 3302-3316.

126. Kaaks, R, Lukanova, A, and Kurzer, MS, Obesity, endogenous hormones, and endometrial cancer risk: a synthetic review. Cancer Epidemiol Biomarkers Prev, 2002. 11(12): p. 1531-1543.

127. Johansson, CB, Youssef, S, Koleckar, K, Holbrook, C, Doyonnas, R, Corbel, SY, Steinman, L, Rossi, FM, and Blau, HM, Extensive fusion of haematopoietic cells with Purkinje neurons in response to chronic inflammation. Nat Cell Biol, 2008. 10(5): p. 575-583.

128. Karin, M, Tracking the road from inflammation to cancer: the critical role of IkappaB kinase (IKK). Harvey Lect, 2006. 102: p. 133-151.

129. Mantovani, A, Allavena, P, Sica, A, and Balkwill, F, Cancer-related inflammation. Nature, 2008. 454(7203): p. 436-444.

130. Coussens, LM and Werb, Z, Inflammation and cancer. Nature, 2002. 420(6917): p. 860-867.

131. Berasain, C, Castillo, J, Perugorria, MJ, Latasa, MU, Prieto, J, and Avila, MA, Inflammation and liver cancer: new molecular links. Ann N Y Acad Sci, 2009. 1155: p. 206-221.

132. El-Serag, HB, Hepatocellular carcinoma. N Engl J Med, 2011. 365(12): p. 1118-1127.

133. Park, J and Conteas, CN, Anti-carcinogenic properties of curcumin on colorectal cancer. World J Gastrointest Oncol, 2010. 2(4): p. 169-176.

134. Farinati, F, Cardin, R, Cassaro, M, Bortolami, M, Nitti, D, Tieppo, C, Zaninotto, G, and Rugge, M, Helicobacter pylori, inflammation, oxidative damage and gastric cancer: a morphological, biological and molecular pathway. Eur J Cancer Prev, 2008. 17(3): p. 195-200.

135. Rutter, M, Saunders, B, Wilkinson, K, Rumbles, S, Schofield, G, Kamm, M, Williams, C, Price, A, Talbot, I, and Forbes, A, Severity of inflammation is a risk factor for colorectal neoplasia in ulcerative colitis. Gastroenterology, 2004. 126(2): p. 451-459.

136. Engels, EA, Inflammation in the development of lung cancer: epidemiological evidence. Expert Rev Anticancer Ther, 2008. 8(4): p. 605-615.

137. Haverkamp, J, Charbonneau, B, and Ratliff, TL, Prostate inflammation and its potential impact on prostate cancer: a current review. J Cell Biochem, 2008. 103(5): p. 1344-1353.

Vitae

EDUCATION:

Doctor of Philosophy, Biochemistry, Virginia Commonwealth University, 2014

Master of Science, Biomedical Sciences, Barry University, 2007

Bachelor of Science, Food Sciences, University of Florida, 2001

Bachelor of Science, Nutritional Sciences, University of Florida, 2001

HONORS:

Keystone Symposia scholarship award recipient for abstract entitled: **Elucidating the Role of Astrocyte Elevated Gene-1 (AEG-1) in Lipid Metabolism**

VCU Massey Cancer Center Excellence in Cancer Research Award Recipient

Presidential Scholar, Scholarship recipient

Kraft General Scholarship Recipient

Coca-Cola Scholarship Recipient

PUBLICATIONS:

7. Genetic deletion of AEG-1 prevents hepatocarcinogenesis.
Robertson CL, Srivastava J, Siddiq A, Gredler R, Emdad L, Rajasekaran D, Akiel M, Shen XN, Guo C, Giashuddin S, Wang XY, Ghosh S, Subler MA, Windle JJ, Fisher PB, Sarkar D. Cancer Res. 2014 Sep.

6. AEG-1 Regulates Retinoid X Receptor and Inhibits Retinoid Signaling.
Srivastava J, **Robertson CL**, Rajasekaran D, Gredler R, Siddiq A, Emdad L, Mukhopadhyay ND, Ghosh S, Hylemon PB, Gil G, Shah K, Bhere D, Subler MA, Windle JJ, Fisher PB, Sarkar D. Cancer Res. 2014 Aug 15;74(16):4364-77.

5. Astrocyte elevated gene-1 (AEG-1) and c-Myc cooperate to promote hepatocarcinogenesis.
Srivastava J, Siddiq A, Gredler R, Shen XN, Rajasekaran D, **Robertson CL**, Subler MA, Windle JJ, Dumur CI, Mukhopadhyay ND, Garcia D, Lai Z, Chen Y, Balaji U, Fisher PB, Sarkar D. Hepatology. 2014 Jul 28.

4. Staphylococcal nuclease domain containing-1 (SND1) promotes migration and invasion via angiotensin II type 1 receptor (AT1R) and TGFβ signaling.
Santhekadur PK, Akiel M, Emdad L, Gredler R, Srivastava J, Rajasekaran D, **Robertson CL**, Mukhopadhyay ND, Fisher PB, Sarkar D.
FEBS Open Bio. 2014 Apr 1;4:353-61.

3. Insulin-like growth factor-binding protein-7 (IGFBP7): a promising gene therapeutic for hepatocellular carcinoma (HCC). Chen D, Siddiq A, Emdad L, Rajasekaran D, Gredler R, Shen XN, Santhekadur PK, Srivastava J, **Robertson CL**, Dmitriev I, Kashentseva EA, Curiel DT, Fisher PB, Sarkar D.Mol Ther. 2013 Apr;21(4):758-66.

2. Astrocyte elevated gene-1 promotes hepatocarcinogenesis: novel insights from a mouse model. Srivastava J, Siddiq A, Emdad L, Santhekadur PK, Chen D, Gredler R, Shen XN, **Robertson CL**, Dumur CI, Hylemon PB, Mukhopadhyay ND, Bhere D, Shah K, Ahmad R, Giashuddin S, Stafflinger J, Subler MA, Windle JJ, Fisher PB, Sarkar D. Hepatology. 2012 Nov;56(5):1782-91.

1. Multifunction protein staphylococcal nuclease domain containing 1 (SND1) promotes tumor angiogenesis in human hepatocellular carcinoma through novel pathway that involves nuclear factor κB and miR-221.
Santhekadur PK, Das SK, Gredler R, Chen D, Srivastava J, **Robertson CL**, Baldwin AS Jr, Fisher PB, Sarkar D. J Biol Chem. 2012 Apr 20;287(17):13952-8.

SKILLS:

Skilled in: Immunoassays, HPLC, Chromatography, Confocal Microscopy, PCR, RT-PCR, Next-gen sequencing and large data set analyses, rodent microsurgery, Cloning, Cell and tissue culture.

EXPERIENCE:

University of Miami, Miami, Florida
***Sr. Research Associate/ Operations Coordinator for Clinical Trial Project
Initiative, Miami Project to Cure Paralysis*** January 2008-August 2009
Responsible for the establishment of assays to translate research endeavors to
industrial biomedical standards

Establishment and maintenance of a GLP facility

Focus on the transfer of manufacturing technology to a cGMP facility including
writing and executing new protocol for the implementation of product testing and
development

Creation of necessary SOP's and training manuals

Development of validation and feasibility studies for proposed processes

University of Miami, Miami, Florida
Research Associate, Miami Project to Cure Paralysis June 2007-January
2008
Responsible for NIH funded research projects with the purpose of identifying
signaling pathways to accurately describe and predict drug functionality on
human cells and tissue

Creation of assays with focus on targeting specific signaling pathways and
modulation of downstream functional pathways

Performance of immunocytochemical, biochemical and molecular techniques to
allow the visualization or measurement of targeted proteins.

Performance of quantitative analyses necessary to determine statistical
relevance of results

Reviewing statistical data to determine accuracy and relevance of research
results

Maintenance of accurate and detailed written and electronic records of each
experiment

Administration of frozen human tissue stock for specific and ongoing
characterization

Performance of necessary purity checks and purification of primary cell lines

Evaluate and redevelop existing protocol for growth and proliferation of human tissue and cells to enhance effectiveness of treatment

Involvement in transfer of manufacturing technology to a cGMP facility including writing and executing new protocol for the implementation of product testing and development

Member of team assigned with the task of creating clear and accurate FDA standard SOP's for translation of emergent protocol to clinical standards

Evaluation of FDA guidelines and correspondence with regulatory bodies to continuously maintain research standards

Maintaining quality assurance for all research team members

Orlando Regional Medical Center, *Orlando, Florida*
Dietetic Research Associate, Nutrition Support Team September2003-
January 2005
Collaborated on the development of nutritional supplements specific to diabetic and cardiac disease states

Created assays for nutritional and pharmacological formulary development

Lead the educational research team responsible for gathering data to modernize formularies

Screened patients to identify nutritional and high dose pharmacological risk

Maintained outcome database that served as multi-study reference base

Calculated parenteral nutrition formulas for critical care groups

Identified and assessed cases of malnourishment and potential food/drug interaction

Initiated and followed enteral, nutritional formularies and TPN for at risk and critical care patients

Avecia Biocides, *Orlando, Florida*
Field Research Chemist February 2002-January 2003
Managed the six person Orlando research and development team

Collected and analyzed data for the development of new biguanide-based biocides

Performed protein and amino group conversions to redevelop polyallylamine polymers

Created specific protocol for new product development and monitored team adherence to protocol

Reviewed and constantly redeveloped research methods to improve efficacy of testing procedures

Hosted local product conferences that pulled together research from multidisciplinary research teams

Trained offsite personnel

ABC Research Corp., *Gainesville, Florida*
Laboratory Technician May 2001-December 2001
Conducted pathogen, spoilage, and microbiological analyses on various matrices

Conducted microbial and chemical analysis using ELISA testing, titration, and gas chromatography devices

Identified sources of food and water contamination

Organized a database for input and reference of recent testing results

Prepared media for and maintained growth of various microbial species

TEACHING EXPERIENCE
Barry University, *Miami, Florida*
MARC/RISE Program Instructor January 2008-July 2009
Developed a GRE test preparatory course for Barry University students enrolled in NIH funded undergraduate research programs

Instructed preparatory course three days per week while holding weekly office hours